Aalto University
School of Chemical
Engineering

Tanja Hautaviita

RHEOLOGICAL CONSIDERATIONS IN PROCESSING NANOFIBRILLATED CELLULOSE IN GEL SPINNING

Master's Programme in Chemical, Biochemical and Materials Engineering
Major in Chemical engineering

Master’s thesis for the degree of Master of Science in Technology submitted for inspection, Espoo, 19 June, 2017.

Supervisor Professor Jukka Seppälä

Instructor M.Sc. Steven Spoljaric

Aalto University
School of Chemical
Technology

Aalto University, P.O. BOX 11000, 00076 AALTO
www.aalto.fi

Abstract of master's thesis

Author Tanja Hautaviita

Title of thesis Rheological considerations in processing nanofibrillated cellulose in gel spinning

Department Polymer technology

Professorship Chemical engineering **Code of professorship** CHEM3027

Thesis supervisor Jukka Seppälä

Thesis advisor(s) / Thesis examiner(s) Steven Spoljaric

Date 19.06.20017 **Number of pages** 98+16 **Language** English

Spinning dopes based on nanofibrillated cellulose (CNF) and poly(vinyl alcohol) (PVA) were characterized to determine correlations between spinnability and rheological properties. Spinnability is important factor presenting the ability and ease of filament formation and if rheology can be related to it, it will help designing better dopes for enhanced spinnability. The demand for more renewable products is increasing thus this work studies the use of 1:1 CNF to matrix dopes, where matrix stabilizes the filament and improves the tensile properties. Previous works commonly use much smaller CNF concentrations and eventhough the rheology of CNFs is well studied it hasn't been correlated to the spinnability.

The effect of dopes consistency to the rheology were tested by changing the solids content from 2 to 4 wt% and altering the matrix composition. The PVA matrix was used as the baseline for all measurements when the effect of adding guar and glutaraldehyde (GA) were tested. Guar was added to increase the high molecular weight portion, that has previously been found to increase spinnability. GA instead was used to study the ability to crosslink the filaments. The crosslinking was tested having the acid in the coagulation bath or in the dope. Thus the effect of acidic and neutral bath were also studied. As crosslinking occurs after the spinning it cannot be related to the rheological properties. Specific rheological measurements (amplitude and frequency sweep and steady state shear) were used to characterize the dopes; this was correlated with observed spinnability. The spinnability qualifications were the wet properties derived from previous gel spinning experiments and the ease of spinning and the tensile properties of the formed filament. Additionally filaments were visually estimated and tested for possible crosslinking.

The best correlation to spinnability of these gel dopes came from the gel strength calculated from the amplitude sweep measurement. The increasing gel strength improved filament stability in the free suface flow. In the air gap filaments started retain the shape attained in capillary with the gel strength of 35 – 45 Pa. Even higher gel strength of 60 – 80 Pa was required for the filament to be enough stable to continue into the bath via an air gap. The storage modulus values instead with the knowledge of the expected entanglement degree allowed the estimation of successful formation of inner structure. This allowed the observation of poor CNF dispersion in the 4 wt% dope containing guar. The linear viscoelasticity region (LVR) instead explained the increased solid like behavior of some of the dope compositions and why they failed to form continuous filament even if they formed filament in the air gap. These parameters were the best for comparing dopes and spinnability. Other parameters gave further insights to the differences between the dopes, but had less effect to the observed spinnability.

Keywords gel spinning, CNF, PVA, filament, rheology, fiber formation

Aalto-yliopisto
Kemian tekniikan korkeakoulu

Aalto-yliopisto, PL 11000, 00076 AALTO
www.aalto.fi

Diplomityön tiivistelmä

Tekijä Tanja Hautaviita

Työn nimi Reologiset tarkistelut nanofibrilloidun selluloosan prosessoinnissa geelikehruussamenetelmällä

Laitos Polymeeriteknologia

Professuuri Prosessi tekniikka **Professuurikoodi** CHEM3027

Työn valvoja Jukka Seppälä

Työn ohjaaja(t)/Työn tarkastaja(t) Steven Spoljaric

Päivämäärä 19.06.2017 **Sivumäärä** 98+16 **Kieli** Englanti

Diplomityön tavoitteena oli karakterisoida selluloosananokuituihin (CNF) ja polyvinyylialkoholiin (PVA) pohjautuvia kehruuliuoksia sekä tarkastella niiden kehrättävyyden ja reologisten ominaisuuksien riippuvuussuhteita. Kehrättävyys on tärkeä ominaisuus, joka kuvaa kykyä ja helppoutta muodostaa kuituja. Jos kehrättävyys saataisiin yhdistettyä reologiaan, auttaisi se kehruuliuosten suunnittelussa. Kysyntä uusiutuvista raaka-aineista valmistettuja tuotteita kohtaan on kasvussa, joten tämä työ keskittyy 1:1 CNF-matriisi-kehruuliuoksiin. Näissä kuiduissa matriisi stabilisoi sen ja parantaa kuivan kuidun veto-ominaisuuksia. Aikaisemmat tutkimukset ovat pääasiassa hyödyntäneet paljon pienempiä CNF-määriä. Vaikka CNF:n reologiaa on hyvin tutkittu, sitä ei ole tutkittu yhdessä kehrättävyyden kanssa.

Kehruuliuosten koostumuksen vaikutusta reologiaan tutkittiin kuiva-ainepitoisuuksilla 2 ja 4 p-% sekä vaihtelemalla matriisin sisältö. Guarin ja glutaraldehydin (GA) lisäysten vaikutusta tutkittiin PVA-matriisin toimiessa referenssinä. Guarin avulla lisättiin korkean molekyylimassan osuutta, minkä on aikaisemmissa kokeissa havaittu nostavan kehrättävyytä. Glutar aldehydiä puolestaan käytettiin kuitujen silloittamiseen. Silloittumista tutkittiin niin, että happo oli joko koaguloitumiskylvyssä tai kehruuliuoksessa, joten samalla tarkasteltiin myös happaman tai neutraalin kylvyn eroja. Koska silloittuminen tapahtuu vasta kehräämisen jälkeen, sitä ei voida yhdistää reologisiin ominaisuuksiin. Tiettyjä reologisia mittauksia (ampliudi- ja taajuuspyyhkäisyä sekä tasapainotilan leikkausnopeutta) käytettiin kehruuliuosten karakterisointiin, mikä puolestaan yhdistettiin havaittuun kehrättävyyteen. Hyvän kehrättävyyden indikaattoreina käytettiin märkäominaisuuksia (johdettu aikaisemmista geelikehräystutkimuksista), kehräyksen helppous ja kuivan kuidun veto-ominaisuudet. Lisäksi kuituja arvioitiin visuaalisesti ja niistä tutkittiin mahdollinen silloittuminen.

Parhaimmat korrelaatiot kehrättävyyteen tutkituilla geelikehruuliuoksilla nousivat geelivahvuudesta, joka laskettiin amplitudipyyhkäisystä. Kasvava geelivahvuus paransi kuidun stabiilisuutta vapaassa virtauksessa. Kuitu alkoi säilyttää kapillaarissa saaneensa muodon, kun geelivahvuus saavutti 35–45 Pa arvon. Vielä korkeampi geelivahvuus vaadittiin, jotta kuitu jatkoi ilmaraon jälkeen muodostumista koaguloitumiskylpyyn. Onnistuneen sisäisen rakenteen muodostumisen arvioimiseen tarvittiin varastomoduulin arvot ja oletettu kietoutumistiheys. Tämän avulla pystyttiin huomaamaan, että guaria sisältävässä 4 p-% kehruuliuoksessa CNF ei ollut kunnolla dispergoitunut. Lineaarinen viskoelastinen alue (LVR) puolestaan selitti havaittua hauraampaa käytöstä, mikä esiintyi muutamilla tutkituista kehruuliuos koostumuksista. Tämä muun muassa selitti, miksi ilmavälissä yhtenäisen kuidun muodostanut kehruuliuos epäonnistui jatkuvan kuidun muodostamisessa kylpyyn. Edellä mainitut parametrit olivat parhaita vertaamaan kehruuliuoksia ja niiden kehrättävyyttä. Muut parametrit lisäsivät tietoa kehruuliuoste eroista, mutta niillä ei ollut selkeitä vaikutuksia kehrättävyyteen.

Avainsanat geelikehräys, CNF, PVA, kuitu, reologia, kuidunmuodostus

Acknowledgements

First I would like to thank the handy people of the workshop that made the experimental part possible. They were able to cut the regular needles into blunt ones with accuracy. With slanted needles the fiber cross section would have been affected and I wouldn't have had any chance of spinning the 2 wt% dopes as they couldn't take the added drag caused by the tip. I should have used their expertise earlier as I waited for the ordered needles for several weeks and thus delaying everything. To this date it remains a mystery to me where the ordered needles ended up.

Then I would like to thank "Sintti" for giving tips with excel and random talk when I needed it. She expanded my knowledge on what can be done with the figures of excel. I would also like to thank my instructor Steven Spoljaric for all the help and guidance he provided during the project. And for sharing his expertise with the machinery used. Jukka Seppälä I would like to thank for giving interesting subject. And lastly I would like to thank my two fur balls for continuing to act as my therapists.

```
  /\_/\
(=^.^=)
  (")(")
```

```
  /\_/\
(=^.^=)
  (")(")
```

Tanja Hautaviita
In Helsinki 19.06.2017

Table of Contents

List of appendix

List of symbols

A	=area
D	=needle inner diameter
DR	=draw ratio
d	=diameter of the particle
E	=Young's modulus
F	=force
G'	=storage modulus
G''	=loss modulus
G^*	=complex modulus
h	=height
K	=cohesive energy density
k	=constant presenting fluids consistency
L	=length of needle
L/D	=length/diameter ratio of needle
l	=length of the particle
l/d	=aspect ratio of the particle
M_w	=molecular weight
$M_{e,\,soln}$	=solution entanglement molecular weight
M_e	=entanglement molecular weight
n	=power law index
$n_{e,soln}$	=entanglement number
ΔP	=pressure difference
Q	=volumetric flow of dope
r_i	=radius of a cylindrical layer
R	=radius to the needle wall
r_{max}	=maximum radius of the filament
t	=time
t^*	=residence time
t_{dyn}	=dynamic relaxation time
t_{long}	=longest relaxation time
t_{relax}	=relaxation time
u	=deflection
v_r	=velocity of the roller
v_s	=average velocity at which fluid is ejected from the die
w	=frequency
w_{cros}	=frequency at storage and loss moduli crossover (G'=G'')
w_m	=frequency value at the maximum value of loss modulus
x	=distance from the needle
x_c	=critical distance from needle where break occurs
γ	=shear strain
γ_{crit}	=critical strain
$\dot{\gamma}$	=shear rate
$\dot{\gamma}_R$	=shear rate at wall
δ	=phase angle
$\tan\delta$	=loss tangent
η	=viscosity
η^*	=complex viscosity
$\emptyset_p$	=volume fraction of the polymer
ϕ_c	=percolation threshold
λ	=wavelength
μ	=growth factor of capillary waves
σ	=shear stress
σ_{rz}	=shear stress at distance r
σ_R	=shearing stress at R
σ_c	=critical stress applied to the filament
σ_y	=yield stress value
τ	=amplitude
τ_0	=amplitude at time point t=0
χ	=die swell

1 Introduction

Cellulose is one of the most abundant materials in the nature [1]. It is the main reinforcing agent in plant cell walls where it is responsible for mechanical strength when lignin and hemicellulose in wood binds everything together [2, 3]. The strength of cellulose comes from its extensive inter and intra chain hydrogen bonding. This also provides a high degree of crystallinity, tensile strength and reactive surface chemistry but also renders them hard to dissolve. Nano cellulose also exhibit unique rheological properties depending on its shape. [4, 5, 2] All these properties make them especially desirable for various applications.

Cellulose can be processed by mechanical and chemical methods to produce cellulose nanofibrils (CNF) [2]. These form a colloidal suspension where at least one of the outer dimensions of the particles are at the nanometer scale [2, 5]. These can be used to reinforce polymers but their use has some challenges due to their hydrophilicity, which is overcome by using water soluble polymers [6]. After dispensing the nanofibrils are randomly oriented and need to be further orientated to reach their full potential. This has been tackled by spinning them into filaments as this process orientates the fibers in the filaments length direction. [7] CNF reinforced filaments have been done by gel spinning method [8, 6, 9]. The addition of CNF even in low quantities has enhanced filaments tensile properties for example increasing the maximum tensile stress and Young's modulus by 60 and 220 % compared to the neat PVA filaments [6].

There are challenges in using the CNF efficiently for reinforcement. This is due to high concentrations decreasing the orientation of the polymer [6], good dispersion being required for adequate stress transfer [10] and CNF:s tendency to act as rheology modifier [11, 12, 13]. The strength of the formed filament as well as the ease of spinning are often referred to as spinnability. It is important factor as it depicts the ease and quality of spinning which is then optimized. This work attempts to find correlations between rheology and the overall spinnability of PVA/CNF based dopes. In addition Glutaraldehyde (GA) and guar were utilized. The GA was used as crosslinking agent in order to test it's applicability in

reinforcing the product by enforcing the interfacial interactions and stress transfer with the matrix polymer. [10] The guar instead was used to increase the portion of high molecular weight that has previously been found to increase spinnability [14].

In the literature review first the gel spinning is explained through comparing it to other commonly used spinning methods and then the second part focuses on how the orientation and filament formation occurs in the spinning process. This is followed by the requirements the dope needs in order to form filaments and similarly how the spinnability is observed from the spinning process. The fourth part extends the knowledge on the raw materials utilized in this study and previous filaments prepared from them. Finally, the rheological background is given and possible rheological parameters are identified for use in the experimental part.

The experimental part details the preparation and composition of the spinning dopes, followed by the spinning and analytical methods. In particular, the various rheological measurements: amplitude and frequency sweep as well as steady shear results are highlighted. The rheological properties of different dopes are compared and correlated with the filament forming ability of the dopes (the ease of spinning, air gap and breaking mass). Additionally these rheological properties are further related to the properties of the dry filament, especially the tensile properties. IR spectroscopy and C^{13} NMR are used to characterize the successfulness of crosslinking within the filaments. Finally, the conclusions and future applicability section highlights the best correlations, possible applicability and issues that could be further studied.

LITERATURE PART:

2 Gel spinning

There are many spinning methods invented for different needs. These include melt spinning [15, 16], solution spinning [15], gel spinning [10, 17, 18] and electro spinning [19] etc. The amount increases with subcategories including dry [15], wet [15, 10] and dry-jet wet spinning [17, 18, 4]. In this work the focus is on gel spinning. Since the requirements of different methods are often similar, it makes the parameters utilized in one method often be applicable for different spinning methods [14]. Thus some analogies will be taken from electrospinning and solution spinning in particular. This section focuses on defining the gel spinning method by comparing it to melt and solution spinning.

Melt, gel and solution spinning differ mostly in regards to the consistency of the dope. Melt spinning doesn't utilize any solvents [15] when gel and solution spinning do [17, 4, 15, 18, 16, 6]. However the difference between gel and solution spinning is slightly vague. Ghae et al. distinguish between gel and solution spinning using the dope solids content; those containing less solids, around 10.5 g/dl are considered as gel spinning while ones at higher solids content, around 20 g/dl are called solution spinning [18]. Other definitions state that gel spinning can contain solvent from 50 – 98 wt% giving it a much broader definition [16]. These names are to differentiate a more gel-like sample from a liquid-like. The viscosity increase comes from the inner network of the material, as the definition of a 'gel' arises from a polymer network having it's whole network volume expanded by a fluid. In other words, a material where a network spanning the whole sample is formed. [20]

Even as melt and gel spinning differentiate from each other due to the presence of solvent in the latter, they are quite similar. In both methods the spinning dope can be quite viscous. Melt spinning is often favored for the lack of the need to remove any solvents. [21] This is due to the high flowability of the melt spinning dope maintained with increased temperature [15]. The only hindrance comes from a lack of melt stability or excessively high melt viscosities which some polymers exhibit.

In order to overcome these challenges, the gel spinning method was developed. There the high solvent content decreases the viscosity by lowering the polymer concentration and thus also the amount of entanglements that cause resistance to flow. [16] Therefore concentration changes can also be used to compensate the need for higher temperature as they have similar effects on flowability [15].

As melt spinning is based on temperature differences, heat being used to turn mass flowable and cooling used to harden the fibers, another noteworthy difference is that there is no mass transfer. Thus, only volume reduction occurring in melt spun filaments is due to thermal contraction. In gel spinning the mass transfer is more significant and leads to higher distortion of the shape, due to the low solids content. The lower volume reduction in melt spinning usually results in the fibers displaying better symmetry and better retaining the initial shape. [15]

The lower solids content with gel spinning dopes is considered to allow higher orientation of the polymer chains inside the filament [16, 18]. This is because there are fewer defects in the structure, that arise from the chain ends and chain entanglements of the polymers. Their amount is naturally decreased when using lower concentrations and higher molecular weight polymers in gel spinning. However, neither defect can ever be fully eliminated; this is further explained in the spinnability section of this literature review. [18] Due to the low amount of defects the gel spun fiber should reach a higher state of orientation than the melt and solution spinning counterparts. A combination of gel spinning with additional drawing is expected to result in an orientation close to morphology in Figure 1a, while the melt and solution spinning methods result in morphologies similar to those in Figure 1b. [21]

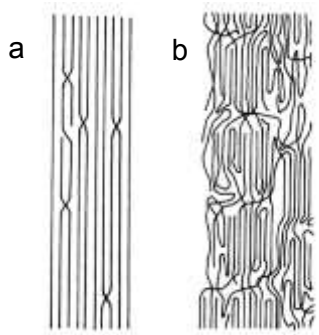

Figure 1. Example of morphology expected from a) gel and b) melt and solution spinning methods, with drawing to extend the molecules (modified from reference) [21].

From the Figure 1 it can be seen that the amount of defects in gel spun filaments is visibly smaller than those prepared from melt and solution spinning. Of course this is idealized example and such 100% orientation cannot be easily reached [9]. The process how this highly oriented structure can be reached by gel spinning and the steps required is further expanded in the following setup and phenomena section.

3 Spinning setup and phenomena

Gel and solution spinning methods can both be divided into sub categories of dry [15], wet [15] and dry-jet wet spinning [15, 4, 17]. In this context, dry spinning means that no liquids were used as a coagulation medium. In this method the coagulation depends completely on the evaporation of the solvent from the dope into the surrounding air. [15] Cellulose acetates [22] and acrylics are some of the most important dry spun fibers [23]. Dry spinning isn't a common method with PVA filaments but has been performed previously [8]. Significantly more common methods are the wet or dry-jet wet spinning, where the coagulation occurs in solvent bath and the dope is either spun straight into the bath or via an air gap [15, 10, 9]. In this work it is expected that wet or dry-jet wet spinning will be the used method thus it is here studied in more detail.

The setup for wet spinning in its most basic form is a container, a nozzle and a coagulation bath. In a laboratory scale the container is often a syringe equipped with a syringe pump to obtain continuous flow. The nozzle in the case of a syringe is naturally a blunt needle that is often also called a spinneret or capillary. [4, 10, 6] The wet spinning method is turned into dry-jet wet spinning with the introduction of air gap between the needle and the coagulation bath which allows some stretching and relaxation to occur [4].

To further orientate the dope constituents, the incipient filament can also be wet drawn within the coagulation bath. This is done by having rotating rollers inside the bath that are rotated at a higher velocity than the filament is ejected. After which the filaments are often allowed to sit in the coagulation bath before being air dried and heat treated which can be either oven drying or heat drawing. [4, 6] The

spinning is often done in parts at the laboratory scale, with the spinning and wet drawing separated from the drying and heat drawing [6]. However, some have complex equipment allowing continuous filament formation [9]. In Figure 2 the process for dry-jet wet spinning is illustrated with wet drawing. In this work the wet drawing is not a possibility due to technical limitations, but the possibility of air gap is considered.

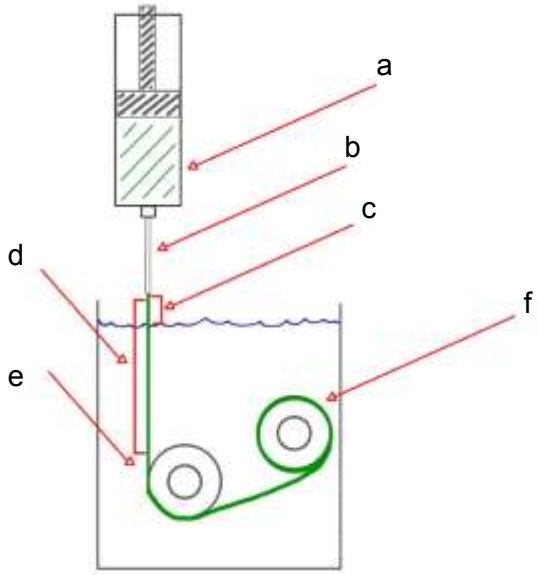

Figure 2. Illustration of the dry-jet wet spinning with wet drawing (adapted from reference) [4, 9].

In the Figure 2 the dope is first held in a syringe (a) and the mass is pushed through the needle that acts as capillary (b) after which the confined flow of of the capillary changes into free surface flow when the mass is ejected from the needle. In dry-jet wet spinning this free surface flow travels through air gap (c). The wet spinning instead lacks the air gap and the dope is ejected straight into the coagulation bath. In the portion after the needle (d) the filament needs to attain some strength immediately to make the drawing possible by the rollers (e). After which the drawn filament can be collected on a coil (f). [4, 17, 6, 9] The formation of the filament structure by these steps is first studied as whole observing the flow profile that then gives the basis on how the different sections affect the final product.

3.1 Flow profile

To understand how a spinning process induces orientation to the fibers, first the spinning process needs to be studied as whole. The different flow behaviors present during spinning are the key in inducing the orientation to the filaments. Initially, the flow profile is expected to be even when the mass enters the needle. There it comes into contact with the walls of the capillary. The interactions with the walls affects the speed profile, forming a parabolic profile in the direction of the flow as the friction causes the outer layers to slow down. The Figure 3 shows this speed profile where the center is least affected by the friction and thus exhibits the highest speed values when the outer layers are approximated to zero. [15, 24]

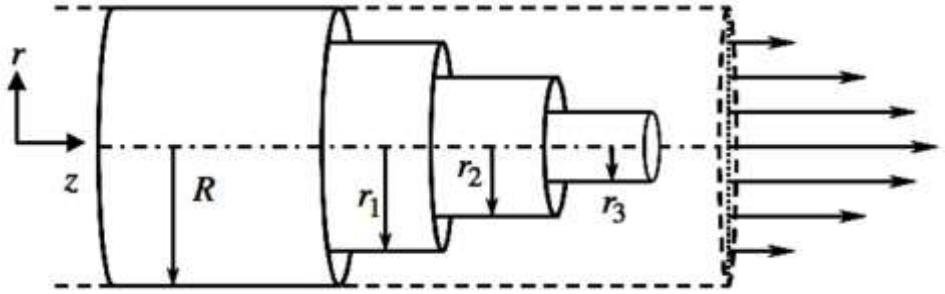

Figure 3. The shearing induced speed profile in cylindrical layers of the forming filament, where the R is the maximum radius and the r_i are the radius of corresponding cylindrical layers [24].

The capillary flow is classified as ‘confined flow’ and shearing is main interaction inducing structure orientation [21]. At the needle exit the flow profile changes as the interaction with the capillary walls and back pressure are no longer affecting. The fluid jet is then drawn away by gravity or added drawing. [15, 4] This stage is called ‘free-surface flow’ which is dominated by elongational flow [21]. During this change from the centrally accelerated into a constant flow, the outside layers previously retarded by friction accelerate to the same speed as the inner portions. Thus a paraboloid speed profile is formed in the opposite direction to the first profile inside the cylindrical filament. This acts to compensate the original profile after which the flow profile is again uniform. [15] The whole speed profile around the needle and free surface flow is presented in Figure 4 showing the changes occurring in the flow.

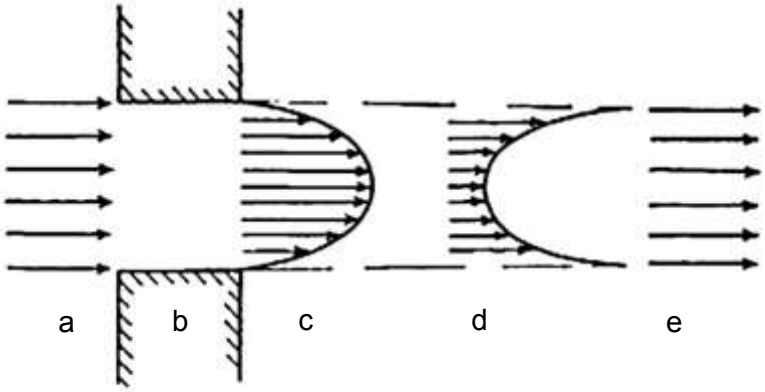

Figure 4. Speed gradient profile for the spinning system, where a) uniform speed at the spinneret entrance, b) spinneret walls, c) speed profile induced by spinneret walls and back pressure, d) profile compensating the original e) uniforms speed (modified from reference) [15].

Building on the flow profile in the Figure 4, the different parts of the gel spinning are studied in more detail in the following sections. First the capillary part forming the confined flow (b and c) studies how the randomly oriented dope attains initial filament shape in the needle. The second part concentrates on the free-surface flow (d and e) explaining the effects of the air gap and drawing. After which the purpose of a coagulation bath and possible additional treatments are briefly introduced. The focus is on how these all steps affect the orientation of the filament and why they are needed or beneficial for spinning.

3.2 Structure formation in a capillary

The needle is the first place the molecules in the dope begin to orientate [21]. There the shear flow that formed the parabola speed gradient (refer to Figure 3) is the factor causing the orientation of the molecules. The speed gradients cause a tilting motion to the chain-like molecules as the parts in the inner layers move at higher speed elongating the molecule and orientating it into the direction of the flow. The higher the speed gradient between the cylindrical layers, the better the orientation effect. Thus the orientation is better at the outer layers and decreases going towards the middle. [15]

The speed gradients are dependent on the magnitude of the shear the mass is subjected to [15]. Also the length of the capillary has an effect since in longer needles the macromolecular chains have more time to relax and orient [17]. This is important as some of the force supplied to overcome the resistance to flow is stored as elastic energy in the polymeric fluid as it is not ideally viscous. In free surface flow it gets released where it causes a decrease in the orientation of the filament. To minimize this the material can allowed to relax and orientate further in the spinneret. This effect is further discussed in the following section. [21]

To estimate the shear stress there are complex equations that are often utilized with the assumption of some degree of Newtonian behavior [14, 24]. Defining the Newtonian behavior with parameter n which is further discussed in the steady shear part of this literature review [24]. How the shear stress can be estimated is shown in Equation 1 to highlight the parameters affecting it [24]. The down side with these equations is that they often use the pressure difference, when the actual spinning is commonly done with a measuring pump instead of pressure control.

$$\sigma_{rz} = \frac{(\Delta P)r}{2L} = \sigma_R \frac{r}{R} \tag{1}$$

where σ_{rz} is the shear stress at certain distance r from the center in the direction of the flow, ΔP the pressure difference, L the length of the capillary, σ_R the shear at the wall calculated with the R inner radius of the spinneret. [24] As already obvious from flow profile, the further from the center the dope mass is the more it is experiencing shear. It is also affected by the force used to move it through the length of the capillary which in Equation 1 is the pressure difference. The shear rate for Newtonian fluid can be expressed as a function of the shearing stress at the wall or as proportional to the extrusion volume flow (Q) which are shown in Equation 2 [24]. In experimental work this parameter has previously been used to compare to the quality of spinning. [25, 26]

$$\dot{\gamma} = \frac{1}{\eta}\sigma_R \equiv \frac{4Q}{\pi R^3} \tag{2}$$

where the $\dot{\gamma}$ is shear rate, η is the viscosity of Newtonian fluid and Q is the volume flow rate. With Newtonian fluids the shear rate is a function of the shearing stress (σ_R), while non-Newtonian ones are more complex and the relationship depends on previous shearing the material has been subjected to [21]. The extrusion rate

is directly related to shear rate and is also important for sufficient speed gradient. Furthermore, the uncurling of the polymers is inefficient with longer chains [25, 15]. More of the shear behaviour of fluids in the steady shear portion of this literature review.

3.3 Structure formation in free-surface flow

The dope jet leaving the capillary is subjected to relaxation, which is visible as die swell phenomenon. In Figure 4 this is shown as part of the flow where the original paraboloid is compensated with the opposite one (d). In the die swell some of the orientation achieved in the capillary is lost. [21] The die swell (χ) is calculated from the ratios of maximum radius of the filament to the inner radius of the spinneret shown in Equation 3. It is also dependent on the shear rate, and the relation between residence and relaxation times. [14] The relaxation time is the measure of time required for the disrupted system to re-arrange [27]. The die swell can be minimized if proper relaxation is reached and thus the residence time needs to be longer than the relaxation time of the dope. The residence time is affected by changes in the needle length and it can be calculated as the time it takes for a volume to pass through the needle shown in Equation 4. [14]

$$\chi = \frac{r_{max}}{R} = \chi(\dot{\gamma}, t^*/t_{relax}) \tag{3}$$

$$t^* = \pi R^2 L/Q \tag{4}$$

where r_{max} is the maximum radius of the filament, R is the inner radius of the spinneret, $\dot{\gamma}$ the shear rate, t^* is the residence time, t_{relax} is the relaxation time, L the length of the needle and Q the volumetric flow of the dope. Liu et al. have bound this die swell phenomena to L/D ratio as it also affects the residence time as it is the ratio of length (L) to diameter (D) of the capillary. They studied the effect of this ratio on the orientation through the spinnability of the filament and found that similarly it has significant effect on the die swell and spinnability until a plateau value. [17] These and other ways to study spinnability are discussed in spinnability in processing part of this literature review.

Because of the die swell phenomena causing some orientation loss right after the spinneret, it is assumed that the technologically most important orientation stage is the extensional flow shown in Figure 4e as the final part of the basic flow profile. This is where drawing is introduced to the fluid jet [21]. The induced drawing is expected to occur closest to the needle where the wet strength is lowest. With dry-jet wet spinning this means the air gap where also some additional relaxation can occur. [15, 4] Wet spinning might not allow as much drawing/relaxation due to fluid jet starting to harden as it hits the coagulation bath immediately [15, 4]. The drawing is used to align and uncurl the molecules by elongating them in the direction of the filament length. When the shear flow relied on the orientation from different speed gradients tilting the molecule the extensional flow exerts different velocities onto the molecule ends, effectively drawing them straight. [21]

In the state when the jet is starting to harden it is only able to absorb low stresses. These stresses can only be as much as the weakest point of the jet near the spinneret is to able carry, which is often not enough for technical applications. [15] The fluid jet needs to gain enough strength immediately in the coagulation bath to be mechanically drawn away which induces the strain into the forming filament [28, 4]. This is done by rotating rollers at a higher velocity than the fluid jet is ejected and the ratio of these velocities is qualified as draw ratio (DR). This is shown in Equation 5. And the average velocity of the fluid can be calculated with Equation 6. [4]

$$\mathrm{DR}=\frac{v_r}{v_s} \tag{5}$$

$$v_s=Q/\pi R^2 \tag{6}$$

where v_r is the velocity of the roller, v_s is the average velocity at which fluid is ejected from the die, Q is volumetric flow and R is the die radius. The drawing can also be expressed by elongation rate that also takes into account the air gap length making the calculation more complex [14]. As the higher draw ratio induces the best orientation it is often pursued. The high orientation then favours crystallization increasing the strength of the formed filament even more. This strain hardening also helps to stabilize drawing. Fluctuations in the strain results in filaments with changing diameter where the thinner portions are only slightly weaker due to strain hardening. [28]

3.4 The effect of the coagulation bath

The coagulation bath itself is just a non-solvent for the polymer that is used to collect the forming filament [4]. There a transition from flowable spin mass into a self-supporting filament structure is accompanied by a viscosity increase of several orders of magnitude. This change is achieved by the removal of the solvent and/or cooling. [15]

The effect of the coagulation bath is based on the fact that the used solvent can't solvate the polymer but the original solvent used to make the spinning dope can solvate in it. So the solvent used to make the dope flowable in the first place is slowly leached from the filament and the polymer content becomes enriched over time. [4] The coagulation can also happen by chemical precipitation where a chemical reaction hardens the structure. This method can be close to instant depending on the reaction rate. Both of these coagulation methods suffer from decreased diffusion rates as the outside layers are first to harden and decrease the diffusion happening in the center part. [15] So basically coagulation is just reducing the mobility of the polymer chains to make the material more stable.

As the structure is starting to set in the coagulation bath it is still susceptible to changes in the polymer chain arrangement. It depends on mobility and relative position of the polymer chains during the hardening period [15]. So similarly as in the die swell some orientation is again lost in the coagulation [28]. The positions and orientation of molecules is disrupted by mass transfer in and out of the fluid jet filament movements inside the coagulation bath. The mass transfer in the coagulation bath is the diffusion of the coagulation bath solvent and dope solvent in opposite directions where their concentrations are the smallest. After the structure has set enough and the filaments are collected and dried, the mass reduction as the solvents are evaporated causes a reduction in the size of the filament simultaneously affecting the orientation and relative places of the chain molecules. [15]

The cross section has previously been able to be manipulated by inducing higher degrees of gelation to the dope. This makes it more elastic and thus also less likely to deform during the spinning process. [17] The sufficient surface tension at

spinneret exit and viscosity in relation to the nature of coagulation medium are the important factors determining how well it is able to hold its form [15].

In previous gel spinning systems with PVA based filaments with cellulose nanofiber the temperatures used have even been as low as -20 °C to -15 °C and coagulation baths of either methanol or ethanol have been used [10, 6]. But with gel spinning other systems have even used as low values as -50 °C [18]. These low coagulation temperatures are often also combined with long coagulation times even up to 48 hours [6]. The need to decrease the temperature in the start of coagulation most likely indicates that before any solvent is leached the viscosity at room temperature isn't enough to form fibers and could possibly cause them to fuse together. Also a cool coagulation bath is believed to produce stronger filaments [28].

3.5 Additional treatments

The spinning process usually leads to only a preliminary orientation even with high wet draw ratio and additional treatments are needed to gain sufficient strength to the filament [21]. Where the additional treatments are usually about inducing further orientation to the hardened filament [15]. Due to this, gel spinning is essentially two-step process as the spinning and additional treatments are difficult to incorporate together [16]. Often in addition to drying the filaments they are also heat treated to make them dimensionally more stable [21], since heating them removes the residual water inducing more hydrogen bonding in the material [6].

Additional drawing requires a plastic state to be performed, which can be reached by swelling or heating the hardened fibers. In some cases the plastic state prevailing during coagulation can be used allowing the additional drawing to be combined with the spinning process. This cold drawing is essentially wet drawing after 'fiber-brakes' to avoid it affecting the weaker part near the spinneret and only inducing drawing to partially coagulated sections that can take more stress. [15]

In the post-spin drawing by heating the used temperature is dependent on the fiber composition. The PVA cellulose filaments has been previously heat drawn by Peng et al. at a temperature of 210 °C. Where the drawing was done by pre-heating the fibers for 30 seconds followed by manually drawing at 3 – 4 mm/s speed. A hot

draw ratio of 13.5 was reached. [6] The post spinning draw ratios are significantly higher compared to wet draw ratios increasing the total draw ratios substantially. For example wet draw ratios of 2 – 3 and hot draw ratios of 13.5 – 6.66 with PVA and cellulose containing systems have been used, where the total draw ratio is the wet draw ratio multiplied with the hot draw ratio. So earlier total draw ratios of 27 and 20 have been reached with PVA cellulose filaments. [6, 9]

4 Spinnability

Spinnability is the term used to refer to the ability and ease of a spinning dope to be successfully spun into a continuous filament [14, 17, 28, 29]. It has a vague explanation and it can be used to indicate that certain dope property and process condition combinations lead or don't lead to filament formation. It can also be used to rate dopes according how well they can be spun or the results they provide. [15, 14]. Although the ability to initially even form filament depends on the dope consistency and its capability to form structure that holds together which is studied further in fiber formers section [15, 29]. The spinnability in processing part also takes the process parameters into account.

4.1 Fiber formers

Spinnability referring to the dope or the polymer is often used to define the lower limit or upper limit at which a filament can be successfully spun. It is often vague and depends on the processing method and conditions. The lower limit is the combination of properties first leading into the formation of stable 3D network structure which is preliminary for filament formation. [15, 29] This network is considered to be the result of three parameters: molecular weight, concentration and entanglements. The latter being the result of the first two, where different combinations of them leads into adequate networks for fiber formation with different properties. [29]

Previously *the entanglements* were referred to as defects that cannot be fully eliminated from the filament. This is because they are the chain junctions forming the network that holds the material together. And the density of the entanglements

arises from the combination of concentration and molecular weight. [29] The chains can slide past each other causing the disentanglement of the junctions which induces viscoelastic behavior into the material. [29, 30] Due to their ability to disentangle they only act as physical network under strain that is greater than their disentanglement time. [29]

The molecular weight affects the viscoelastic properties by determining the distances between physical entanglements affecting the extensibility and thus also the speed of the disentanglement. With same entanglement density per chain, lower molecular weight reaches lower extensions and disentangles significantly faster. [29] Thus the maximum elongation of the spinning fluid has been related to the average molecular weight of the solution where spinnability increases with the portion of high molecular weight fraction [14].

For the molecular weight to affect and entanglements to form there needs to be a certain *solids concentration* of chainlike molecules present in the solution. As concentration affects the intermolecular distances, higher molecular weight requires lower concentrations. Thus the concentration affects the network properties and the flow of the solution. Low concentration can be compensated with temperature decrease as it also acts to retard the chain mobility. [15, 29] The viscosity increase caused by decreased chain mobility is an important parameter in spinning affecting the formation of filaments as it slows down the initial thinning dynamics and stabilizes the spinning process [4].

Shenoy et al. further examined the dependence of molecular weight, concentration and entanglements on the spinnability with an electro spinning method. Insufficient entanglements formed due to low molecular weight or concentration, leading to the formation of beads. When increasing the values first resulted in a mixture of beads and fibers and eventually only fibers were formed. The parameters at which only fibers were formed was identified as stage when stable spinning can occur. This was at the entanglement number ($n_{e,soln}$) value of 3.5. This is defined as the ratio of the polymer molecular weight to its solution entanglement molecular weight shown in the Equation 7. [29]

$$n_{e,soln} = \frac{Mw}{M_{e,\,soln}} = \frac{\emptyset_p Mw}{M_e} \qquad (7)$$

where for polydisperse system, the M_w is molecular weight often replaced with weight average molecular weight, $M_{e,\,soln}$ is the solution entanglement molecular weight, M_e is the entanglement molecular weight corresponding to the average molecular weight between entanglement junctions and $\emptyset_p$ is the volume fraction of the polymer. The entanglements per chain can be calculated by deducting one from the $n_{e,soln}$ value as all entanglements involve two chains. Thus the $n_{e,soln}$ value of 3.5 corresponds to 2.5 entanglements per chain. [29] Haward et al. have confirmed that this minimum value also applies to the dry-jet wet spinning process. They also detected significant increase in relaxation time of the dope and the Hencky strain when increasing the value to the minimum by changes in concentration. This further confirmed that some inner structure formed at this threshold. [4]

Shenoy et al. also list other ways to promote the fiber formation if the concentration and molecular weight are too low for adequate network formation allowing the fiber formation. These are: crosslinking, enchancement of polymer-polymer interactions and addition of solvent able to induce gelation. All these methods are based on enchancing the 3D network similarly as the chain entanglements. [29]

Crosslinking affects the effective molecular weight of the polymer, and those covalent bonds between polymers lack the chain entanglements ability to disentangle by chains sliding past one another. Thus it affects the viscoelastic behavior of the material. [29, 19] Hydrogen bonding as a common polymer-polymer interaction has less of a finality due to being a weaker connection compared to the covalent bonding [29]. The solvent inducing gelation to the solution is one that brings about favorable interactions with the polymer to form a network. One such example is exploiting permanent dipoles in the polymer structure with appropriate solvent. [17]

Shenoy et al. have illustrated the impact of hydrogen bonding by comparing the minimum molecular weight and concentration of nylon spinning to the spinning of polystyrene. The absence of hydrogen bonding caused the need for a higher molecular weight and concentration in the latter. There the nylon was spinnable from 25, 000 g/mol and 2.5 wt% when styrene needed up to 190,000 g/mol and 34 wt%. [29] Similarly the effect of crosslinking in electro spinning has been proven

[19]. Furthermore, the addition of solvent to induce gelling was tested with gel spinning [17]. Even though their usability has been proven, some still consider crosslinking and gelation detrimental for the spinning as it can eliminate solubility and act against flow [15, 30].

4.2 Spinnability in processing

Even when the dope passes the requirements set out in the fiber formers the formation of the filament is still dependent on the relationship between the spin mass characteristics and the processing conditions [15]. As previously mentioned certain conditions are required for the entanglements to act as a network holding the material together.

Spin mass characteristics are often studied by rheology as it does give some indication of things favorable for spinnability but cannot give the absolute values for the best spinnability on its own. The ideal values are highly dependent on the variables like consistency and process parameters. Thus rheology can only compare the dopes against each other and thus practical observations need to be done as well. Even then the rheology cannot always explain the differences observed in the spinnability. [14, 28] The rheological comparison of the dopes is explained in the rheology part of this literature review. Here the focus is on practical observations of spinnability in processing and how the lower and upper limits are determined and how they can be used to compare spinnability of dopes.

Previously in the spinning setup and phenomena the free-surface flow was identified as the most important factor in forming the well oriented structure [21]. Since the filament is at its weakest and is subjected to drawing forces, the limitations observed in this part are most likely to limit the spinnability of the dope the most. Thus the stability and strength of the fluid jet are of interest. [28] As in the free surface flow, filament breaks or instabilities are common reasons for limiting spinnability or completely preventing the formation of continuous filament. [14] The breaks in the filament can occur by three already identified methods or be a combination of them [28, 14]. These are the: capillary, ductile and cohesive break up and they are presented in Figure 5 [14].

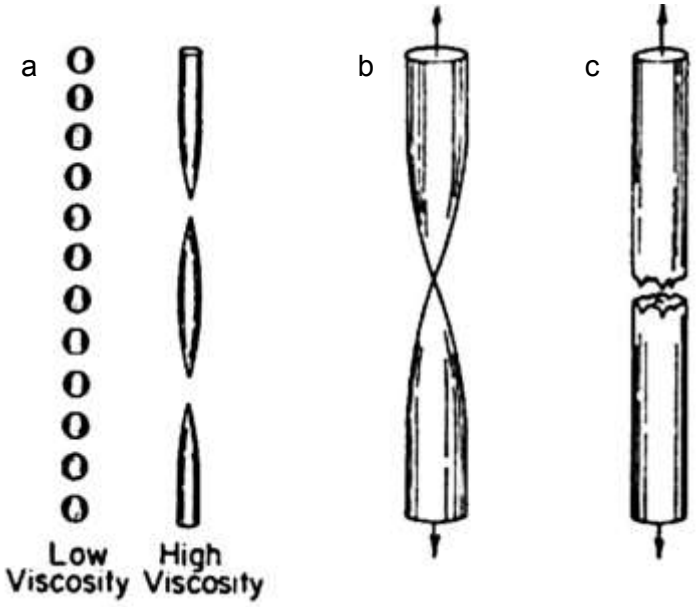

Figure 5.The failure modes of filament in spinning a) capillary break up for low and high viscosity dope, b) ductile and c) cohesive break up(modified from reference) [14].

Of these methods the capillary one is considered to be related to surface tension where the break results from capillary waves as the forces holding the filament together aren't sufficient. Thus it presents the lower limit for the spinnability. Whereas the cohesive break up presents the upper limit. This is because the material requires certain relaxation time in comparison to the applied strain to behave like a viscoelastic material or it is susceptible to fracture. The relaxation time required increases with strain and molecular weight. The ductile failure occurs between the two extremes. [29, 14]

The capillary method is explained to result from capillary waves causing filament to break up into drops or ligaments when the other two methods are the result of excessive force applied to them [14]. The propagation of the waves is represented by the amplitude of the capillary wave which is a function of time and distance from the needle tip which is presented in Equation 8 and visually in Figure 6. When the amplitude τ rises to be equal with the radius of the fluid jet it will cause it to break [17].

$$\tau = \tau_0 \exp(\mu t)\cos(2x/\lambda) \quad (8)$$

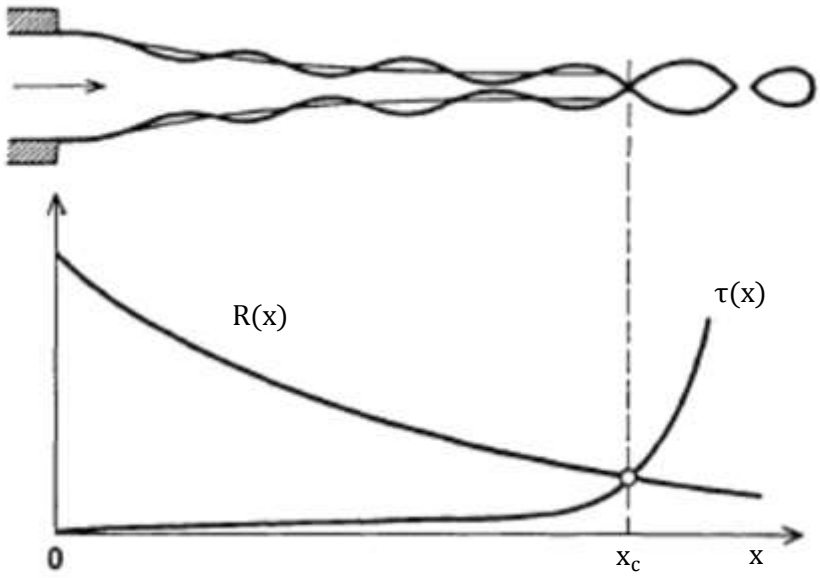

Figure 6. Propagation method of capillary wave (modified from reference) [14].

where τ_0 is the amplitude of capillary waves at time point t=0, μ the growth factor of capillary waves, t the time, x the distance from the needle where the x_c is the critical distance where break occurs, and λ is the wavelength. This equation for example allows the estimation of the lower limit for extrusion velocity and spinneret radius [14]. This is because increasing the velocity the distance is reached faster and increasing the radius of the filament requires higher amplitude to cause the break [28]. Additionally the increase in air gap length has been found to prolong the amplitude [17].

The upper limit for the cohesive fracture comes from the strain being excessive causing it to lose its viscoelastic behavior required for spinning. The break up then occurs due to excessive storage of elastic energy [14, 17]. This means that the tensile strength of the filament is exceeded. This occurs when the critical stress level is reached that can be expressed by Equation 9. [17]

$$\sigma_c = \sqrt{2KE} \quad (9)$$

where σ_c is the critical stress applied to the filament, K is the cohesive energy density and E is the Young's modulus of the fluid flow [17]. The point of break indicates the point where this critical stress reaches the value of the filament tensile strength [14]. In addition to leading to cohesive fracture, extensive strain can lead to structural disruptions of the polymer chain changing the characteristics of the

dope [15]. Hashim et al. also witnessed roughness on the filament surfaces due to excessively elevated speeds. At the same the outer diameter was affected as the molecules weren't appropriately relaxed. [25] This highlights the importance of the relaxation time to enhance the materials ability to behave like viscoelastic fluid and to avoid the fracture.

Ductile failure resembles the cohesive fracture as it is also caused by excessive force. The local stress results in a 100 % reduction in cross section of the filament. Rather than fracturing it [14, 28] With melt spinning it has been found that intermediate molecular weights are more likely to cause ductile failure when high molecular weight polymers are prone to cohesive break up [14].

Excessive thinning of a portion of filament without breaking can also cause a phenomena called draw resonance, where steady oscillation of the filament diameter occurs [14]. This often takes place when there are weaker defects in the structure. These portions are then excessively thinned as they are not capable of distributing the force evenly. This forms a cycle as then the following portion isn't stretched properly leaving it thicker and capable of transmitting the force upstream causing new over thinning to occur. This can cause filament break within few cycles. [28] The only reliable way to avoid this is to ensure homogenous composition of the dope [15, 14].

As the drawing applicable to the dope is one requirement for good spinnability the early spinnability studies were executed by pulling polymer fluid threads with a rod and observing maximum attainable draw lengths and draw velocities. [14] Contemporary similar studies can be performed with capillary breakup extensional rheometry [4, 17]. Furthermore, easier rheological measurements like the oscillatory measurement in combination with the results from practical spinning studies are more commonly used [28, 14]. The rheological parameters are then used to distinguish differences between the materials [31]. In this work the combination of practical spinnability observations are used with the oscillatory and flow measurements.

In the practical spinning studies, the spinnability is often considered to exhibit itself as increasing the maximum draw ratio attainable [17, 14]. Previously the effect of

different solvents on the dope has been tested by Hauru et al. [28]. The effect of weight fraction of the high molecular portion has been tested by Saastamoinen [14]. Liu et al. instead compared the effect of relaxation times both in the spinneret and in the air gap by increasing the L/D ratio and the air gap length. The result for this is shown in Figure 7 to highlight their importance. [17]

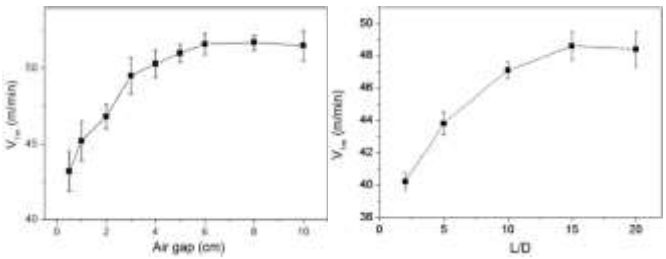

Figure 7. The effect of relaxation to the drawing a) the effect of air gap with 15 L/d ratio needle b) the effect of L/D ratio with 30 mm air gap [17].

As shown in Figure 7, the effect of the changed variable to the drawing is visible as indicated by the increasing curve. With the L/D ratio and air gap effect can also be seen that even though they have significant effect on the drawability they can only increase it to certain extent. With their dopes the air gap of 3 cm and L/D ratio of 15 were the start of a plateau after which they had barely any effect. The spinnability studies aren't restricted to drawability studies as other properties of the filament can also be compared. The enhancement of desirable properties can be taken as an indication of better spinnability. As the drawing affects the orientation thus the strength attainable in the product, the tensile properties of final fibers is one common qualification for spinnability. [17]

5 Material information

In this section the materials used in this work are further studied. The aim is to distinguish how cellulose nanofibers differentiate from other nanocellulose and how the manufacturing method also affects their properties. The matrix part concentrates on compatibility and interactions between the cellulose particles and the matrix forming portion. Also the basics for the matrix forming water soluble polymers PVA and guar are given and the reasons why they were chosen for this work. Also the previous filaments prepared from PVA and nanocellulose are discussed and the crosslinking ability of GA on PVA and cellulose is examined.

5.1 Cellulose

Cellulose is a typical biomass having a wide variety of uses. It can be used as gelling agent in cosmetics, coating in papermaking, nano reinforcements in polymer matrixes and adhesives or as rheology modifiers. [2, 11, 5] It's best properties are it's high surface area, low density, good mechanical strength, availability, biodegradability, nontoxic nature and reactive surface chemistry. [2, 11] And for nanomaterial's use as a reinforcement in addition to good orientation also a good dispersion and interfacial interactions and stress transfer with the matrix polymer are important. [10] Nanocellulose's properties affect how it behaves, especially the particle size and surface properties [27].

Nanocellulose can be defined to have at least one of its dimensions [5] or all at the nanometer scale [3]. In this work the previous definition is used. Due to their small size the nanoreinforced composites cannot be treated as a diphase system. Since the size of the particles are close to the size of the polymer macromolecules causing the distance between the particles to be relatively small. Thus the polymer-particle interactions also need to be extended over the whole volume. Strong interactions can cause particle aggregation that can be controlled with chemical surface modifications. [12, 13]

But strong interactions with the polymer can also enhance the mechanical strength also limiting the amount of reinforcement usable due to significant increase in viscosity [27]. For example hydrogen bonding is one strong interaction that can increase the compatibility with the polymer and increase the strength of the composite but can also lead to aggregation of the particles and decrease the stress-transfer efficiency. Chemical modifications reduce the amount of hydroxyl groups (-OH) on the particle surface decreasing it's effect on the rheology. [32, 27]

The dispersion stability of the cellulose particles is affected by the preparation method where different sizes, shapes and surface properties are possible. Spherical cellulose nanocrystals SCNCs and cellulose nanocrystals CNCs prepared by sulfuric acid or mixed acid hydrolysis (containing some sulfuric acid) lead to zeta-potential values of -30, 98 mV and -39,61 mV that are above the threshold value that forms a stable colloid (±30 mV). When the native cellulose has a value of – 15 mV. Which results in the CNF flocculating faster when the SCNCs

and CNCs formed dispersions that stayed stable longer. This difference comes from some of the hydroxyl groups being replaced by negatively charged sulfate groups. [27]

In addition the morphology of CNF is highly different to CNCs and SCNCs. This also has significant effect on the resulting product properties as it affects the rheological behavior of polymer-particle suspensions [27]. This is often studied by combing the effect of particle size and shape into aspect ratio (l/d) where the length (l) is divided by the diameter (d) of the particle. This can be further used to estimate the percolation threshold (ϕ_c) in Equation 10 for cylindrical nanoparticles. [6]

$$\phi_c = \frac{0,7}{l/\mathrm{d}} \tag{10}$$

This is similar to the entanglement degree studied in the fiber formers section. As the combination of dimensions and concentration eventually lead to the formation of a network structure. The percolation threshold solves the weight percentage needed of nanoparticles in a certain aspect ratio to form the 3D network. [6, 10] The formed network acts to hinder the chain mobility and has also been found to hinder a matrix polymer's degree of crystallinity [6].

Even though high aspect ratio decreases the matrix polymers crystallinity, CNFs have been found to exhibit stronger reinforcements in polymer matrix due to their significant aspect ratio and thus also higher percolation ability. This causes them to affect the mechanical properties of the composites more compared to low aspect ratio ones. [27] The networks formed with polymer by different aspect ratio cellulose nanoparticles are shown in Figure 8.

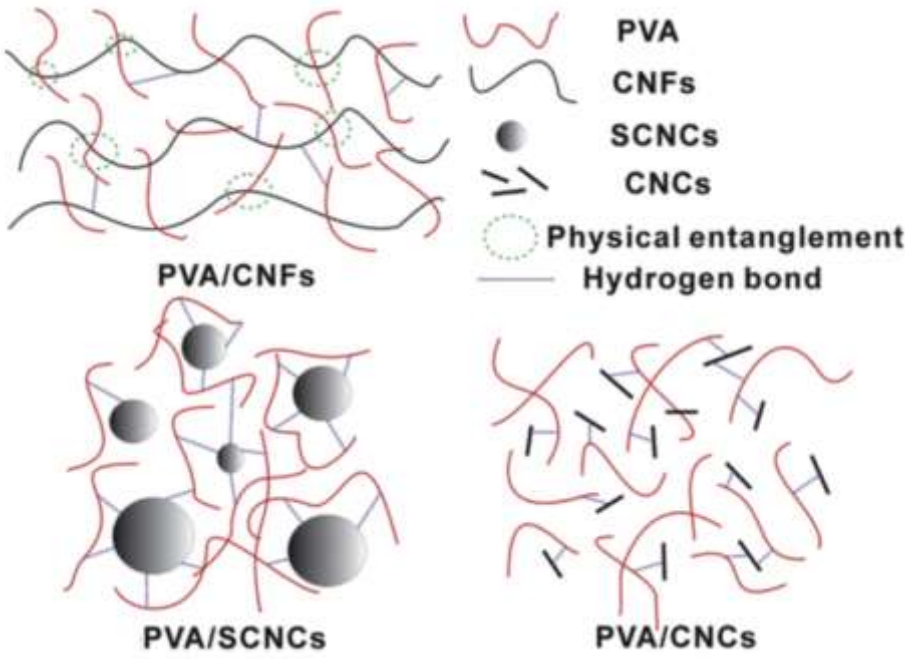

Figure 8.The networks of different nano celluloses with PVA matrix and the effective interactions [27].

The high flexibility of CNFs can be seen to further enhance the physical entanglements with the polymer. Where the flexibility arises from the combination of amorphous and crystalline regions in the structure. [27, 31] The CNCs instead are highly crystalline as the amorphous regions are removed [32]. Thus the CNCs have higher tensile modulus of 138 GPa when CNF only reaches values 10 – 35 GPa [6]. Even then the CNF have higher reinforcing effect due to the increased physical network formation. As with the CNCs the lower aspect ratio and higher crystallinity causes the 3D network to mainly rely on the hydrogen bonding, which is also hindered by replacing some of the hydroxyl groups with sulfate groups when processing with sulfuric acid. [27] There is also variation in the reinforcing ability of CNFs due to different manufacturing methods leading to differences in product properties [3].

The fibrillated celluloses are usually manufactured from wood pulps due to their availability [5]. The first microfibrillated cellulose materials were prepared purely by mechanical disintegration and the process was first enhanced by increasing the number of passes the mass was fed through the system [3]. The mechanical manufacturing methods are for example grinding, homogenization of microfluidization. The mechanical disintegration separates the microfibrils that

form the cell walls and this results into a viscous gel [5]. The extracted CNF are usually aqueous cellulosic suspensions (1 – 2 wt%) and are used as they are. Since further drying can promote irreversible agglomeration, known as hornification. [33]

The disintegration process can be further enhanced by incorporating chemical or enzymatic pretreatments. These ease the fibrillation by making the small fiber dimensions easier to reach, decreasing the energy consumption while also turning the process more environmentally friendly. [5, 2] This usually results into the nanofibrillated material to being more homogenous [5]. Even energy savings up to 91 % can be reached by incorporating the pretreatment methods [3].

Enzymatic pretreatment subjects the cellulosic fiber to a mild hydrolysis [2]. The enzymatic treatment is performed to the roughly mechanically treated slurry incubating at 50 °C [6]. Endoglucanase is one commonly used enzyme which is assumed to degrade the cellulose from the amorphous regions [5]. When chemical pretreatments used on CNF production are for example selective oxidation with 2,2,6,6-tetramethylpiperidinyl-1oxyl (TEMPO) and carboxymethylation [3, 5]. In the selective TEMPO-oxidation the radical catalyzes the process where surface hydroxyl groups (-OH) are modified into carboxylate groups ($-COO^-$) [2]. Carboxymethylation also introduces a charge to the fibers in a process including solvent exchange (water to ethanol), impregnation with monochloroacetic acid and addition of NaOH in methanol isopropanol mixture. With this method even one pass through a homogenizer can be enough to reach sufficient size and uniformity. [3]

These extraction processes lead to different morphology, DP, aspect ratio, physicochemical surface properties, like surface charge, and mechanical properties. All these affect their rheological behavior in an aqueous suspension. [2, 3] The mechanical treatment alone and combined with enzymatic pretreatment results into a more polydisperse suspensions of fibrillated materials than the chemical pretreatment methods. Where they contain both the micro- and nanoscale elements that are the partially fibrillated cellulose fibers and elementary fibrils or bundles of fibrils. They usually range in the size between 5 – 100 nm in width and 1 – 10 µm in length. When the chemical pretreatments can lead to 3 – 6

nm diameters with 1 – 2 µm lengths that are mostly individual fibrils but can contain some fibril bundles. [2]

The chemically pretreated CNFs are more transparent resulting from homogenous suspension forming due to the electrostatic repulsions of the anionically charged sodium carboxylate groups [2, 9]. They have a zeta potential of -50mV when the mechanically and enzymatically pretreated ones only have -15mV as those methods don't change the zeta potential of the cellulose. The low zeta potential of enzymatically and mechanically treated ones causes them to exhibit floc sizes of 50 – 100 µm and seem more opaque even at low loading levels. Even with these differences the CNFs prepared by different methods exhibit similar behaviors in flow rheology (yield, shear thinning, shear stress plateaus) that are studied further in the steady shear part of this literature review. [2]

5.2 Matrix

Due to the hydrophilic nature of cellulose, water-soluble polymers are the best candidates for preparing blends or composites, allowing easy dispersion and better compatibility. [6] The two main interactions would be physical entanglements and inter or intra hydrogen bonding [27]. The pronounced entanglements among CNFs increases the probability of polymer chains contacting and forming physical junctions with them [31].

Within potential polymer candidates for mixing with CNF, the low molecular weight ensures lower viscosities and easier orientation leading to higher crystallinity [21]. High polymer weights instead have led to better dispersions especially with graphene oxide nanoparticle containing systems affecting the dispersion and aggregation behavior of the nanoparticles [13]. The concentration has the opposite effect and high concentration has previously been found to lead to poor dispersion of CNFs due to strong interactions caused from excessive amount of hydroxyl groups. Which causes significant viscosity increase. Where in previous experiment the addition of CNF to 15 wt% PVA solution so that the CNF concentration was 0.45 wt% increased viscosity at 1 1/s strain from 0.145 to 1.897 Pas. [27]

The percolation tendency of CNF can be affected by the polymer where it can either favor or hinder its formation. The flexible chain structures are favoring due to them having higher adsorbed level on the particle surface compared to semi rigid ones. These adsorbed and non-adsorbed polymers chains affect the dispersion stability differently. The adsorbed ones have bridging effects promoting the formation of the percolation network allowing it to form at lower particle concentrations. The non-adsorbed chains instead have depleting effect where the polymers can have strong electrostatic repulsion that result in shielding effect increasing the percolation threshold. This causes the percolation structure to form later at higher loading levels. The effect that adsorbed and non-adsorbed polymers have on nanocrystalline cellulose (NCC) suspension network structure are shown in Figure 9. [11]

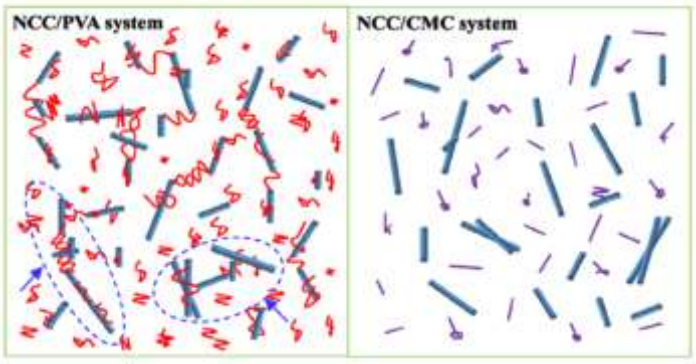

Figure 9. The effect of flexible poly(vinyl alcohol) and semi rigid carboxymethyl cellulose polymers on nanocrystalline cellulose dispersion state [11].

From the Figure 9 can be seen that the flexible chains significantly bind the NCC particles together. Whereas the semi rigid ones the polymer chains are dispersed with the NCC particles and don't exhibit physical entanglements. [11] Structural formation is often described through flocculation where first small clusters are formed and as the polymers further incorporate into the network structure a network spanning the whole sample is formed. This stage when the network reaches the whole material, can be detected from rheological data as the gel point. This is discussed more in the rheology part of this literature review. [34]

5.2.1 Poly(vinyl alcohol)

Poly(vinyl alcohol) (PVA) is a synthetic polymer that is highly hydrophilic and thus also water soluble. In addition it has a flexible chain structure, high crystallinity, non-toxic nature, is biocompatible, non-carcinogenic and environmentally friendly. [35, 10, 31, 11] With PVA the method of preparation with the hydroxyl group density are the main factors affecting its rheological properties. Due to significant amount of hydroxyl groups PVA can form chemically and/or physically crosslinked network structures. Crosslinking can happen by substituting the hydroxyl groups with acid or aldehyde groups. [31, 34] And due to it's highly hydrophilic nature the final product usually contains a significant amount of water [34]. The repeating unit of PVA is shown in Figure 10.

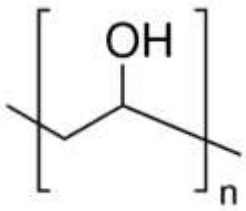

Figure 10. The repeating unit of poly(vinyl alcohol) [36].

PVA has broad range of possibilities among industrial and technical applications due to its nature. Filaments based on PVA are attractive choice in tissue scaffolding, filtration materials, membranes, optics, protective clothing, drug release and reinforcement for concrete and cement materials. [6, 10] In building materials it is especially desirable alternative for asbestos when resistance against earthquake is needed. In these materials it enhances the ductility, toughness and crack resistance [10]. PVA as reinforcement can also be used to reduce bulk weight [6]. Also in building materials the high resistance to alkaline environments and good adhesive strength of PVA are especially attractive [10].

Previously PVA has been used to spin reinforced filaments with both enzymatically [6, 8] and TEMPO-oxidized [9] CNFs and other cellulose nanoparticles like cellulose whiskers [10]. Where the PVA molecular weight varied between 66,000 to 195,000 g/mol and the used PVA concentration varied between 5 – 20 wt% [9, 6, 10, 8]. In addition PVA is used with CNF and other nanoparticles to form reinforced hydrogels. That have previously been crosslinked with glutaraldehyde and borax. [32, 31]

Some of the PVA cellulose filaments were spun from dopes heated to elevated temperatures of 75 °C [10] or 90 °C [9] when others didn't state the spinning temperature [6] or were spun at room temperature [8]. Those that stated spinning speed used 0,38 ml/min volumetric speed [10, 6]. And the inner diameters of the used needles ranged between 0.33 – 0.686 mm [6, 8]. These previous filaments were all gel spun and the wet spinning seemed to be the most favored method [6, 10] but also dry-jet-wet spinning [9] as well as dry spinning [8] were used. Basically any gel spinning method seems possible as long as the rheological properties/wet strength are favorable for the intended method and system parameters.

The coagulation baths used in the spinning systems were either cold methanol or ethanol. Temperatures of the baths ranging from 5 °C [9] to -15 – -20 °C [10, 6]. This could indicate that high viscosity increase in the coagulation bath is needed for filament formation. Which is further confirmed with the need to keep them immersed for 24 – 48 hours to extract water [6, 10]. But then again the dry-jet-wet spun prepared in the semi continuous process was allowed to be immersed for only 5 minutes before further processing by heat [9].

Some of these were subjected to wet drawing [9, 6] while others were just collected in the bath [10] and the one dry spun was attached to dry under tension [8]. Of the ones spun into baths, one of them were then only air dried [10] when most were also heat drawn [6, 9] or dried at oven to remove the water from the structure increasing the amount of hydrogen bonding [8]. Heat drawn were subjected to even 230 °C [9] when the one just oven dried was dried at 120 °C [8]. The ones subjected to both wet and hot drawing a total draw ratios of 20 – 27 were reached [6, 9].

5.2.2 Guar

Natural gums are polysaccharides able to induce significant increase to the solution viscosity already at small concentrations. They can be derived from plants or microbial sources and are classified according to the source. Guar gum is a seed gum as it is obtained from embryo of the seed where it is stored as a food reserve [37]. The plant Cyamopsis tetragonolobus from which guar is extracted is mainly grown in semi-arid regions of South Asia [38]. The natural gums are gaining

interest due to their abundance, non-toxicity, biodegradability, biocompatibility, renewability, and cheap price [4, 37].

More specifically guar is in the endosperm part of the seed accounting for 35 – 42 wt% of total mass of the seed. The extraction takes advantage of the difference in hardness of the various seed components in multistage grinding and sieving process. Guar is then commercially available in powder form which contains 75 – 86 % galactomannan, 8 – 14 % moisture, 5 – 6 % protein, 2 – 3 % fiber and 0.5 – 1 % ash in weight. [37] The name galactomannan comes from the mannan units of (1→4)-β-D-mannopyranosyl forming the backbone and the galactose units of α-D-galactopyranosyl attached by (1→6) linkages as the side chains. The ratio of mannose to galactose has been studied to be from 1.6:1 to 1.8:1. [37, 39] The structure is shown in Figure 11. Due to their natural origin the molecules show significant variation in length of the mannose back bone and the branching characteristics which affects the molecular weight. [37] The molecular weight can vary between 1000, 000 g/mol – 2000, 000 g/mol [39, 37]. The variation causes fluctuation in the solubility rate and viscosity from batch to batch [37].

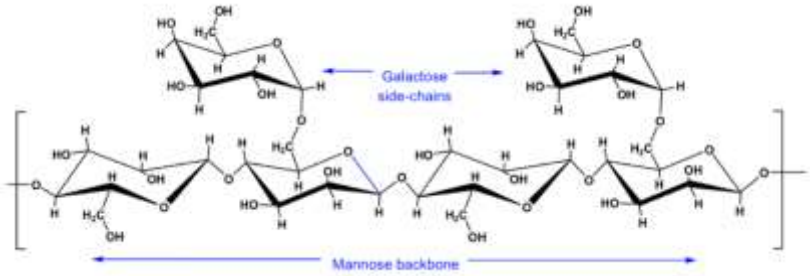

Figure 11. The structure of guar where the mannose backbone is the horizontal chain and the galactose units form small side chains [37].

Guar is water soluble and doesn't solvate to most organic solvents like hydrocarbons, alcohols, esters and ketones. The high molecular weight contributes to high viscosity but in addition the formation of hydrogen bonding and possibly even superstructures/aggregates in aqueous solutions lead into excellent water thickening and viscosity increasing properties. [39, 37] It is said to have even up to eight times the thickening capability compared to corn starch. [40] In addition guar doesn't require prolonged cooking like most other natural gums to reach the viscosity maximum. It can reach this even in cold water where its solvation is also

relatively fast. The aqueous solutions of guar are stable in wide pH range from 4 to 10.5 due to it's non-ionic nature. [37]

Guar is used in industry application as additives that are used to modify the rheology of structured and complex fluids [4]. As food additive Guar emulsifies, thickens, stabilizes and suspends many liquid-solid systems. It can prevent stratification of orange juice thus increase the shelf life of these products. These thickening and suspensing properties are also used in cosmetics. [37, 38] Guar can also act as a dispersant for organic systems due to its numerous hydroxyl groups enhancing the hydrogen bonding with other materials or as a coagulant for inorganic ones. In papermaking guar has been used to break up agglomerated cellulose pulp and disperse them forming uniform slurry simultaneously enhancing also other paper properties. [37] The high amount of hydroxyl groups also impart guar with strong water absorbing ability allowing it to retain large amount of water [38, 37]. The suspending properties can come in handy if there is difficulties keeping the dispersed state of cellulose nanofibers. Previous uses of Guar in gel spinning or spinning was not found.

5.2.3 Glutaraldehyde

Glutaraldehyde (GA) is a water soluble dialdehyde that is used for chemical crosslinking [19, 32]. But it can also solvate in ethanol [41]. It has two active sites which undergo intermolecular bonding with the material to be crosslinked forming a closed loop like structure [42]. The aldehyde groups of GA can react either with hydroxyl or amino functional groups of the material in the presence of strong acid [19, 32]. Previously HCl has been used to lower the pH of the solution to 2 for the crosslinking reaction [35]. At room temperature, the crosslinking reaction is quite slow taking up to even 24 hours [35] but faster at elevated temperatures taking only 390 – 430 s to reach the gel point at 50 °C in small sample studied in cone and plate geometry. Where it was dependent on the frequency value used [34]. The crosslinking reaction between PVA and GA is depicted in Figure 12.

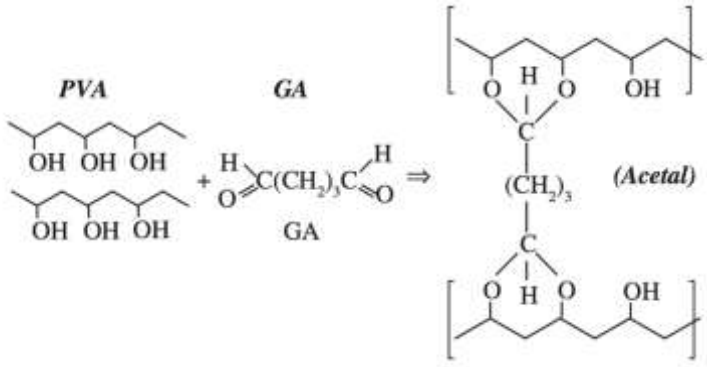

Figure 12. Crosslinking reaction between PVA and GA by formation of acetal linkage [35].

The effective molecular weight of the polymer is increased with crosslinking as it affects the polymer entanglements by forming intermolecular crosslinking [19]. More of how the covalent bonds act in comparison to normal chain entanglements is in the fiber formers section of this literature review. The structural formation starts as small clusters of molecules and the network slowly extends to span the whole sample. When it is extended to whole sample, the gel point can be observed from rheological data of storage and loss modulus. As networking further continues the molecules and particles are further incorporated to the formed network structure. [34] Tang et al. found out that the storage and loss modulus were not convenient parameters to observe the extent of crosslinking from as they were also dependent on the concentrations. The phase angle showing the relation of storage and loss modulus correlated better for determining appropriate crosslinking stage. As the phase angle decreased from 90° to 10° during crosslinking allowing the precise determination of processing window when the properties were desired. [19]

Chemical crosslinking is used to modify polymers especially to improve their mechanical properties and chemical and thermal stability [35]. The mechanical properties are already affected by increasing the relative molecular weight resulting from crosslinking the polymer but also by enforcing the interactions between polymer and reinforcing particles. This allows the stress to transfer from the matrix to the reinforcement. [32] As glutaraldehyde is able to crosslink the materials by their hydroxyl groups it is able to crosslink cellulose, PVA and guar [37, 32]. The crosslinking reactions can occur between any possible unique two material combinations resulting in six possible reactions with three materials. The covalent bonds formed are assumed to be vital for stress transfer at low nano-reinforcement

concentrations and in higher concentrations it is combined with effect from hydrogen bonding. [32]

As sometimes the applications of the polymer can be limited by its hydrophilic nature the chemical crosslinking can be used to improve it's stability. For example the stability in an aqueous media is increases as crosslinking decreases the solubility. [19, 35] This was studied by Tang et al. by electrospinning in situ crosslinked PVA/GA fibers. Where the stability was compared against the mole of GA to mole of PVA ratios. At low mole ratios (bellow 27:1) the spun fibers dissolved in water. With intermediate ratios (between 27:1 to 90:1) the fibers fused together when immersed. When high ratios (over 90:1) the fiber morphology was maintained in immersion but swelling was observed. At this ratio the wt% of GA to the mass of PVA was 7.09 and with the 127, 000 g/mol PVA this translates to 0.4963 wt% of total mass. [19] The wt% ratio of GA to dry mass could be used as a guideline in this work to ensure that enough crosslinker is used. Although as it can also solvate into ethanol it might be partially dissolved before all can react in crosslinking reaction.

6 Rheology

Rheological measurements can be used to determine a material's behavior during the spinning process. Basic phenomena can be identified, named and given reasons for their occurrence but the rheological requirements for the dope are harder to evaluate as they depend on the system and dope properties. [15] The rheology portion of this literature review is based on understanding the chosen materials in the view of rheology and identifying measurements that could have correlation to spinnability.

There are multiple types of fluids: pure substances, mixtures, dispersions and solutions. Each of these have a unique behavior when subjected to stress, which is the heart of rheological testing. Structured fluids like PVA solution with dispersed CNF has rheological behavior that is dominated by the interactions between the constituents. These kind of materials have complex rheological properties, where it's behavior is influenced by the viscosity of the liquid medium, the particle size,

shape, concentration and any forces between the particles and medium. [43] The rheology behavior can thus predict the properties and reveal dispersion microstructure [27].

In this work, the most relevant and interesting data relates to oscillatory and flow measurements. The oscillatory tests can be used to characterize the materials when the shear rate measurements predict the flow properties of the dopes. [43] Where the flow measurements are conducted by continuously rotating the measuring probe and oscillatory measurements are based on back and forth motion inducing the oscillation. The Figure 13 illustrates the difference between these rheological measurements and the two different modes of oscillatory measurements where either the amplitude or frequency is changed [44]

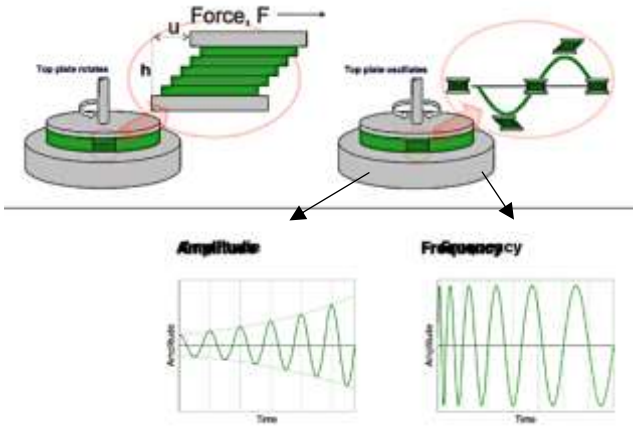

Figure 13. The difference between flow and oscillatory measurements and the two different oscillatory modes amplitude and frequency (modified from reference) [44].

Even though the rheological measurements affect the material differently they all work with the same basic parameters that are used to present the system by the shear stress (σ), shear strain (γ) and shear rate ($\dot{\gamma}$). These are used to describe the deformations the material is subjected to in the measurements and to calculate further material properties. Shear stress presents the force per area, while shear strain is the displacement of the material divided by its height and shear rate is the change in strain in time. These are shown in Figure 14 and given in Equations 11 – 13. [44]

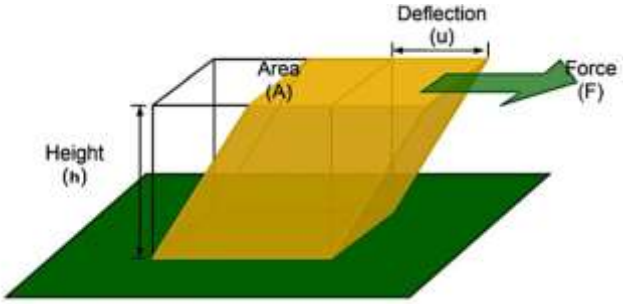

Figure 14. The basic forces applied to the material in rheological testing (modified from reference) [44].

$$\sigma = \frac{F}{A} \tag{11}$$

$$\gamma = \frac{u}{h} \tag{12}$$

$$\dot{\gamma} = \frac{d\gamma}{dt} \tag{13}$$

As the rheological measurements apply similar forces to the material the difference in the measurements arises from the various modes of applying the force as the materials response to them is different [44]. The stress, strain, and shear rate can then be used to further derive viscosity (η), storage modulus (G'), loss modulus (G'') and phase angle (δ). Of these storage modulus, loss modulus and phase angle are used in the oscillatory measurements (amplitude sweep and frequency sweep) and viscosity from the flow measurements. [44]

The viscosity (η) depicts a material's resistance to flow [44]. When the storage modulus (G') is the measure of stored energy or elasticity and loss modulus (G'') is the measure of dissipated energy in a material under deformation [45, 46]. Where the storage and loss modulus are the complete opposites to each other as the storage modulus indicates of materials ability to recover from deformation and loss modulus presents the portion attributed to viscous flow. As opposites their relation to each other can be used to estimate materials physical state. [27, 46] The phase angle (δ) is also indicative of the materials behavior. It is determined from the difference between applied and measured signal shown in Figure 15 depicting also the signals for purely elastic and viscous materials. The ways to determine the viscosity, storage and loss modulus are presented in Equations 14 – 16. from the previous parameters are shown [44]

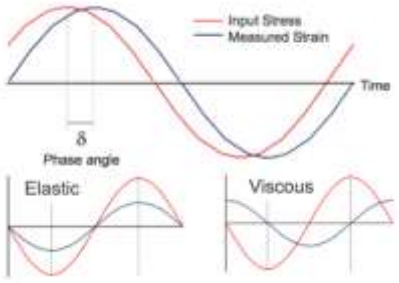

Figure 15. The applied signal and the resulting signal in determining the phase angle (δ) and examples of elastic and viscous signals (modified from reference) [44].

$$\eta = \frac{\sigma}{\dot{\gamma}} \tag{14}$$

$$G' = \frac{\sigma}{\gamma}\cos(\delta) \tag{15}$$

$$G'' = \frac{\sigma}{\gamma}\sin(\delta) \tag{16}$$

where viscosity (η) is a function of shear stress (σ) and shear rate ($\dot{\gamma}$), and storage and loss modulus are functions of shear stress and shear strain (γ) multiplied by trigonometric functions sine and cosine of the phase angle (δ). In the Figure 15 no lag between the input stress and measured strain signals ($\delta = 0°$) indicates of elastic material (solid) when ¼ of cycle (δ=90°) indicates of viscous material (liquid). [44] Most real materials exhibit both elastic and viscous nature at the same time ($0° < \delta < 90°$). This is called viscoelastic behavior and it is important for spinning as indicated in the spinnability in processing section of the literature review. [46, 44] Also previously in the Material information part for the Glutaraldehyde the phase angle has been used as an indication of crosslinking degree as the material changes from more viscous to more elastic behavior during the crosslinking [19]. The following subheadings dive into the amplitude and frequency sweep from the oscillatory and the steady shear from the flow measurements.

6.1 Amplitude sweep

Amplitude sweep, also known as strain sweep, is an oscillatory measurement where a material's response to a varied strain rate is measured. The strain (γ) is often varied from 0.01 to 100 % [31] or 0.1 to 1000 % [28, 27] with constant frequency value of 1 Hz for example [28, 31, 27, 12]. The major reason for executing amplitude sweep experiments is to determine the linear viscosity region (LVR) for samples. Inside this region the material's response to deformation is independent of the applied stress causing the material to behave like viscoelastic solid. [31] Operating inside this region allows the comparison of the relationships between the molecular structures and the viscoelastic behavior of the dopes. [47] Furthermore relationships between gel strength and amplitude sweep parameters have been proposed. [31, 28, 48, 49].

The range of the LVR is determined from the storage modulus values (G') [31]. As inside the LVR the storage modulus values are independent of the strain amplitude. This is why the deviation from constant G' value is the indication of the end of the LVR. Some define it as 5% deviation from the plateau values. [31] But the end of the LVR is considered ambiguous as the decline of storage modulus is gradual [28]. This decline in the storage modulus is also an indication of the decomposition of a material's internal structure. The strain value at which this occurs is often called either the terminal [12] or critical strain [31] and in this work the critical strain (γ_{crit}) is used.

The range of the LVR is dependent on the material's physical state. As the range gets shorter with increased solidity of the material [31]. Other parameters influencing this are temperature and frequency. Where increased temperature extends the LVR range while increased frequency shortens. [45] Inside the LVR region a strain value is chosen that is then used in the frequency sweep [31, 27, 12, 50]

In addition the LVR determination Hauru et al. have listed three simple ways of defining gel strength from an amplitude sweep experiment. The first is the stress value at the end of the LVR range when critical strain is reached. Second is the stress at the crossover point of the storage and loss moduli (gel point). And third

is the yield point defined as the maximum elastic stress the gel can endure. [28] Castro et al. have also identified the second and third methods as potential ways of defining the strength of soft solids. And indicated that both the second and third methods estimate the same yield stress. [49]

The first method which uses the critical strain from the LVR definition was deemed ambiguous by Hauru et al., which is due to the gradual decline of G' and the difficulty in determining the strain value [28]. Due to its definition as the end of the LVR it relates the gel strength to the start of decomposition of the specimen's internal structure. [12]

The second method that uses the stress value at the crossover of storage and loss moduli implies the point where the G' and G'' values are the same. [28]. The crossover is a point where elastic and viscous behaviors are at balance. This point acts as the transition point between the two behaviors. [46] This means that the internal structure of the material has already been partly broken down as the storage modulus is approaching the value loss modulus. There the material is no longer solid nor is it liquid yet, hence it is also referred to as the 'Gel point'. [43] However, this method is in accurate and can overestimate the gel strength by up to 40% [28].

The third method used by Hauru et al. [28], Castoro et al. [49] and Yang et al. [48] used the storage modulus and strain values to find the maximum value that indicated the yield stress (σ_y). Where the maximum from Equation 17 of the in-phase stress component presents the yield stress value. This method when used with plate rheometer can underestimate the yield stress if grip between sample and instrument is insufficient. Also its usefulness is hindered by facture issues but is used due to fast measuring and low sample amounts. [49]

$$\sigma_y = \max(G'\gamma) \tag{17}$$

where G' is the storage modulus and γ is strain. The importance of yield was further discussed in the shear rheology section of this literature review. This method of defining yield stress has previously been used for soft solids [49, 28]. Hauru et al. used it to compare the spinnability of cellulose from ionic liquids. In their studies they estimated the gel strength reached in different IL solutions with addition of

weighted amount of water in the mixture. This was then related to fiber hardening in coagulation bath. The higher gel strength indicated better hardening of the core of the filament stabilizing the spin line from inside leading into better spinnability. [28] With the gel spinning in this work the gel strength could indicate better wet strength overall in the spinning process allowing higher air gap and more stable spinning process even when no drawing is subjected to the filaments.

6.2 Frequency sweep

Frequency sweep is also an oscillatory measurement which is the opposite to amplitude sweep as there the strain is kept constant and the frequency is varied. Frequency is presented as angular frequency either as 1/s [11, 34, 50] or rad/s [13, 4, 27, 31]. The frequency is usually varied from 0,01 or 0,1 to 100 Hz [11, 34, 50, 13, 4, 27, 31]. Frequency sweep results are used to understand the viscoelastic properties of the material. For example it has been used to determine the effect of different kinds of cellulose nanoparticles on hydrogels. It can also be used to estimate the dominating behavior (elastic or viscous), entanglement degree, strength of hydrogel and relaxation times. [31]

The G' and G'' values are used to estimate a specimen's dominating behavior at different frequency values [27]. The polymer-based solutions usually change from liquid like to solid like when the frequency is increased. In relation to G' and G'' this translates to the G' first exhibiting smaller values than the G'' and with the increase of frequency the G' increases to higher value compared to G''. Where the G'<G'' indicates that the liquid behavior is dominant in that region whereas G'=G'' indicated the cross over, also called gel point. [27, 31] This is because it indicates the entanglement of polymer chains that causes the formation of an elastic network as previously indicated in the the glutaraldehyde part under material information. After which the G'>G'' indicates that the solid like behavior is dominant. And the G' is then increased until a plateau is reached that is indicative of the entanglement density through the rubber elasticity theories. Where the crosslinking density should follow the G' order of magnitude. [31]

It is also possible that material only exhibits one dominant behavior in the frequency range if it lacks the gel point in that region. [31] In cellulose suspensions

the high particle loading can cause the crossover point to shift to values lower than the testing region. [11] This effect of particle loading causes a network formation [27]. Where the elastic behavior is attributed to the percolation of particles in the solution which were studied in matrix and cellulose parts under the material information section of this literature review. There the flexible chains adsorbing on the surface, strong surface interactions and increasing the particle dimension were the enhancing properties. [11]

The relation of G' and G'' at the frequency value of 0 Hz and the observed changes in δ can also be used to classify the material into three general behaviors. The G'>G'' and increasing δ over the frequency range indicates of viscoelastic solid. Gels instead have G'>G'' and δ is independent of frequency staying constant over the whole range. For viscoelastic liquids the G'<G'' and the phase angle is descending. These are shown in Figure 16. [44]

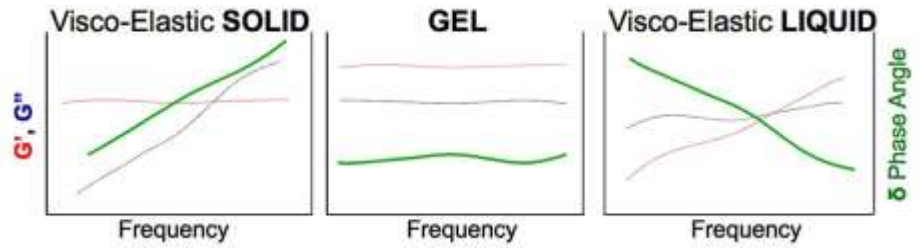

Figure 16. The classification into solid, gel and liquid through frequency sweep results (modified from reference) [44].

The solid samples are thus broken with the increase of frequency and the liquids are turned solid as the network acts as a solid under higher disruption. The gels instead have a sample spanning network resembling a solid but are not broken under increasing frequency. The dominating behavior of the material can also be examined with the use of loss tangent ($\tan\delta$). Which compares the individual points of G' and G'' values and the dominating behavior can be seen from the result. As the material is liquid like if $\tan\delta$>1 and the cross over point can be found from $\tan\delta$ =1 and at values $\tan\delta$ <1 it is solid like. [27, 31] Where $\tan\delta$ is also said to represents the ratio of dissipated energy to stored energy during the stress deformation and it is shown in Equation 18 [31].

$$\tan\delta = \frac{G''}{G'} \quad (18)$$

In frequency sweep the sample can also turn from solid-like behavior back into fluid-like with increasing frequency. In CNF containing suspensions this can occur due to the structure resisting the low oscillation and retaining solid/gel-like behavior. This resisting behavior from entanglements and hydrogen bonding is then lost as the frequency is increased and the relaxation time is shortened. Then the shorter relaxation time no longer promotes the re-arrangement of the entanglements and hydrogen bonds. The higher CNF ratio has previously been found to shift this transition frequency to higher values also yielding tighter structure. [27]

Also the complex modulus G^* utilizes the relation of the G' and G'' combining the two different material behaviors into one. Thus it is the measure of materials soft solid structures, the rigidity when it is exposed to stresses inside the LVR region. It is also said to be the indicator of visible attributes like flexibility or stiffness [46]. The higher this stiffness, the tougher the material and thus it should be similarly usable as the gel strength from amplitude sweep [44]. It is calculated from storage and loss modules shown in Equation 19. The complex modulus instead can be used to calculate the complex viscosity and to plot complex viscosity shear profiles from frequency data that could be used to estimate the flow curve with the Cox-Merz relation shown in Equation 20. [31, 14, 4]

$$G^* = \sqrt{G'^2 + G''^2} \tag{19}$$

$$\eta^* = \frac{G^*}{w} \tag{20}$$

where G^* is complex modulus, G' storage modulus, G'' loss modulus, η^* complex viscosity, w frequency. Complex modulus, complex viscosity and loss tangent have also been found to estimate hydrogel properties by Han et al.. They found that samples with highest G^*, η^* and smallest $\tan\delta$ within the whole frequency range were the indication that the sample was the strongest and most elastic hydrogel among the samples. These properties allowed the sample to withstand more deformation without damage. Thus the sample exhibited highest elasticity and flexibility with outstanding damage-tolerance and efficiently dissipated energy. [31] Considering filament formation there might be a degree to which this could be

beneficial but extensive amount could prevent the structure formation in the filaments by not allowing the sliding of polymer chains in relation to each other.

Han et al. also utilized relaxation times in the characterization of hydrogels. Predicting with Chompff-Duiser theory and modified Rouse theory that the relaxation spectrum would show the maximum of entanglement slipping mechanism. They used the dynamic relaxation time (t_{dyn}) related to the crossover point and the longest relaxation time (t_{long}) related to frequency at G'' maximum value. The relationships between the gel point and G'' max values to the aforementioned relaxation times are presented in Equations 21 and 22. [31]

$$t_{dyn} = \frac{1}{w_c} \tag{21}$$

$$t_{long} = \frac{1}{w_m} \tag{22}$$

where w_{cros} is the frequency at storage and loss moduli crossover (G'=G'') and w_m is the frequency value at the maximum value of loss modulus [31]. The (t_{dyn}) is connected to the longer lifetime of the entanglements or crosslinks under physical forces. Often caused by denser polymer entanglements or higher crosslink density. Therefore increasing this value acts to reduce the speed of shear-induced rearrangement occurring and dissociation of the crosslinks under oscillatory shear. Where higher t_{dyn} value (t_{dyn}>10) allowed the sample to be molded while lower values (t_{dyn}=0,34) were not moldable. The t_{long} was instead described as the time for macromolecules to disentangle from neighboring polymer chains. [31] Where high value in t_{dyn} could be beneficial for the formation of filaments allowing it to take the shape of the capillary as spun. When the t_{long} instead needs to be high enough for the polymers initially to form filaments.

6.3 Steady shear measurement

Unlike the oscillatory measurements the shear measurements study the flow properties of materials as viscosity against the shear rate. Shear rate represents the velocity gradient in the direction of shear flow quantifying the speed of shear flow resulting form the application of shear stress. [43] The steady shear is often measured across a wide shear range from 0.1 to 100 or 1000 1/s [27, 4, 34] The

steady state, unlike in the sweep measurements, the individual measurements points are extended until a constant value is reached or specified time to find the constant value has been used. This makes it a slow measurement as the points where the values are not constantly experiencing change and are not influenced by stress or rate are measured. [45] The steady shear measurements can be used to determine the network properties of the material and gives important information about its performance in processing as it measures the flow behavior [27, 43].

The flow behavior of the material in the low shear rate region is related to storage behavior and dispersion stability [51, 43]. This is because within dispersions, an elevated zero shear viscosity can be vital for inhibiting the sedimentation. Thus it attributes to suspension and emulsion stability. [51, 46] This is due to the amount of chain entanglements increasing with increasing molecular weight and the entanglements then act to oppose the dislocation [15, 29]. This could allow some comparison of effective molecular weight with samples having the same concentration.

In the flow curve the zero shear is the viscosity value corresponding to the lowest reachable shear value. Thus presenting the closest approximation for the viscosity value for material at rest. [46] The materials that have zero shear viscosity flow instantly when stress is applied [43]. In addition there are fluids that don't flow at rest and require a critical level of stress to initiate the flow. The material behaves like solid absorbing the stress and opposing the deformation if the value is insufficient to induce the flow. So instead of zero shear they have yield stress [43].

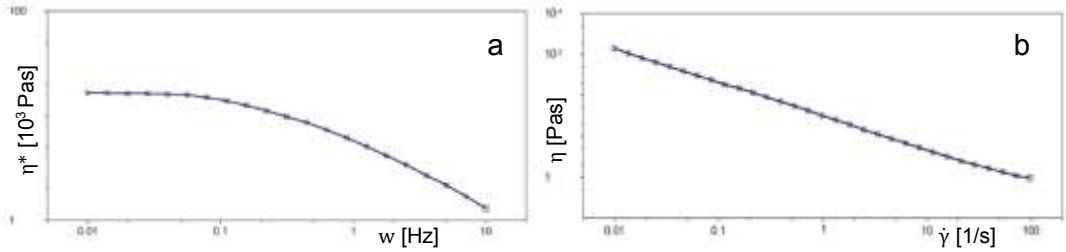

Figure 17.Two different low shear behaviors a) zero shear where the material flows at rest and b) yield stress before flow is initiated (modified from reference) [44].

A material exhibiting yield can easily be stretched until the yield point, indicating the transition from solid to liquid [44]. High concentrations can lead to the disappearance of the low shear rate viscosity completely due to increasing the

yield stress so that it can only be reached at high shear rates [43]. Previously CNF suspension were found to have yield stress at low concentrations of even 0.25 and 2 wt% [2, 27]. The zero shear combined with shear thinning behavior results in pseudoplastic flow. Whereas the material with yield stress and shear thinning is considered as plastic flow. [43] The shear thinning flow is only one of three flow modes possible in the whole flow region. These are: shear thinning, Newtonian and shear thickening flow. Of these the Newtonian flow is the simplest having a constant viscosity profile over the shear rates. The shear thinning and thickening ones are affected by the shear rate. Shear thinning indicates that the viscosity decreases whereas the shear thickening causes an increase in viscosity. Thus the shear thinning gives in to the flow and shear thickening opposes the change. And these flow behaviors are presented in Figure 18. [44]

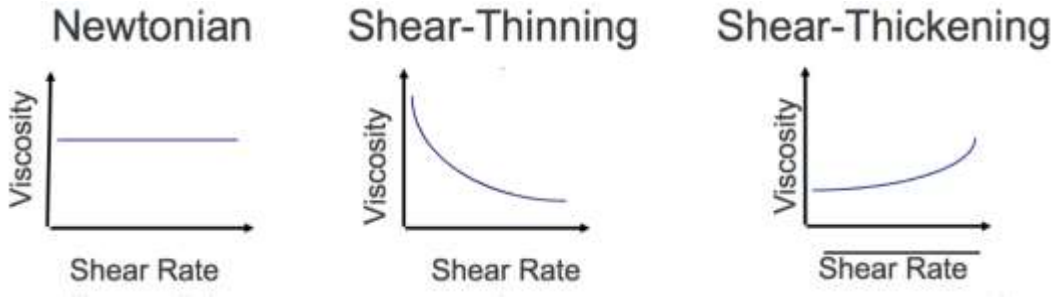

Figure 18. The basic flow modes and their viscosity profiles (modified from reference) [44].

Of the materials used in this work the PVA exhibits Newtonian flow in 5 to 15 wt% solution when Guar and CNF both exhibit shear thinning flow [37, 27, 30]. Most real liquids exhibit combinations of different flow behaviors [44]. Thus before comparing the viscosity of two samples wider portion of flow curve needs to be studied [46, 15]. For example with pure CNF suspensions Zhou et al. identified four characteristic regions from the flow curve; two shear thinning regions (regions 1 and 3) and two Newtonian plateaus (regions 2 and 4) shown in Figure 19. Similar to CNF suspensions, the same behavior was found with composites. The low molecular weight polymers exhibited this behavior visibly but the high molecular weight polymers diminished the effect and the plateau regions were less obvious or could be completely eliminated. [13].

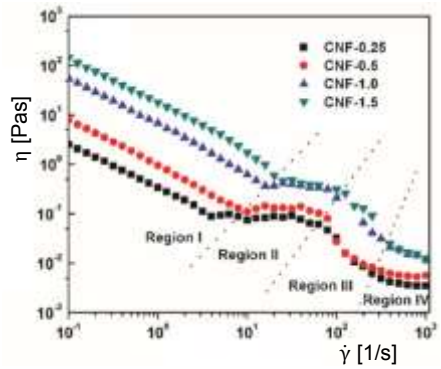

Figure 19. The shear behaviour of CNF suspensions [27].

The shear thinning regions are where the orientation occurs [27]. Increased concentration of CNFs intensifies the shear thinning behavior due to causing decreased molecular mobility [27, 43, 30]. And as the shear thinning occurs due to increasing orientation in the material it approaches a constant value corresponding to a completely oriented state [30, 15]. Within the plateau regions a temporary entangled network with hydrogen bonding and Van der Waals interactions forms. These temporary networks are able to retain the viscosity value constant over narrow shear rate region or they can also increase the viscosity momentarily. [27] With the Newtonian plateaus the CNF concentration was found to affect their starting point, since as in lower concentrations, the orientation is reached in lower shear rates. [27] The overall differences in the shear rates are connected to structural differences in the material arising from the inner network [43, 27].

The shear thinning behavior can result in fiber quality fluctuations as it is highly dependent of the shear rate in the beginning of the flow curve. For stable spinning, a region where the viscosity is relatively stable should be favored. [30] The shear thinning behavior of material in the shear measurement can be further studied with the Ostwald-de Waele power law shown in Equation 23 that can be used to model the shear dependent viscosity [52, 30].

$$\eta = k\dot{\gamma}^{n-1} \tag{23}$$

where the apparent viscosity (η) as it is often called with shear measurements can be calculated with the constant value (k), power law index (n) and the shear rate ($\dot{\gamma}$). There k is the measure of the fluids consistency and higher value indicates higher apparent viscosity, while n is a degree of non-Newtonian behavior. [52] The n value indicates which of the three behaviors is present. When $n<1$ indicates

shear thinning where the degree of shear thinning increases with lowering n value. The n=1 instead indicates Newtonian flow and n>1 is shear thickening. The power law index also allows the estimation of the shear rate at capillary wall. The Equation 2 which estimates the shear rate at wall for the Newtonian fluid can be corrected to work with non-Newtonian liquids as well shown in Equation 24. [24]

$$\dot{y}_{wall} = \left(\frac{4Q}{\pi R^3}\right)\left(\frac{\frac{1}{n}+3}{4}\right) \quad (24)$$

where Q is the flow rate, R is the radius and n is the power law index. The shear rate during the spinning is expected to be in the higher shear rate region. With a dissolved cellulose system it was over 100 1/s. The high shear rate leads to improved product quality due to the viscosity not being so sensitive in that region. Whereas excessive shear can only increase energy consumption. [30] Using these equations and solving the shear in the capillary and comparing that to the flow curve could estimate how stable the spinning is.

EXPERIMENTAL PART:

The goal of the experimental section was to correlate dope/filament properties to the results with spinnability. The matrix to CNF ratio of PVA/CNF based filaments were kept at a 1:1 ratio. The effects of wt%, glutaraldehyde, guar and pH in the dope and in coagulation bath were the properties which effect on spinnability was observed. Rheological measurements listed in the literature review were used to determine the properties of the dopes that most affected the spinnability while also trying to detect if crosslinking by GA was possible. These observed trends were then correlated to the actual spinnability and the tests adapted from the spinnability section of the literature review and the tensile properties of the resulting filament. In addition the crosslinking was studied by IR spectrometry and ^{13}C NMR measurements as well as the tensile properties.

7 Raw materials

Poly(vinyl alcohol) (Mowiol 56-98, M_w ~195,000 g/mol, guar, glutaraldehyde (50 % wt) were obtained from Sigma Aldrich. Hydrochloric acid (HCl, 32 % wt) was obtained from Fluka and technical grade ethanol was purchased from Altia. To ensure the same thermal history to all dopes, PVA and guar were dissolved in similar conditions. Solutions of 4 wt% PVA and 3 wt% PVA with 1 wt% of guar was dissolved in milliQwater in a water bath of 90 – 95 °C for 1.5 hours at 250 rpm mixing speed with a magnetic mixer. HCl was diluted to 5M concentration for use in acidic coagulation bath and 1M for lowering the dope pH. Glutaraldehyde was diluted to concentration of 5M for it's use in dopes as crosslinking agent.

Cellulose was provided by UPM and it was mechanically disintegrated by passing it 6 times through fluidizer. The CNF was used in its initial concentration and dried to over 4 wt% for preparing the more concentrated samples. This drying was performed in a 60 °C oven. The dry weights for these raw material solutions are presented in Appendix 1. Bellow in Figure 20 the CNF composition is observed with SEM imagining from 0.5 wt% solution dried up into a film.

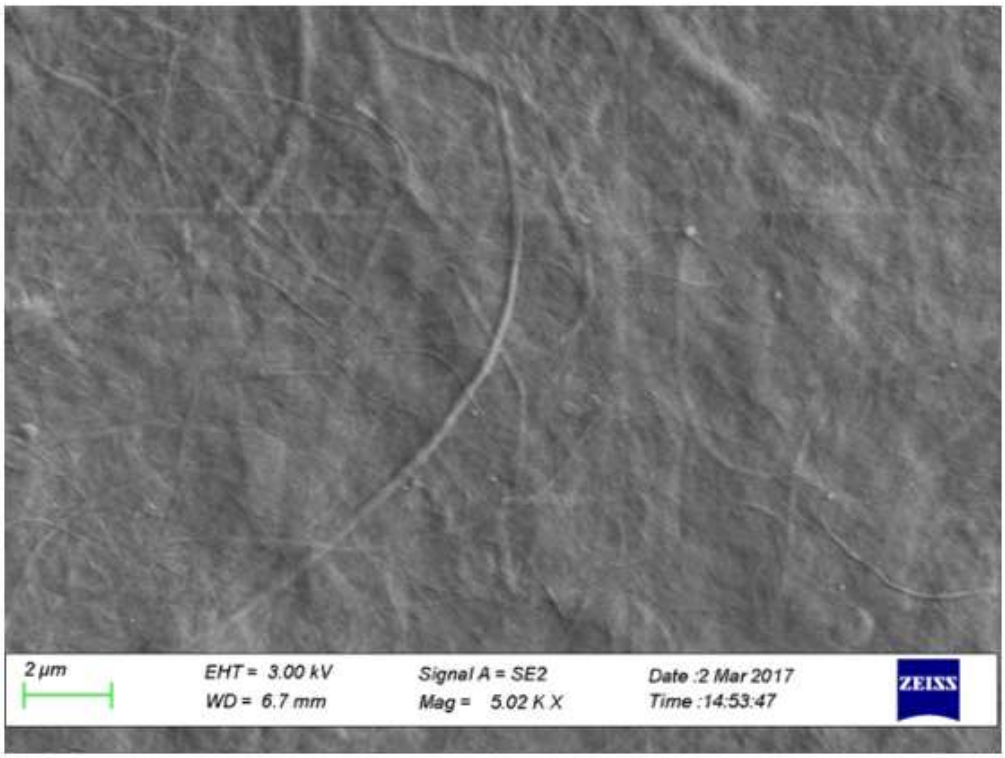

Figure 20. SEM image of CNF fibers at 5K magnification.

The Figure 20 cannot be used to accurately estimate the CNF sizes. This is because from SEM image cannot be seen whether they are formed of single fibers of bunch of fibers agglomerated together like in TEM image of Zhou et al. [27]. The visible sizes seem to wary between 2 – 15 µm in length and 0.05 to 0.2 µm in diameter. This is close to the approximation given for the mechanically and enzymatically treated ones in the material information portion of this literature review. Where they were estimated to range between 1 – 10 µm in length and 5 – 100 nm in width. Due to the possible overestimation of the fiber diameters the aspect ratios of the fibers/fiber bundles in the used solution could be even 50 – 100. Thus estimating the percolation threshold using the Equation 10 would indicate that 3D network for these would form at concentration range of 0.7 – 1.4 wt%

8 Dope preparation

The dopes were prepared in 2 and 4 wt% solid contents by mixing specific amounts of previously prepared polymer solutions with dried or undried cellulose. The concentrations were corrected to desired values by milliQwater. The aforementioned low concentrations were chosen due to using higher molecular weights and aspect ratios with increased CNF concentrations compared to previous filaments [6, 8, 9, 10]. And these concentrations still yielded dopes that were possible to mix by hand in 10 minutes. Thus allowing the GA and HCl to be incorporated relatively fast avoiding long processing times before rheological testing and spinning could be performed.

Dope sets containing only PVA solution and CNFs were used as the baseline. These were named PVA2 and PVA4 dopes. The GA dopes were similarly prepared from PVA solution and CNF by adding 10 wt% of GA compared to the PVA/CNF dry weight. The GA+acid dopes also had the same base as GA dopes but some acid was used to adjust the pH to value of pH 2. The Guar dopes were prepared from the polymer mixture of PVA and Guar. The GA and acid used in the dopes were incorporated just before the measurements and spinning. In the Table 1 is the afore mentioned dope compositions presented as wt% to the total mass of the dope.

Table 1. Summary of dope compositions.

	PVA4 [wt%]	Guar [wt%]	cellulose [wt%]	GA [wt%]	pH
PVA2	1	---	1	---	---
GA2	1	---	1	0.2	---
Guar2	0.75	0.25	1	---	---
Ga+acid2	1	---	1	0.2	2
PVA4	2	---	2	---	---
GA4	2	---	2	0.4	---
Guar4	1.5	0.5	2	---	---
GA+acid4	2	---	2	0.4	2

The specific data for the dope contents is in Appendix 2. These dopes were prepared in advance before their use. During this time the cellulose-polymer samples had time to equilibrate their physical networks and form hydrogen bonds.

9 Characterization

9.1 Rheological measurements

Rheological measurements were conducted to determine the properties and differences between the dopes. These measurements were performed with a Physica MCR 301 rheometer from Anton Paar with a CP25-2/TG cone that had diameter of 24.967 mm and angle of 1.998° and 0.049 µm trunctuation. Testing methods used were stability test, amplitude sweep, frequency sweep and steady shear. Where all methods were used to determine trends correlating to better spinnability.

Material stability was assessed from oscillatory measurement where strain and frequency values were kept constant for 20 minutes. The strain value was kept as 1 % and frequency value was 1 1/s across the measurement range where the measurement interval was 60 second. This was used to determine if the ones with GA and especially the ones also containing HCl showed signs of crosslinking.

Amplitude sweep was run over the range of 0.01 – 1000 % with 1 1/s frequency. The data was recorded on logarithmical scale with 6 points per decade slope. This deformation data was used to determine the LVR and gel strength.

Frequency sweep was executed over the range of 0.1 – 500 1/s with 1 % strain. The data was recorded similarly on logarithmical scale with 6 points per decade slope. The data was then used to define the materials behavior and strength.

Steady shear was measured from the range of 0.1 – 1000 shear rate on a logarithmical scale with 20 points per decade using the steady shear rate algorithm in Rheoplus software for the measurement. This flow data was used to estimate the inner structure of the materials and the actual shear they experience in the spinning and thus the effect of orientation

For all rheological measurements the samples were loaded and then the gap was decreased to 0.059 µm for trimming. After that optically clear silicon oil was added and the cone was lowered to 0.049 µm. These samples were then let to equilibrate at 25 °C for 10 minutes before measurement.

9.2 Spinning tests

Spinning of the dopes was performed with a customized setup including syringe, syringe pump and a needle acting as the nozzle. Where the syringe was 2ml (3ml HSW Norm-JECT – 2-part disposable luer [53] and it was fitted into an in-house built compression based syringe pump. The needles used were 18G 400 mm from Terumo [54] 20G 70 mm from Braun [55]. As these had long bevel they were cut in-house to blunt needles in the lengths of 1.8 and 2.6 cm. The needles used and their naming is shown in Table 2.

Table 2. Summary of the used needles and their dimensions.

needle	gauge	diameter [mm]	length [cm]
thin	G20	0.9	2.6
normal	G18	1.2	2.6
short	G18	1.2	1.8

Filament spinning and spinnability tests were performed at a velocity of 0.4 ml/min into a coagulation bath held at room temperature. The coagulation bath was either pure technical ethanol or technical ethanol adjusted to pH 1 – 2 with HCl. PVA samples were spun into both neutral and acidic baths whereas the Guar and Ga+acid samples were spun to neutral baths and GA samples were spun to acidic baths. These spun filaments were then immersed in the baths for 24 hours. The spinning was done from zero air gap. When in the spinnability tests inspired by the spinnability in processing section of this literature review were conducted from infinite air gap and finding the maximum air gap possible.

The *breaking mass* was used as an indication of the force the filament could endure inspired by the ductile and cohesive failure modes. Where the breaking mass could indicate of the maximum force the filament could carry. For this a set of six samples containing a minimum of 40 droplets were collected to minimize the effect of air bubbles causing filament breaks.

As the maximum *air gap height* has been previously connected to better spinnability at least with drawing, it was also tried to estimate [17]. This was measured as the distance of the coagulation bath from the needle tip that still led to the filament connecting with the bath before it broke off. And due to the interference from the bubbles the maximum height was the one where this occurred couple times within 1 minute.

The *spinning quality* was assessed from the spinning with the "normal" needle (G18 in the length of 2.6 cm) for the ease of spinning and wet quality. Where the wet quality consisted of visual evaluation and the ease of pulling them out of the coagulation bath and laying them to dry on a polypropene film as they indicate of the wet strength of the filaments [56]. The visually evaluation of the filaments was performed with *optical microscopy* with an Olympus BH-2 optical microscope equipped with NeoSPlan 5 NIC 0.13 (∞/-f=180) lens and a Nikon Coolpix 990 camera.

9.3 Filament evaluations

The final filaments were tested for tensile strength which combined with SEM imagining worked as the quality observations thus were related to spinnability. When also basic water stability was tested. In addition the successfulness of glutaraldehyde crosslinking was examined with IR and ^{13}C NMR.

Freeze dried samples were also used in *SEM imaging* to get a better picture of the surface smoothness of the dried filaments. The SEM imagining was performed with a Zeiss SIGMA VP scanning electron microscope. The samples were coated with 4 nm layer of gold palladium prior to imagining. An acceleration voltage of 3 kV was used with detector that allowed shadows for understanding of the shape.

Water stability of the filaments was tested from air-dried filaments by visually observing changes during 48 hour immersion in milliQwater.

The *tensile testing* was performed with an Instron universal testing equipment 33R4204 equipped with 100N load cell. The used gauge length of 2.5 mm and extension rate of 0.254 mm/min was used for tensile testing. The filaments were subjected to 50 % relative humidity and 25 °C for four days prior to measurements. Then ten parallel measurements were done trying to avoid the end of the filaments and parts that had more imperfections. *The Young's modulus and maximum tensile stress* were measured with the expectation of round cross section.

For the detection of crosslinking and *IR and ^{13}C NMR* measurements were used. The IR measurements were performed with a Unicam Mattson 3000 FTIR spectrometer that was equipped with PIKE Technologies GLadiATR that had diamond crystal plate. The spectra were scanned within the range of 400 – 4000 cm^{-1} with the total of 16 scans carried out and resolution of 32 cm^{-1}. This gives indication if there is any crosslinking on the surface. Whereas the ^{13}C NMR gives better image if there is any crosslinking in the whole structure. The ^{13}C NMR spectra was measured with a Bruker AVANCE-III 400 MHz spectrometer was used to operating at 100.6 MHZ for ^{13}C used with spinning speed of 8000 HZ and contact time of 2 ms and delay between pulses 5 s. The samples were first freeze-dried and cut small prior to analysis.

10 Results and discussion

During the mixing some bubbles were entrapped in the dopes due to high surface tension. And they were not able to be removed as sonification bath was found not to affect the amount of bubbles when used in low temperatures for avoiding possible crosslinking. This can be expected to affect the spinning process negatively. The dopes are presented in Figure 21 as thin layers of approximately 2.5 mm. From where the relative amounts of bubbles can be estimated.

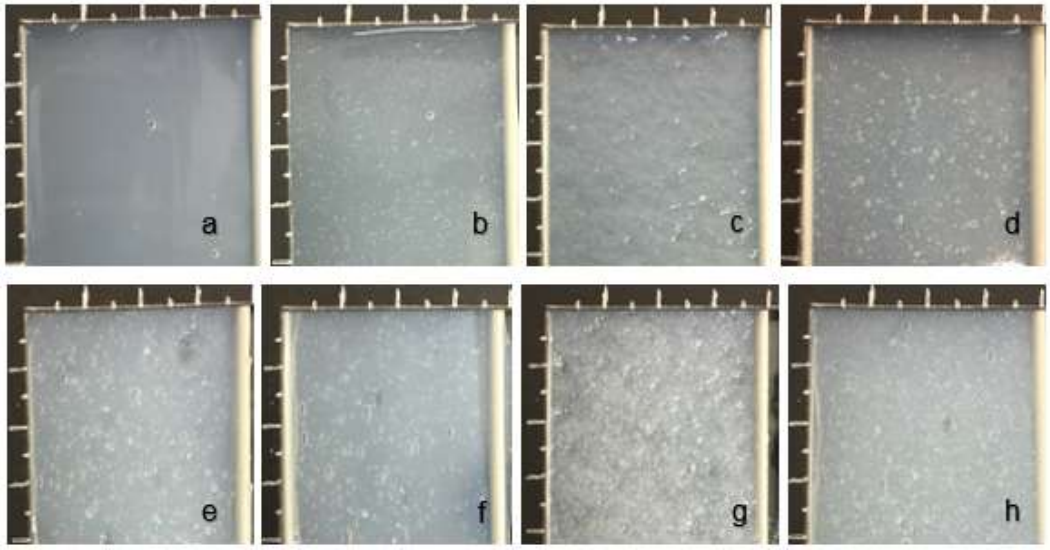

Figure 21 The dopes made into a thin layers a) PVA2, b) GA2, c) Guar2, d) GA+acid2, e) PVA4, f) GA4, g) Guar4 and h) GA+acid4.

From the figure can be seen that the 2 wt% dopes had less bubbles and the bubble size seems to be larger with the 4 wt% ones. Of the samples the PVA2 was clearly the best having least bubbles. The Guar dopes instead exhibited an uneven surface in addition to the bubbles when all the others exhibited smooth surface. Whereas the GA+acid exhibited thickening when the acid was incorporated into the structure.

In the ***stability test*** visually the samples were relatively stable in the logarithmical scale. There most significant value change was visible in storage modulus and the initial and value change are presented in Table 3. Also the phase angle was studied as it has been previously used to detect crosslinking explained in the material part for glutaraldehyde. The GA containing dopes were compared to the other ones to see if any crosslinking occurred. The phase angle values during the 20 minute testing time (t) for stability test in room temperature are shown in Figure 22.

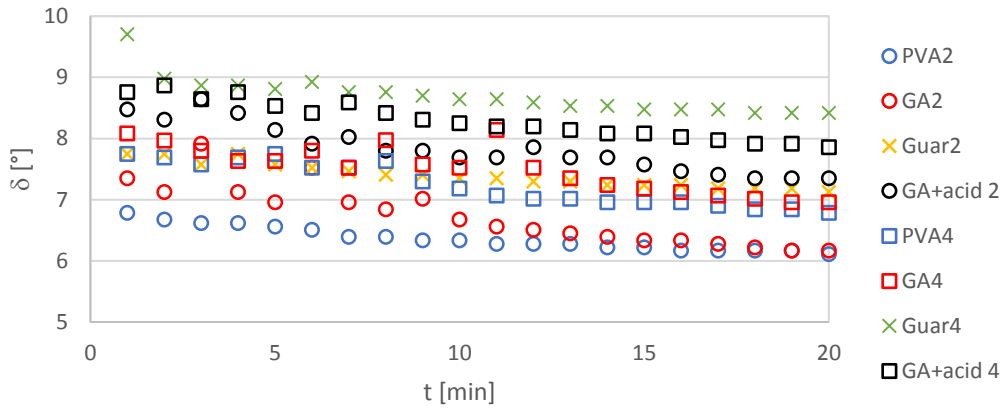

Figure 22. The phase angle values over the 20 minute stability test.

Table 3. The variation in storage modulus values.

dope	storage modulus		
	initial value	change	[%]
PVA2	97.4	+8.6	8.1
GA2	109	+25	18.7
Guar2	853	+29	6.1
GA+acid 2	1180	+153	15.1
PVA4	448	+110	11.4
GA4	1490	+170	12.6
Guar4	857	+150	9.1
GA+acid 4	2820	+170	5.7

From the Figure 22 it is obvious that some change in the values of phase angles occurs although overall they seem to be rather stable. With a numerical inspection of the storage modulus values the comparison of the initial and end values are more significant. Even then trends suggesting that some crosslinking would have occurred isn't visible at least in the 20 minute time frame in room temperature as all the samples containing GA or at least the samples also containing acid don't exhibit a similar trend. Although the decline of GA dopes is visibly steeper compared to PVA dopes. Even then the values of GA dopes seem to rather approach the values of PVA. This could be that due to slight wt% increase from small molecules of glutaraldehyde it needs slightly longer time to reach stable values in the constant frequency and strain. Thus it should be safe to say that the dopes are rather stable in the short time periods it takes to measure the rheology and to spin.

Also interestingly from the phase angle the 2 wt% dopes behave more like solids in the chosen deformation rates as they reach the lowest phase angle values. Which has been previously seen also in the work of Zhou et al. with pure CNF suspensions. Increasing concentration increases the phase angle closer to the value 1 thus decreasing the elastic behavior. [27] Thus this change could be expected to be arising from the differences in the inner network where guar due to higher amount of hydrogen bonding and high molecular weight and acid crosslinking favor the formation of the 3D network more than the PVA or GA. Where the rearrangement time for the more elaborated 3D structure is longer thus it doesn't reach it between the deformations.

10.1 Amplitude sweep

The LVR is here visually evaluated from Figure 23 at a logarithmical scale. To help the determination a horizontal line was fitted to GA+acid4 curve. From this can be seen that the storage modulus values deviate from this horizontal line significantly already between 0.6 to 1 % strain. The PVA2 instead follows the major gridline even up to values 4.5 to 6 % strain

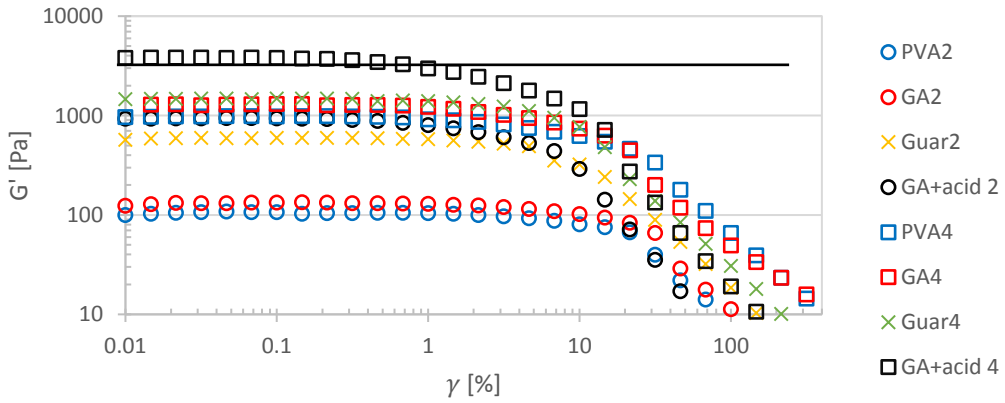

Figure 23. The plotting of the LVR from storage moduli.

Due to difficulties estimating the deviation point visually only rough estimation of the LVR lengths of the dopes compared to each other were made from the shortest one to longest: GA+acid4≈GA+acid2<Guar4≈GA4≈PVA4<Guar2<GA2≈PVA2. Indicating that the crosslinking effect from acid solidified the structure more than the addition of guar.

For the ***5 % deviation method*** the values between 0.01 to 0.1 were considered to form the plateau and their average value was used to compare when the deviation was 5 %. The exact value at 5 % deviation was calculated using the two closest measurement points and fitting a linear equation and solving that at the 5 % deviation point. The method is shown in Equation 25 for PVA2.

$$x = \frac{y_{dev} - y_1}{k} + x_1 = \frac{y_{dev} - y_1}{\frac{y_2 - y_1}{x_2 - x_1}} + x_1 = \frac{-5 - (-4.968)}{\frac{(-8.104) - (-4.968)}{3.16 - 2.15}} + 2.15 = 2.160 \quad (25)$$

Where the y values are the deviation values from the plateau the y_1 value being the lower deviation and the y_2 the one greater than 5% when the x_1 and $x_2$values are the corresponding strain amplitude ((γ)). The x value is the searched critical strain ($\gamma_{5\%\ \mathrm{dev}}$) at the deviation value specified as 5%. The critical strain values for this are gathered in Table 4.

Table 4. Critical strain values for 5% deviation point.

dope	$\gamma_{5\%\ \mathrm{dev}}$
PVA2	2.160
GA2	2.398
Guar2	1.523
GA+acid2	0.415
PVA4	0.916
GA4	0.989
Guar4	1.025
GA+acid4	0.295

The values from the 5% method are significantly lower than the ones visually evaluated. The GA+acid4 leaving the plateau already at value 0.3 is half the value of the lowest visual evaluation. Similar difference is observed with the LVR range of PVA2. Although the order for the dope LVR lengths is mainly the same as from visual. The order with 5% methods is: GA+acid4<GA+acid2<PVA4≈GA4≈Guar4 <Guar2<PVA2≈GA2. The 5% methods is able to produce numerical values easier but as the measurement points are sparse the accuracy is still a concern.

The order of shortest LVR lengths seem to correspond to the maximum storage modulus values within the wt% sets; with higher the storage modulus values resultingin a lower the LVR. The GA+acid dopes displayed the highest storage modulus values and shortest LVR ranges. As the shortness of LVR indicates of

more solid like behavior the GA+acid dopes are the most solid ones of the dopes at their wt% sets. Which is due to the acid causing crosslinking of the dope that was not taken into account as the pH 2 was only expected to allow the glutaraldehyde to crosslink at room temperature over 24 hours.

After which the Guar2 dope stands out as significantly more solid than the PVA2 and GA2. Which is most likely due to higher molecular weight of 1,000,000 compared to 195,000 of the PVA used. As this increases the entanglement density and due to the significant amount of hydroxyl groups also the degree of hydrogen bonding is expected to be higher. Although there seems to be limitation for the effect caused by guar as the Guar4 dope is highly equal to the PVA4 and GA4. Thus the effect present in the lower concentration of Guar2 dope is affected by high concentration where possibly poor dispersion limits it. At least the higher polymer concentration has previously been found to limit the effect of CNF in flow measurements due to poor dispersion [27].

Because the value of strain used in frequency sweep was decided according to visual evaluation of GA4, the chosen strain value of 1 was out of the LVR for some. This could cause some problems with the frequency sweep as not all are in the region where the materials are. Although since the decline is quite gradual it is expected that the results should be somewhat comparable but should be considered when viewing the results.

The gel strengths were estimated using the second and third methods presented in the literature review portion of amplitude sweep that estimate the yield stress. The first method related to the end of LVR was not used due to the ambiguity. Of the used methods the second method relied to the crossover point to evaluate the yield value and the third to the maximum yield value from Equation 17. These methods are not completely accurate due to the sparse datapoints withing the yield stress range. The raw data obtained from rheological measurement was used for these methods by choosing the values from closest datapoint to the cross over and the maximum calculated by the Equation 17. These results are shown in Figure 24 for both methods.

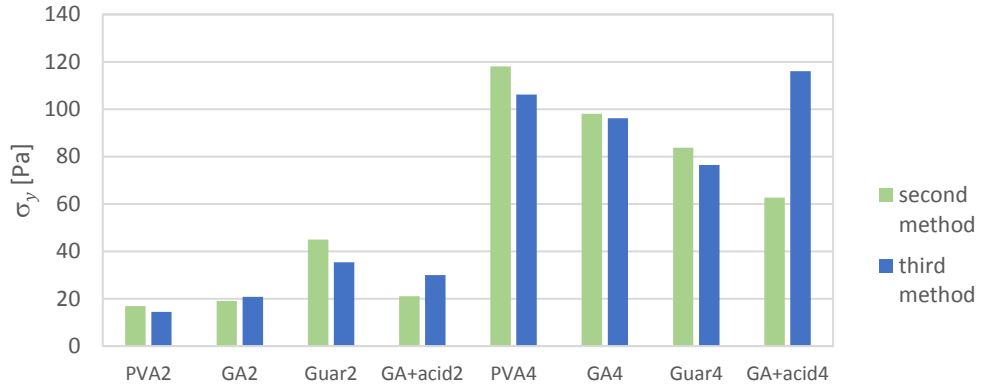

Figure 24. The yield stress values for the dopes using the second and third methods mentioned in the literature review section.

These two methods seem to agree well with each other. Most significant variation is with the GA+acid4 as the methods don't agree if it is the strongest or the weakest of 4 wt% dopes. The strengths of 2 and 4 wt% dopes seem to be the opposites of each other. As the strength order from weakest to strongest in 2 wt% is: PVA2<GA2<Guar2 when in the 4 wt% it is Guar4<GA4<PVA4. The GA+acid dopes don't follow this trend as closely unless the average value of the two methods is examined. In this case they would be in line with others. Later this property arising from the yield stress is called gel strength without separating the two methods used to measure it.

The differences observed most likely arises from the 3D network as in the 4 wt% dopes the thickening from guar can for example cause aggregation or poor dispersion and then due to this optimal network cannot be formed and thus the required yield stress is lowered compared to the dopes not containing excess guar. In the lower wt% region increase in entanglements favors the formation of a 3D network and thus increases the yield stress. It was visible that Guar worsened the gel strength in the 4 wt% dopes and then leading to the best gel strength within the 2 wt% dopes. Similar observation can also be done using the average values of the two methods for the GA+acid dope indicating that the crosslinks formed are favorable in the 2 wt% and detrimental in the 4 wt%. Although the effect is significantly lower compared to the guar. Thus this implicates that using lower concentrations with GA, Guar and Ga+acid compared to the 4 wt% PVA dope would have possibly increased their gel strengths and resulted them being comparable to PVA4.

10.2 Frequency sweep

As mentioned in the amplitude sweep results the chosen critical strain value was high for some of the dopes. This can cause that the results of the samples outside their LVR to be more frequency dependent than others. Bellow in Figure 25 is the PVA2 dope as an example for the *G', G'' and phase angle*. The other ones are presented in Appendix 3. By definition Zhou et al. used the dopes would be qualified to have solid dominated behavior [27]. A more closer definition arising from the G' and G' relation and the phase angle would qualify them as gels due to the G'>G'' and phase angle being independent in the low region. Instead they resemble solids in the higher frequency region.

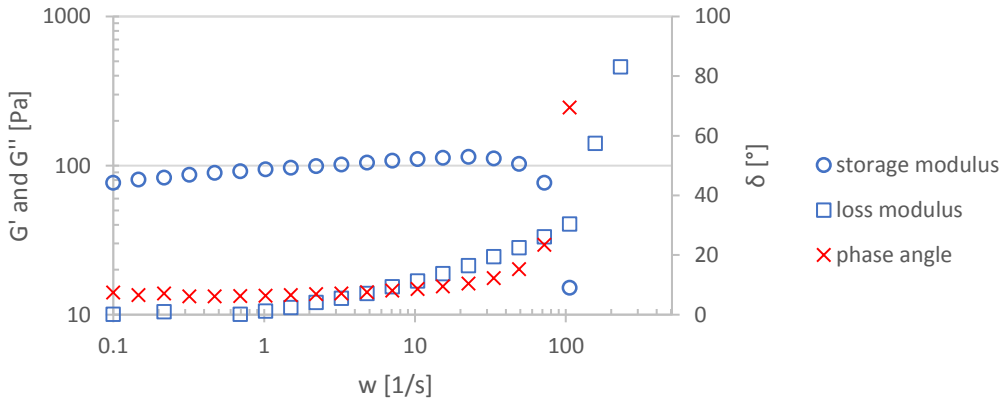

Figure 25. The G', G'' and δ values for PVA4

These dopes don't exhibit the liquid to solid transformation in the low frequency region so they don't have the crossover point needed for *dynamic relaxation time*. Nor does the loss modulus exhibit maximum value within the range from where determination of *the longest relaxation time* could be done. Instead the loss modulus increases towards high frequency values indicating that the structure is turning to more liquid like. Due to this, these factors cannot be used to compare the dopes. *The storage modulus* value instead should give some indication of the entanglements and crosslinking in the material. Thus the average values and maximum and minimum values for the storage modulus in the whole range is shown in Figure 26.

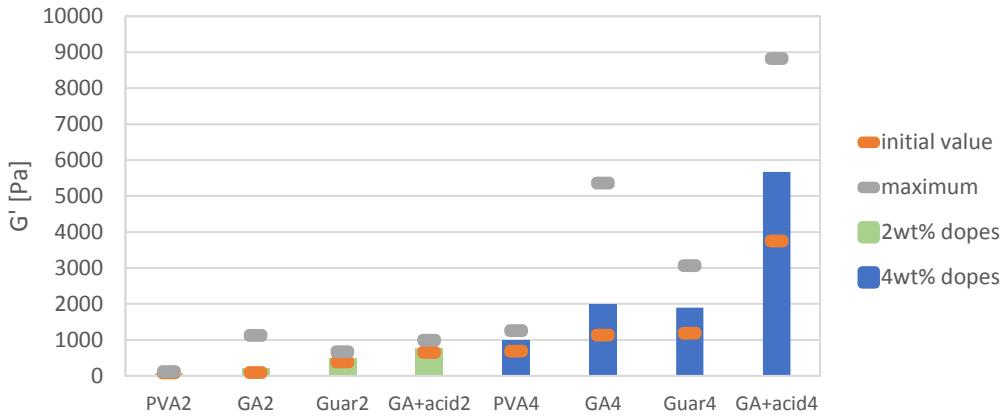

Figure 26. Storage modulus average values.

In the Figure 26 the 2 wt% dopes have significantly less entanglements than the 4 wt% dopes due to lower concentration. In the Figure 26 in addition to the average values the initial values at 0.1 1/s frequency and maximum values reached within the measurement range are shown. In the results Guar and acid crosslinking can be seen significantly increase the entanglement degrees of the dopes as they reach higher initial values compared to PVA and GA dopes. From the maximum values can also be seen that the GA dopes have different behavior at high frequency values. There the interactions with the arising from the addition of GA molecules seem to increase the maximum entanglements. The average storage modulus values are compared as relative entanglement degrees relating them to the entanglement degree of the PVA dopes used as the baseline. These are shown in the Figure 27

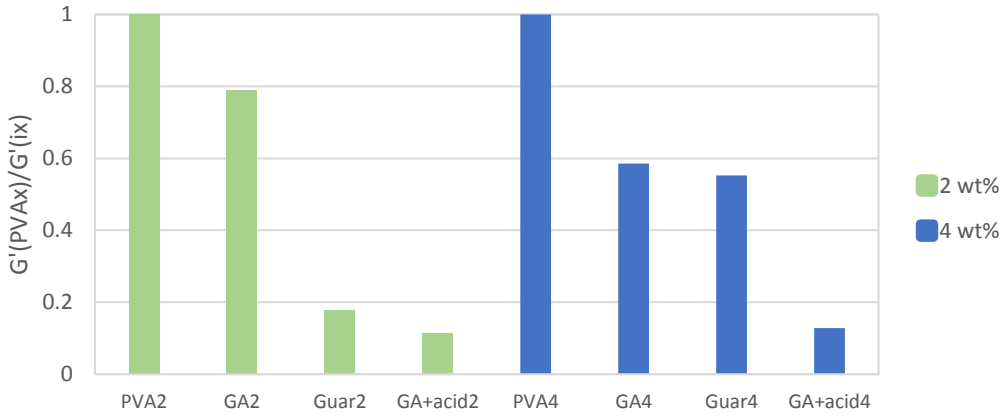

Figure 27. Comparing the entanglement degrees to the base values from PVA dopes where i refers to GA, Guar and Ga+acid dopes and the x to the wt%.

From the Figure 27 can be seen that the relative entanglement degree of Guar4 is significantly less than Guar2 when comparing them to the PVA dopes. The GA dope can be seen to increase in relative entanglement with the increase of concentration and the GA+acid dopes reach highly similar values. The effect with guar would further suggest poor dispersion reached in the 4 wt% system. The acid instead doesn't affect this, as the dispersion of CNF is performed before the addition of GA and acid. After which the addition of acid only multiplies the amount of experienced entanglements. The increased entanglements caused by acid would explain the shorter LVR observed for the GA+acid dopes. The entanglement degree also relates to the gel strength where the increased entanglements in 2 wt% are favorable and then hinder the gel strength in the 4 wt% dopes.

The tanδ values are used to further compare the materials state, as it is the easier repsentation for the relation of G' to G'' by using the Equation 18. As mentioned in the theory part it is also used to estimate which of the samples is the strongest and can dissipate energy the best. The lowest tanδ over the whole range is the qualification for strongest gel. As already visible from the G' and G'' values the loss tangent also confirms that the materials are solid dominated as all the values are initially bellow 1 as shown in the Figure 28.

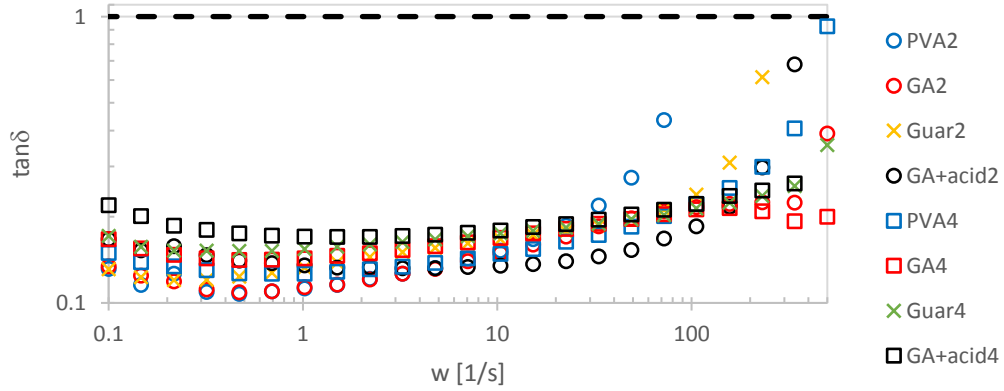

Figure 28. The tanδ curves for dopes.

The tanδ values of the dopes in Figure 28 reach highly similar values to each other. They all exhibit small decline in low frequency range and slight increase in the high frequency range. The increase in the tanδ value would suggest some kind of decomposition of the inner structure, which seems to be more visible with the 2 wt% dopes. This means that even though the dopes are solid first they seem to

turn more liquid like as the frequency increases. Dopes determined to contain less entanglements at high frequency turned liquid like in lower frequency values. Zhou et al. noticed similar behavior with their PVA5/CNF suspension where the higher CNF concentration (0.15 – 0.45 wt% of total) led to higher frequency value at point where the tanδ=1 was reached [27]. As these tanδ values are in flux and one dope doesn't reach the lowest values over the whole scale it cannot be used to determine the strongest dope. The order the dopes leave the solid like behavior instead could possibly be related to spinnability, if similar conditions are reached in spinning conditions.

In addition to the lowest tanδ value the high values of G^* *and* η^* could also used be used to evaluate the strength of the dopes. These would be expected to give similar results to the tanδ as the G* is also calculated from G' and G'' values by Equation 19 and the value of G* is then further used to solve the η* using Equation 20. These results are shown in Figure 29 and Figure 30 in a logarithmical scale.

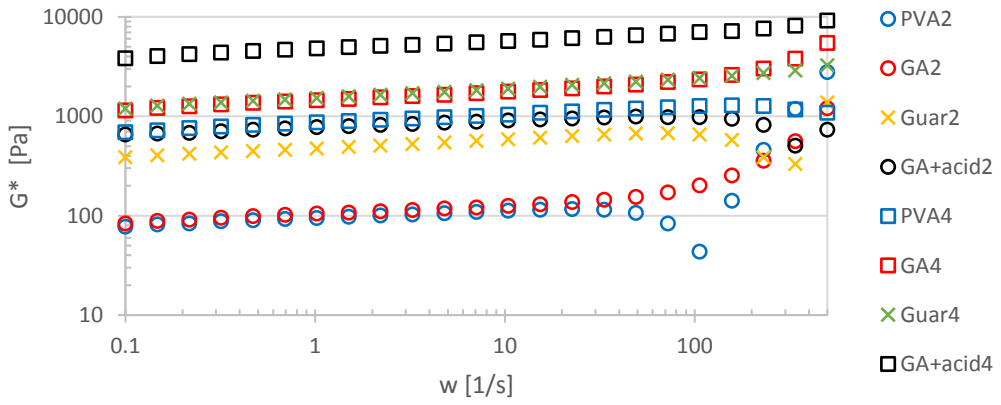

Figure 29. The complex modulus.

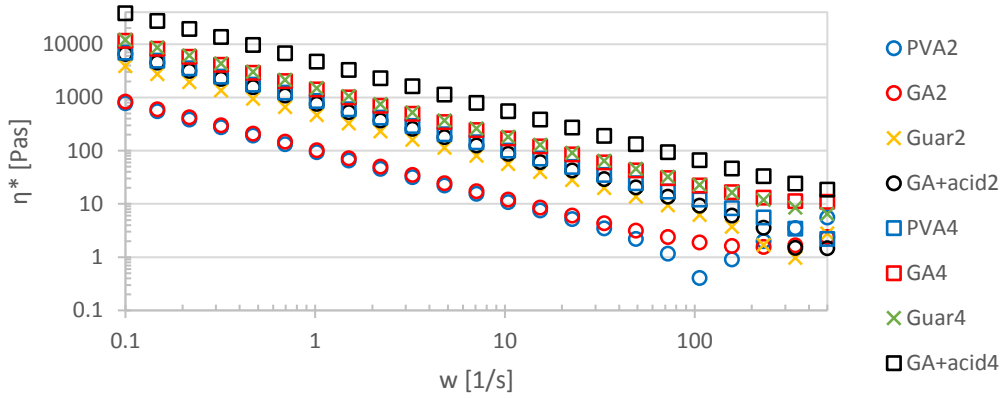

Figure 30. Complex viscosity.

As the G* is the rigidity of the material under deformation it seems to significantly follow the storage modulus values of Figure 26 indicating of the entanglement degree. The η* indicates shear thinning flow which is expected as the orientation increases. Thus the combination of the G*, η* and tanδ can be expected to give estimation of the strongest dope. Compared to the tanδ values, the G* and η* are more consistent, whereas the order received from them is completely different to tanδ values at low frequency. The order from G* and η* don't seem to have other connection to observed gel strength than that they follow the degree of entanglements from the storage modulus

10.3 Steady shear measurement

The zero shear of the dopes was in the form of a yield. This is visible in the Figure 31 where the low shear rate is shown. This indicates that none of these dopes flow at rest. To have better idea of the low shear rate behavior shear rates should be studied at lower values. But the fact that these have yield behaviour is supported by enzymatically fibrillated CNF having similar behaviour at 2 wt% even down to shear rates of 0.001 1/s [2].

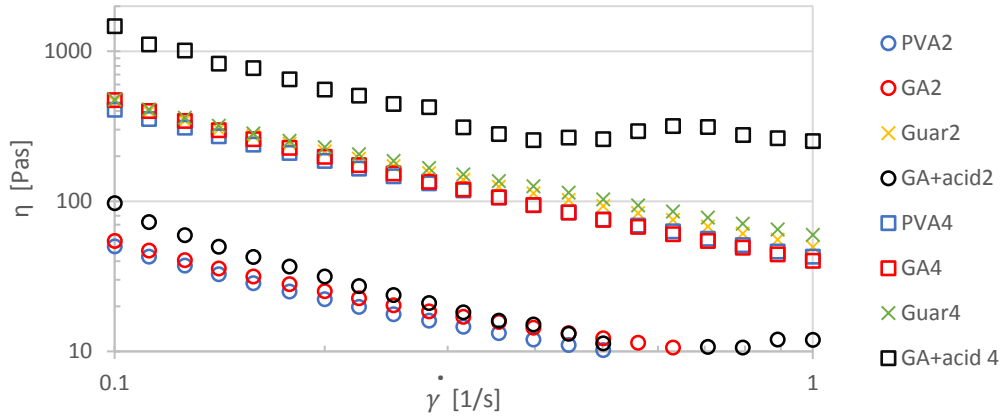

Figure 31. Zero shear viscosities.

The zero shear is indicative of the effective molecular weight, indicating that the networks formed with PVA2 and GA2 are highly similar in low shear whereas the GA+acid2 only has slightly higher experienced network due to acid crosslinking. The PVA4, GA4, Guar2 and Guar4 instead are highly equal in the logarithmical scale, which would indicate to be the maximum network attainable with hydrogen bonding and molecular weight in the used composition. Further network formation is disrupted by agglomeration and dispersion difficulties. This further confirms the results observed from storage modulus. Similarly the increase in experienced network caused by acid increase is in same relation to GA4 dope as it was in the storage modulus values. The similarity observed in the 2 and 4 wt% Guar dopes is even more significant than previously expected.

In previous experiments the amount of CNFs in PVA solution has been seen to increase the zero shear viscosity as the percolation network increases [27]. Thus the difference between the PVA and GA dopes with 2 and 4 wt% solids were expected but then the Guar dopes defy this trend. The main cause is most likely the poor dispersion and possible aggregation. The high molecular weight portion increases the entanglements and thus viscosity so that the Guar2 is in multiple tests reaching closer to the values of the 4 wt% dopes like the LVR, yield, G* and η*. This is due to it reaching similar network as the Guar4 even in low concentration. The viscosity values at point 0.1 1/s have been listed in Table 5, from which the effect of guar forming network can be seen.

Table 5. The viscosity values from 0.1 1/s.

Dopes	PVA2	GA2	Guar2	GA+acid2	PVA4	GA4	Guar4	GA+acid4
Viscosity	50	54.3	464	96.9	408	472	475	1470

The zero shear values follow the similar trend as the storage modulus values used to indicate of entanglements. With the low entanglement degree also the formed network stays insignificant. Thus there is significant gap between the 2 and 4 wt% dopes with the storage modulus and the zero shear values. Even the acid crosslinking has lesser effect due to the increased distances between the molecules resulting from low concentration. There seems to be experienced network value that can only be exceeded by acid crosslinking in this experiment.

Previously similar values have been reached with CNFs. Zhou et al. reached values of 50 Pas with 1 wt% CNF in water suspension. These fibrils were similarly mechanically treated by passing through a microfluidizer five times. [27] Martoia et al. also reached values around 50 Pas with 2 wt% enzymatically fibrillated CNF in water solution [2]. The enzymatically fibrillated CNFs require higher concentration due to the lower aspect ratio reached with the enzymatic pre-treatment. The PVA raw material was found to have significantly low steady shear of bellow 0,1 Pas so the similarities with CNF water suspension is promising. Also the matrix will affect the percolation network formed by the CNFs as the semi-flexible molecules adsorb on the surface.

The whole shear rate is shown for the dopes in Figure 32. As was already said from the η^* curves the dopes are shear thinning. What the η^* curves could not tell was the fluctuation caused by the formation of intermediate internal network structures as the molecules orientate referred in the literature review of this work.

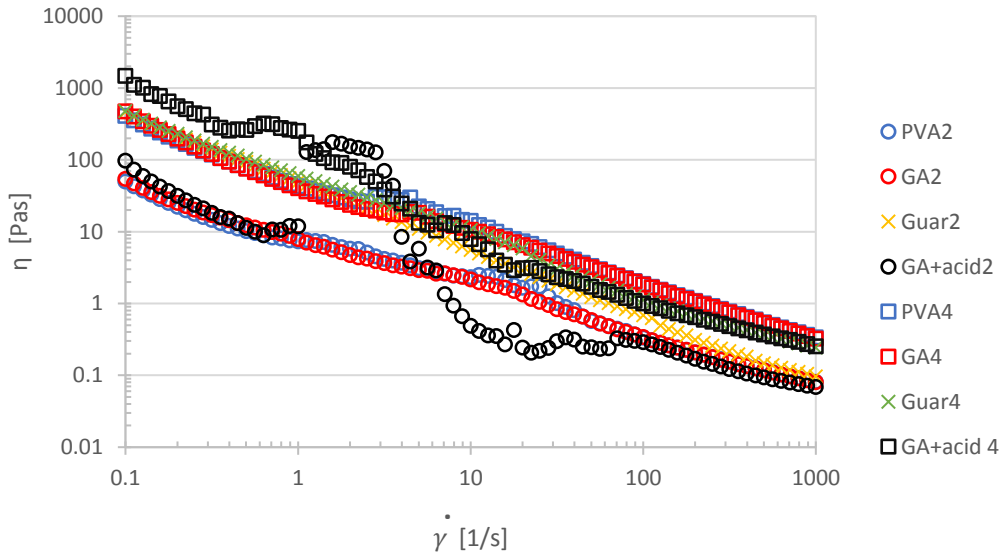

Figure 32. Whole shear rate and inner structure formation in flow curve

From the flow curve of Figure 32 can be seen that the same wt% dopes approach same values at the high shear rate region regardless of their initial values. The viscosity values at shear value of 1000 1/s also resembles the order received from gel strength values from the amplitude sweep. It can also be seen that most significant inner structure is observed with the GA+acid dopes causing a viscosity increase instead of Newtonian plateau, while the PVA and GA dopes instead have relatively faint structure formation. The individual plateau regions can be better observed from the individual figures shown in Appendix 4 comparing the 2 and 4 wt% dopes. In the logarithmical scale it seems like none of these would reach the final plateau value, when in reality at high shear rates the viscosity values are relatively stable. Thus they should also prove relatively stable in the spinning process.

From the curves of the PVA dopes in Fiqure 1 of Appendix 4, it can be seen that they exhibit clear Newtonian plateaus. The PVA4 only exhibits one single plateau, when the PVA2 exhibits two Newtonian regions; one at low shear rate and other at a higher shear rate. The PVA2 reaches the first Newtonian plateau at around 1 1/s shear rate when the PVA4 reaches this around 2 1/s. The second more complicated inner structure of the PVA2 dope is reached at 9 1/s followed by multiple transition from shear thinning to Newtonian again. After which it continues as shear thinning again. The difference of the Newtonian behavior reached comes

from the less concentrated dope reaching the oriented structure easier with lower deformation. Thus the 4 wt% one only exhibited one orientation structure. This follows the trend also found with CNF suspensions by Zhou et al. [27].

The GA dopes exhibit highly similar behavior as the PVA dopes but with them the Newtonian plateaus are much less prominent and the Newtonian plateau especially in the 4 wt% dope has shifted to higher shear rate of 3 1/s. In the curve of GA2 the Newtonian regions observed in PVA2 are visible as only slight deviations and not as proper Newtonian regions. These values are reached slightly earlier at rates 0.8 1/s and 8 1/s. This Indicates that GA addition is detrimental for inner structure formation making the inner structure harder to reach. This can be caused by the increase in solids concentration of the small glutaraldehyde molecules disrupting the original structure formation affecting differently on other sides of the ideal wt%.

The guar dopes displayed no visible plateau values. As it was previously stated in the shear section of the literature review, guar suspensions exhibit shear thinning flow. Therefore, within guar samples containing two raw materials which exhibit shear thinning flow, inner structures were prevented from being formed in the flow system. The shear thinning flow was also observed to occur already with the PVA3/Guar1 raw material. Additionally, an interesting factor is that the 2 wt% and 4 wt% dopes reach similar values at 0.1 but differentiate towards the high shear rates. This further confirms that the guar solutions have a similar effect where the more concentrated dope only differs in the ease of orientation.

The GA+acid dopes instead exhibit the strongest inner structure related behavior as the viscosity is even momentarily increased. This behavior could arise from the crosslinking occurring from the acid addition but it is highly unlikely that the shear rates are able to produce enough heat to cause the glutaraldehyde to crosslink. The oriented structure is reached earlier in the 4 wt% dope compared to the 2 wt% dope. This is the opposite to the expected order. Could be that the 2 wt% reaches it’s first inner structure outside the measurement range as the higher entanglements from acid should similarly restrain the formation of inner structure. Or it could be from the acid crosslinks being more parsely in the lower concentration dope. Thus the point when the acid crosslinks are broken is reached

later, when the reached viscosity increase of the inner structures are almost the same.

As the shear rate experienced during spinning are expected to be above the 100 1/s region, the shear thinning region in the high shear rates were drawn and power law trend lines were fitted to them. The diagrams and the fitted trend lines are in Appendix 5 and *the k and n* values are shown in Table 6, where the n value is solved from the exponent n-1.

Table 6. The k and n values from the power law equations.

dope	k	n-1	n
PVA2	7.963	-0.678	0.322
GA2	11.070	-0.737	0.263
Guar2	42.992	-0.909	0.091
GA+acid2	5.138	-0.639	0.361
PVA4	80.362	-0.805	0.195
GA4	64.757	-0.772	0.228
Guar4	58.100	-0.826	0.174
GA+acid4	22.278	-0.660	0.340

In the Table 6 the value of k is the measure of fluids consistency and a higher value should indicate higher apparent viscosity. Thus the order of this could be also estimated from the corresponding flow curve region, but this seems to only apply within the different wt% dope sets. The order in 2 wt% dopes from highest to lowest value of k is: Guar2>GA2>PVA2>GA+acid2 and for the 4 wt% dopes it is: PVA4>GA4>Guar4>GA+acid4. The relative order of these correspond with the measured gel strengths if the GA+acid dopes are overlooked.

The power law index instead comes from the shear thinning behavior of the dopes that arises from them orientating and thus decreasing resistance to flow. The most shear thinning being the one with lowest power law index n value. Similarly to the k values this quality could be evaluated from the slopes on a logarithmical scale. The n values vary between 0.121 to 0.411 so all the dopes are quite non-Newtonian as Newtonian behavior is qualified to have the value of 1. The order of dopes from most shear thinning to least shear thinning is: Guar2<Guar4<PVA4≈GA4<PVA2<GA2<GA+acid4≈GA+acid2. This should be affected by the relative ease the dopes reaching orientation. According to this the

Guar dopes should within the power law region be in a state where it is experiencing significant orientation. Although because the power law is only fitted to the high shear region it doesn't well represent the overall orientation reached. Thus it is hard to compare the shear thinning to the previous results. Only the weakness of the acid containing dopes can be seen as the initial entanglement increase is completely lost at high shear rates. Also the 2 wt% seem to orientate before the 4 wt% dopes. Except the Guar2, possibly due to Guar4 being so much harder to orientate due to larger quantity of high molecular weight portion, when poor dispersion keeps it in the same range as the others.

The shear at the capillary walls was estimated for the dopes and for a Newtonian liquid using the n value of 1. As the accurate inner diameters of the needles were unknown the shear rates were calculated for diameters ranging from 0.7 to 1.2 mm. The equation is initially meant to be used solving the non-Newtonian behavior from capillary measurements but is here used with values solved from cone and plate geometry, which can cause error in the values. Below in an Equation 26 is the shear at wall solved for Newtonian liquid using the process parameters used to spin the samples and needle diameter of 0.7. The results for shear rate at the wall are then presented in Figure 33 for the various capillary diameters.

$$\dot{\gamma}_R = \left(\frac{4Q}{\pi R^3}\right)\left(\frac{\frac{1}{n}+3}{4}\right) = \left(\frac{4\,\frac{0.4\ ml/min}{1000000m^3\cdot 60s}}{\pi\left(\frac{\frac{0.7}{2}}{1000}m\right)^3}\right)\left(\frac{\frac{1}{1}+3}{4}\right) = 197.9769943\ 1/s \qquad (26)$$

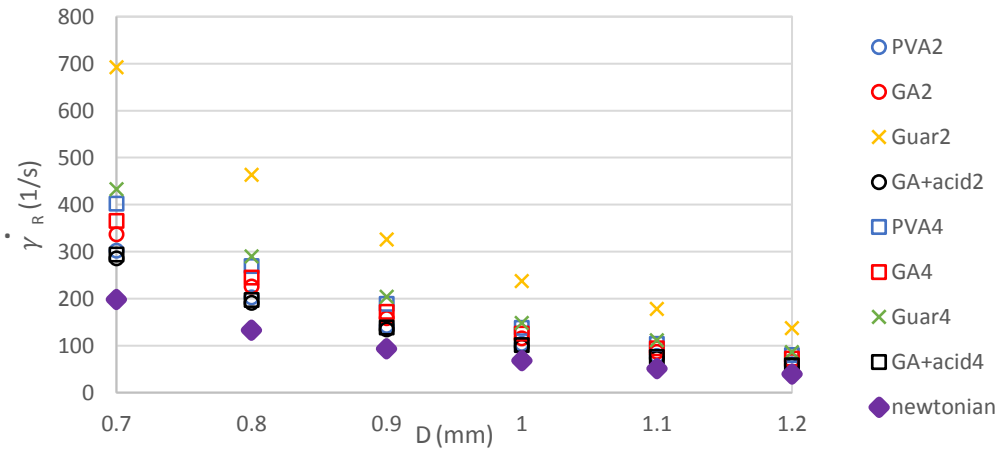

Figure 33. Shear rates at the needle wall.

where Q is the feeding speed of the dope and R is the radius of the capillary wall. From Figure 33 can be seen that the increase of shear thinning increases the experienced shear rate when decreasing the needle diameter increases the differences between the dopes. Although the order of shear rates experienced remains the same even if the needle diameter is changed. The dopes approach the same shear rate as Newtonian liquid when the needle is increased. The shear rates the dopes experience with the used parameters would be from the highest to the lowest: Guar2>Guar4>PVA4>GA4>GA2>PVA2>GA+acid4>GA+acid2. The higher the shear rate experienced the better the orientation forces but as the dopes have different entanglement degrees it doesn't correlate straight into the best orientation reached. Due to the differences in the shear rates experienced in 1 mm diameter needle being relatively small the best orientation could be expected to be reached in the dopes with least entanglements.

10.4 Spinnability in the spinning process

The *breaking mass* with the slow speed of spinning was determined to be in the mode of ductile failure. Due to the low speed there was no spraying or significant instabilities. As more of the filament was extruded, the increasing mass of the forming filament caused the cross section to slowly decreased and the filament was cut off. Thus it correlates to the maximum force the filament can carry. Here these are used to just estimate the relative order of the dopes. Breaking of the filaments are shown in Figure 34 for the normal needle. The images were taken just before the filaments broke off. In the figure the sizes of the droplets are just indicative as the angle and zoom vary between the images. But as can be seen from the Figure 34 the dopes had inconsistencies that affected the result and thus the large sample amount.

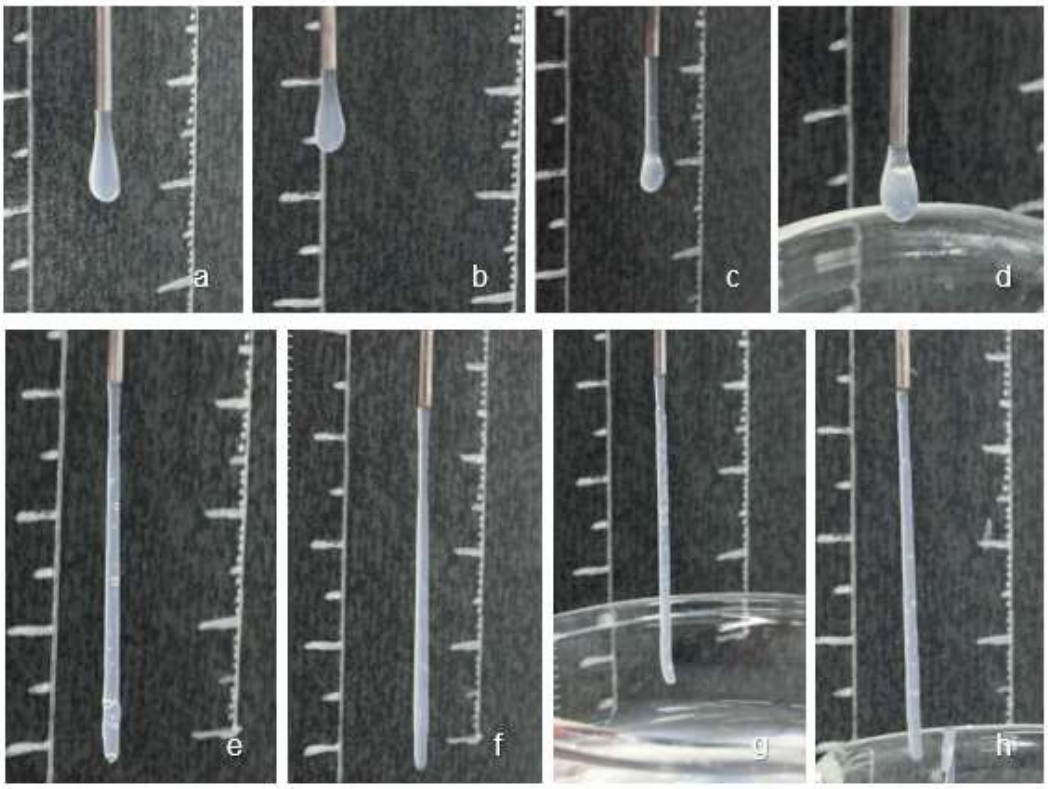

Figure 34.Breaking mass of the dopes a) PVA2 b) GA2 c) Guar2 d) GA+acid2 e) PVA4 f) GA4 g) Guar4 h) GA+acid4.

This shows that the 2 wt% dopes mostly formed a droplet before they stretched out and broke off. The 4 wt% dopes instead all formed a filament that eventually gave in near the needle when the mass increased. This trend of filament formation instead of just drops seemed to follow the **gel strength** from amplitude sweep, **zero shear** and $\mathbf{k}$ indicating the fluids consistency from the steady shear. As with all of those parameters the weakest ones were the ones only forming droplets (PVA2, GA2, GA+acid2) and the ones significantly stronger formed the initial filaments.

Although from these 3 methods the gel strength best correlated with the order of the dopes as it can also explain the significantly weaker tendency of Guar2 to form filament. This indicates that gel strength of 35 to 45 Pa caused the transition to the filament formation in air gap. The zero shear and k also help to predict which ones have the ability to form filament in the air gap, but they don't exhibit a trend that would explain why the filament formation of Guar2 is weaker compared to the others.

The breaking mass results for the dopes are then presented in Figure 35 where the average drop weights have been calculated from the average of 40 drops and 6 samples. The raw data is in Appendix 6. This data could not be ideally used to estimate the force the filaments could carry as the diameters of the forming filaments could not be accurately measured or estimated due to them being in such weak state before any solvents were extracted.

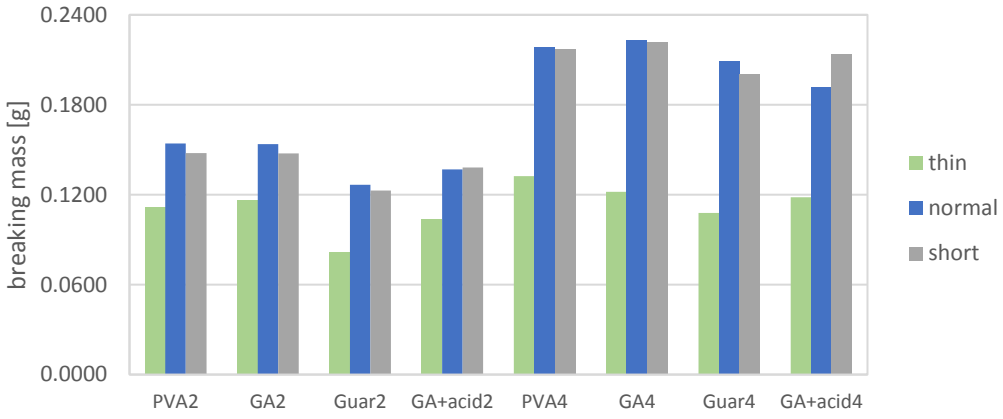

Figure 35. The average drop weights for different needles.

With the thin needle there was barely any difference between the 2 and 4 wt% dopes. Which could be due to the 2 wt% ones having tendency to form dropled at the end of the needle thus having larger cross section to hold the weight when the 4 wt% ones formed extremely thin filaments. With both the 2 and 4 wt% dopes can be seen that the Guar and GA+acid dopes are slightly weaker than the PVA and GA dopes. The high amount of bubbles in the dopes makes the correlation of such small differences inaccurate. This result best correlates with the **storage modulus** as the higher entanglement degree is harder to orientate. This is because the increasing storage modulus value within the dope sets seems to cause lower breaking masses. How ever this battles against the shear rates in different diameter needles as the normal and short needles that should exhibit the least shear rate to the forming filament result into highest breaking masses with the 4 wt% dopes. This is due to the breaking mass not being able to correlate to the filament diameter and the 2 wt% dopes forming a droplet in the end of the needle. Thus the effective diameter for the ones forming droplet is increased compared to the dopes that retain the shape and size of the capillary.

Additionally the high amount of bubbles especially with the formation of thin filaments can favor filament breaks as the bubbles are large compared to the cross sectional area and thus cause extremely weak points. Compositions with less bubbles or lower tendency to form filament in air gap are subsequently less likely to break off. Thus the observed differences in the breaking masses could also have been due to higher amount of bubbles.

With the normal and short needles there is more significant difference between the 2 and 4 wt% dopes as the droplet formation no longer leads into superior cross section. But there is same order with the dopes as with the thin needle suggesting that the same factors dominate also in the wider capillary. As the filaments diameter are closer to the same as droplets have they are able to carry more weight except the Guar2 which is the weakest. With these dopes the difference between the short and normal needle were such insignificant that the $\mathrm{L/D}$ ratio can be expected not to affect the reached orientation much. The exact $\mathrm{L/D}$ ratios could not be calculated due to not knowing the inner diameter of the needle but estimating from the outer diameters the ratios of short and normal were 15 and 22. The ratio of 15 has previously been the start of a plateau for pre-gelled gel spinning executed by Liu et al. thus also explaining the insignificant effect [17].

The ***air gap height*** proved more complicated to determine, as the different dopes didn't behave similarly in the test. Some of them connected to the coagulation bath but broke almost instantly inside the bath, not forming proper continuous filament. Some instead were so riddled with bubbles that estimation, when it formed a continuous filament was severely affected. Thus with some of the filaments continuing in the bath over 20 second window was considered as forming continuous filament. These measured heights are presented in Figure 36 and the data is in Appendix 7.

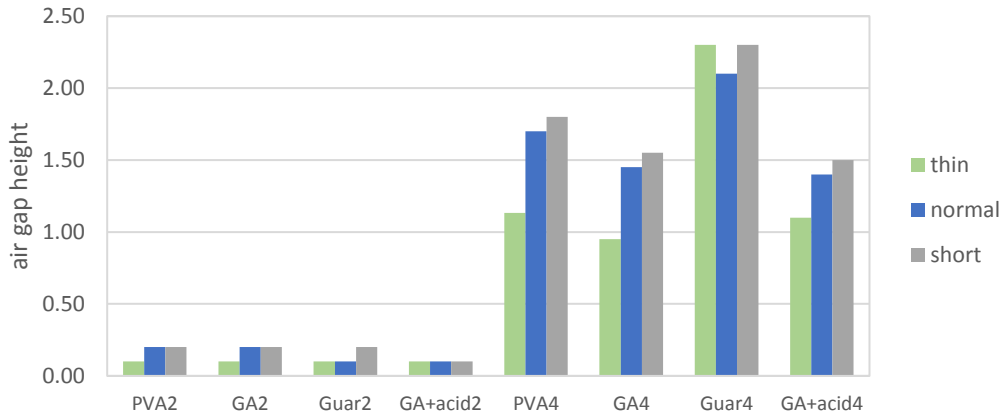

Figure 36. Air gap lengths for 2 wt% and 4 wt% dopes.

For all 2 wt% dopes this was between 1 and 2 mm and due to the inaccuracy in the measuring they can all be expected to be the same. With these even if longer or heavier droplets were formed in air gap decreasing the air gap height caused the droplet to break off. This happened when it came in contact with the coagulation bath surface until the height of 1-2 mm. Whereas the 4 wt% dopes could instead be spun from a higher air gap. Of which the PVA4 and GA4 filaments continued to the bottom of the bath if they initially started forming filaments, while the Guar4 and GA+acid4 were breaking so often due to bubbles. Thus the lowered expectations were used with these and they were considered to form continuous filament in the bath if some entered the coagulation bath 1 cm before breaking. Hence the results might not be comparable.

As there was difficulties conducting this experiment the results are expected to be just indicative of the differences between the 2 and 4 wt% dopes. The best correlations are from the **gel strength**, the **viscosity values at high shear rates** and **storage modulus**, as these are the only ones properly explaining why example the Guar2 didn't form filaments at higher air gap. This is due to certain gel strength, entanglement degree are needed for the material to retain network that causes the viscosity so that the material can retain its shape. **Zero shear** and $\mathbf{k}$ values also give some correlation but fail to explain the Guar2 dope.

For the *spinning quality* these dopes were rated from easy (1) to impossible (5). Their behavior in air gap was not included in this as the actual filament spinning was conducted at zero air gap due to the amount of breakages occurring in the air

gap resulting from the bubbles. This caused the weaker points to be included in the formed filaments but also allowed filaments of appropriate length for tensile testing to be formed. Thus the ease of spinning only consists the observations of the spinning into the coagulation bath and then retrieving the filaments that were immersed for 24 h to dry them. The ease of spinning didn't always correlate with the ease of pulling them out. The ratings for all the dopes are listed in Table 7. As can be seen from the table not all the dopes were able to form filaments in the used conditions and even if filaments were formed not all could be recovered.

Table 7. Fiber formation of dopes and the ease of handling.

dope	bath	formation of fibers	fibers recoverable	ease in recovering (1 easy - 5 impossible)
PVA2	neutral	yes	no	5
PVA2	acidic	yes	yes	2.5
GA2	acidic	yes	yes	2
Guar2	neutral	no	no	5
GA+acidic2	neutral	no	no	5
PVA4	neutral	yes	yes	4
PVA4	acidic	yes	yes	1
GA4	acidic	yes	yes	1
Guar4	neutral	yes	yes	4.5
GA+acidic4	neutral	no	no	5

As visible in the Table 7 from the dopes only PVA2 spun in an acidic bath, GA2, PVA4 spun to both neutral and acidic bath, GA4 and Guar 4 formed fibers that could be gathered. The Guar2, GA+acid2 and GA+acid4 instead broke to pieces inside the coagulation bath during the spinning process. Of which the Guar2 and GA+acid2 were so fragile that they broke to small flakes almost immediately after exiting the needle. The GA+acid4 instead formed filaments that broke due to the twisting motion present when the filament gathered on a coil in the bath. These behaviors are visible in Figure 37 where the breaking of GA+acid4 is highlighted.

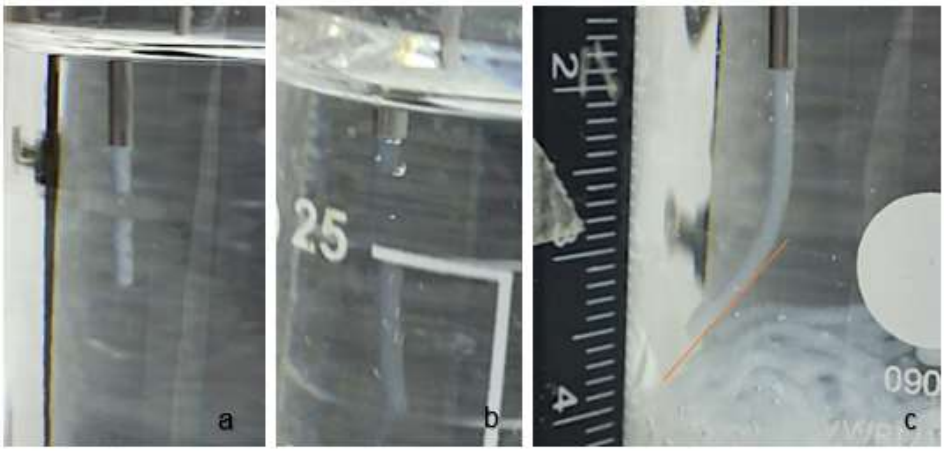

Figure 37. The spinning of a) Guar2, b) GA+acid2 and c) GA+acid4 from zero air gap.

The breaking behavior could arise from **storage modulus**, **LVR**, **gel strength** or the sum of these. Insufficient orientation arising from higher entanglement degree, increased solid like behavior or worse gel strength all could be the reason for this. Although as the entanglement network affecting the LVR making the two things almost the same. When the Guar2 and GA+acid2 seem to lack the inner network formation needed for them to retain the filament shape the GA+acid4 seems to just be too solid like resulting into fragile breakage of the filament. Thus most likely LVR and gel strength need to be in certain relation for the dope to not be fragile. For 2 wt% dopes the LVR continuing to strain value of 2 % seems to be enough as the PVA2 did initially form filaments in the neutral bath. Instead for the 4 wt% dopes the reguired LVR range seems to be up to strain value 1 %. The difference could be expected to arise from the gel strengths being in different scales.

After the initial formation of filament not all were recoverable from the bath. Especially the PVA2 spun into neutral bath initially formed filaments in the shallow coagulation bath. The filaments were spun approximately at 2 cm height from the bottom of the bath. There the filament structure broke down during the 24 h immersion time, which was most likely due to the low entanglement degree. The entanglements needed for filament formation were lost in the bath as the mass transfer from dope solvent and coagulation bath solvent caused them to disentangle. The same dope could be successfully retrieved from acidic coagulation bath as the acid induced some crosslinking and thus more stable network structure. Before similar fibers have been spun into -15 to -20 coagulation

baths [6, 10]. Thus the room temperature was not optimal for increasing the viscosity and so retaining the fiber structure but the acidity worked to compensate the effect of temperature allowing the dopes with lower gel strength to be spun.

Of the dopes that could be recovered, the ease of pulling them out and lying to dry varied. The ones spun in neutral bath PVA4 and Guar4 were extremely fragile compared to the ones spun into acidic bath PVA2, PVA4, GA2, GA4. The coils from neutral baths could be easily lifted from the bath but when trying to gently pry the coils open they broke to tiny bits from where the bubbles weakened the structure. Thus only extremely small sample amounts were recovered of the PVA4 and Guar4 from neutral coagulation baths. Filaments in acid baths could be uncoiled easily by attaching one end to the drying surface and then lifting the coil to the other side. Only the 2 wt% ones exhibited slight difficulties if the coil had been out of the bath a while as the ethanol evaporated fast allowing only few straight strands to be collected from one coil before it had dried too much. Thus the 4 wt% filaments could be said to stay separate better and could even be held elevated from both ends by hand when placing them to dry.

Again the most significant effect arises from the network as the acidic bath is able to induce network formation. Thus the filaments spun into the acidic bath were more stable. The differences in the ease of pulling out observed between PVA4 and Guar4 spun into neutral bath are rather insignificant, and are due to the bubbles in the structure and differences in orientation due to entanglement degree and gel strength. For the filaments spun into the acid bath, the difference was only significant between the 2 and 4 wt% ones and thus correlates with about everything from LVR length, G', shear both at low and high rates and consistency. The spinning of these dopes that could be recovered is shown in Figure 38. The importance of the filaments ability to form coil comes from the fact that the bath is held stationary and thus all the product is formed as a coil before a formation of new coil is started. If drawing could be induced the tilting would depend on the diameter of the rollers possibly allowing more solid like and less flexible filaments to be formed.

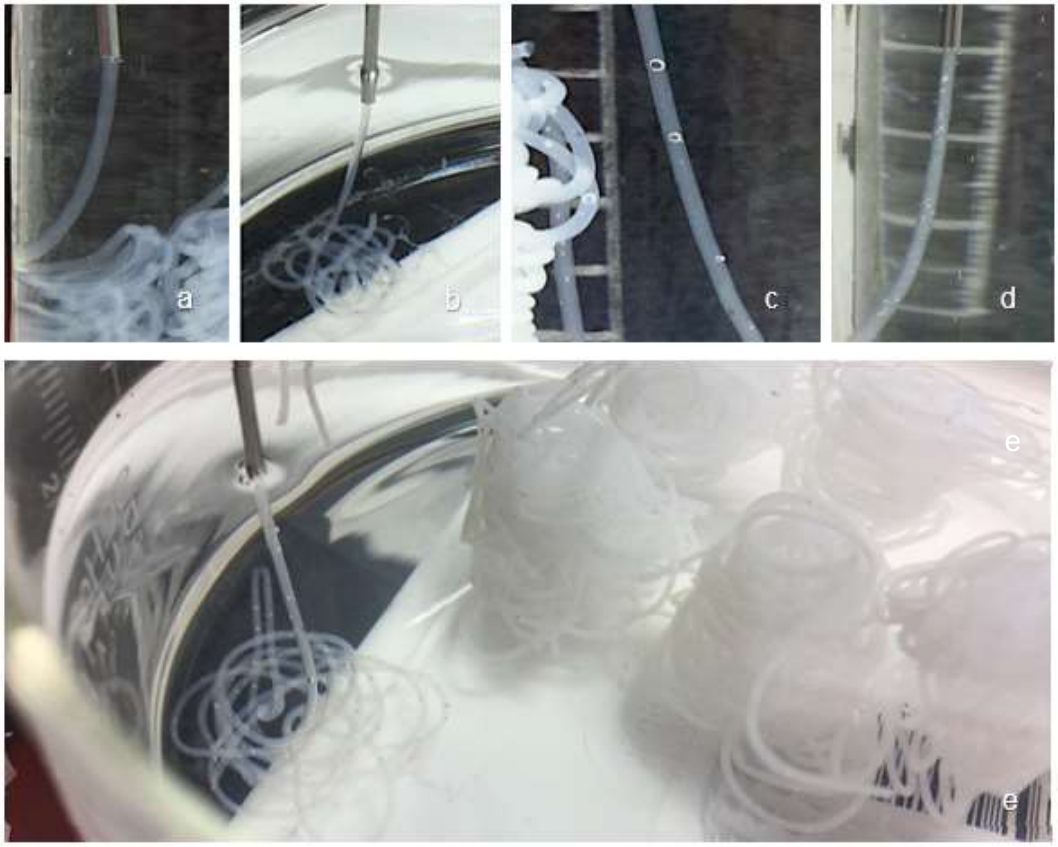

Figure 38. The spinning of samples a) PVA2, b) GA2, c) PVA4, d) Guar4 and e) GA4 from zero air gap.

From the Figure 38 can be seen that the 2 wt% dopes had hardly any visible imperfections. The 4 wt% dopes instead were riddled with bubbles and even some nearly the size of the filament diameter could be trapped in the forming filament. Whereas the PVA4 and GA4 were plagued with bubbles ranging from large to small the Guar4 mainly had small bubbles but in larger quantity. That helps to explain the variation present in the results.

A distinctive feature of these filaments were that initially they were quite transparent and then turned to opaque after some time in coagulation bath. Arising from the fact that the amount of water decreased in the filaments causing the water soluble polymers to precipitate, which is best visible from PVA4 in the Figure 38 as previously spun coil is next to newer just forming filament. The mass transfer of water out of the filaments must have also contained some PVA and CNF as a sedimentation was formed in the bottom of the bath. Due to the dopes being spun into coagulation baths of varying sizes and varying dope amounts the degree of this behavior could not be evaluated. The sedimentation was first an even layer in

the bottom but then flaked as the filaments were pulled out. An example of the sedimentation is shown in Figure 39 that depicts the coagulation bath used for GA4 after most of the fibers are pulled out and the sedimentation has gathered as small clusters instead of even layer.

Figure 39. Sedimentation flakes in the coagulation bath.

The formed wet filaments were also observed with *optical microscopy*. As the cross section of the wet filaments spun with the normal needle were somewhere in 1 mm scale only small portion of the surface could be focused on with the microscope. The images were taken with the same magnification and shrunk into 1400x1536 pixel sized images to retain some comparability. This was done so that the sizes could be compared due to the lack of a measuring scale. These are shown in Figure 40.

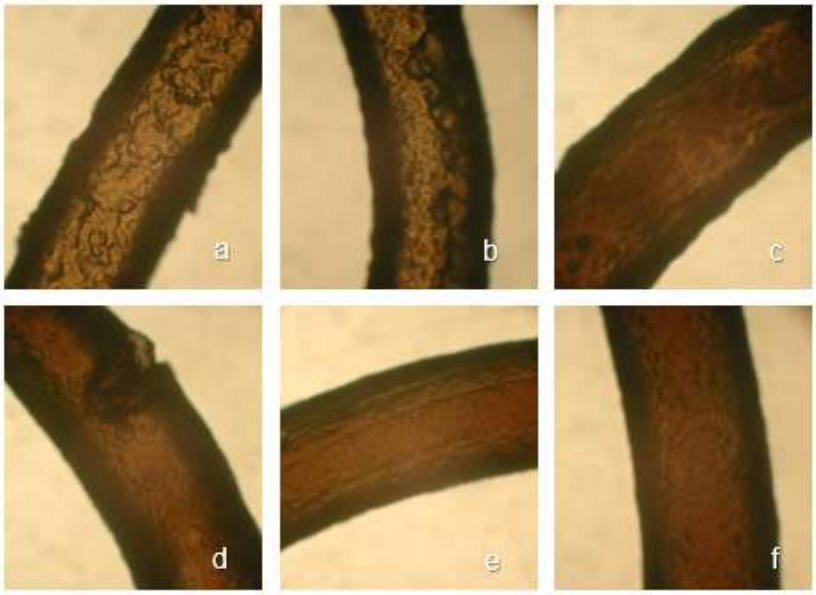

Figure 40. Optical microscopy pictures of the wet filaments a) PVA2 b) GA2 c) Guar4 d) PVA4 neutral bath e) PVA4 acidic bath f) GA4.

From optical microscopy figures can be seen that all the formed filaments are initially the same size when they are still moist as they were all spun with same needle. A noticable difference is that the 2 wt% dopes (a and b) are more translucent than the 4 wt% ones (c – f) due to concentration. The GA4 (f), PVA4 (d) and (e) seem to be more even on the surface than PVA2 (a), GA2 (b) and Guar4 (c) if the hole left by bubble in the PVA4 in neutral (d) filament is disregarded. This indicates that the PVA4 and GA4 dopes were best oriented in the system. Difference to Guar4 arises from the molecular weight when with the 2 wt% counterparts either the experienced lower shear didn't reach as good orientation of the mass transfer in coagulation bath relaxed the orientation more in less entangled network. The PVA4 in acidic bath (e) seems to have retained the shape from spinning as the grooves on the surface are most likely the result of in-house cut needles. The fact they are missing on GA4 could be just an indication of different needle being used with those or the grooves being only on one side.

10. 5 Fiber quality and evaluation

When the wet filaments were more in the size of a fine sock yarn with an approximately a diameter of slightly under 1mm, the dried filaments had shrunk to the size of a fishing line in the diameter range of 0.1 to 0.25 mm. Bellow in Figure 41 is the dried and collected filaments of PVA2 and PVA4 from acid baths as an example. From this can be seen that the larger bubbles caused significant imperfections to the filament. These imperfections weren't equally distributed along the filaments, indicating that some air could have gotten into them when loading the syringes.

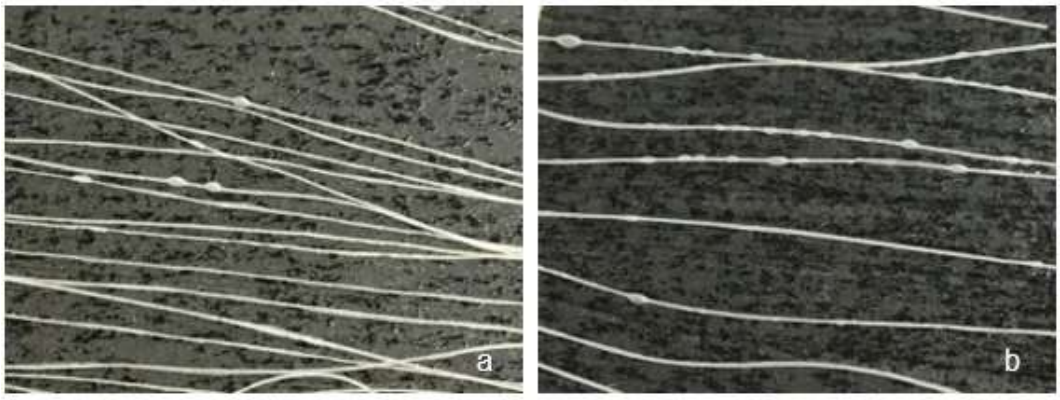

Figure 41. The dried filaments of a) PVA2 and b) PVA4.

The 2 wt% dopes were visually flatter compared to the 4 wt% ones and this was further studied in *the SEM images*. The SEM images from the cross sections are presented in Appendix 8 shows that none of the filaments are completely round. Some deformation caused to the cross section due to drying on a flat surface is visible. When with the 4 wt% ones only slight flatness indicated where it had lay on the drying surface, the 2 wt% ones formed thin flat parts on both sides of the thicker center. This was because those parts had attached to the surface and as the rest of the filament shrunk to the middle. The 4 wt% filaments displayed better shape stability because of better inner network only small portion touched the surface. SEM images also show that PVA2 was increasingly angular when the GA2 remained quite round. Possibly indicating that the inner sections of GA2 had crosslinked and thus better inner network was formed. The solvation of glutaraldehyde in ethanol could explain why it still formed similar flaps as the PVA2 dope.

Only rough estimation of the filament diameters can be made from these as the shapes vary even within the same dope and bubbles in the structure also interfere the estimation. Even then it is clear that the cross sections of the 2 wt% dopes are significantly smaller, indicating that they have shrunk the most in the drying. For the 4 wt% dopes, the higher concentration and entanglement degree resulted in better shape stability. As short LVR, higher yield stress, storage modulus, zero shear and consistency value all seemed to explain the differences between the 2 and 4 wt% dopes.

The SEM side view images are also presented in Appendix 8. In the side view images the 2 wt% filaments resembled eels with their fins, being cylinder shaped and having flat pieces protruding from the sides. From these can also be seen that the surfaces are rather smooth but the orientation of the fibers can be seen. Although compared to filaments in [6] without close to no surface roughness, the filaments prepared in this work had a coarser texture. They are also better than ones prepared by crosslinking before spinning where the increased degree of entanglements due to crosslinking has caused imperfections in significant heights [8]. In the filaments formed in this work, only PVA4 in neutral bath and the Guar4 dopes exhibited slightly different surface qualities. Most can be attributed to the neutral bath not forming the crosslinks like acidic bath. Thus the PVA4 neutral

looks more rough compared to the acidic bath one. As the height of imperfections is roughly the same only difference is that with the PVA4 in neutral possibly more PVA and CNF has come off with the mass transfer of water or just the orientation reached in the needle were decreased by the mass transfer. The Guar4 also has a higher molecular weight which makes it harder to orientate, resulting in larger imperfections.

Water stability of the filaments were expected to be relatively good as the raw materials needed the temperature of 90 °C to dissolve. Also due to small sample amount only basic visual evaluation was performed as the sample amounts were insufficient for weight analyses. All the samples retained the form of a filament the duration of 48 hours they were kept immersed. And visually no significant swelling was visible as they stayed virtually the same size as when dry. Although the immersion in water made them more bendable and also relaxed the shape the filaments were initially dried to. This difference didn't make them fragile and they could be easily recovered. This allows the filaments to be straightened out easier as the filaments don't swell and retain higher strength compared to the initial wet strength after spinning.

As *tensile testing* was executed with the expectation of round cross section it can be seen from the angularity in SEM images that it will overestimate the properties of the 2 wt% filaments. The stress strain curves are shown in Appendix 9. From these can be seen that the 2 wt% dopes were stronger compared to their 4 wt% counterparts. This is affected by the possible lesser orientation of 4 wt% dopes that causes them to retain higher cross-sectional area. Thus the maximum force in addition to maximum tensile stress will be studied to compare the effect of cross section to the results.

In the results the glutaraldehyde used in the GA dopes can be seen to result into more uniform quality indicates that some crosslinking might have happened during the 24 hour immersion time. The crosslinking from acidic bath alone also had slight effect but not as significant compared to glutaraldehyde. The effect of acidic bath in PVA filaments arises from the combination of the better retention of the inner structure during the mass transfer from the acid crosslinks thus being able to pull out as longer filaments where the end portions experiencing more contraction

during drying can be excluded. For all these reasons the orientation reached in the filaments spun to neutral baths are not expected to be as good as in the acidic bath. Especially as a slight increase in the diameter of them can be observed in the Table 8 where the Young's modulus and maximum tensile stress values are presented.

Table 8. Tensile testing results Young's modulus and maximum tensile stress with fiber diameter.

dope	filament diameter [mm]		Young's modulus [MPa]		maximum tensile stress [MPa]	
	mean	stdev	mean	stdev	mean	stdev
PVA2	0.110	±0.018	1380	±421	125	±39.98
GA2	0.111	±0.007	1225	±166	132	±15.94
PVA4 neutral	0.193	±0.006	624	±120	62	±17.03
PVA4 acidic	0.176	±0.013	821	±163	72	±15.08
GA4	0.177	±0.008	801	±225	74	±6.64
Guar4	0.226	±0.036	426	±158	34	±18.53

The Young's modulus and maximum tensile stresses had significant variation in the values resulting the standard deviation being up to half the mean value. Thus the data was tested for outliers by grubs test using the Young's modulus values [57]. The stabilizing effect of glutaraldehyde can be seen as better standard deviation but the effect to the average tensile property values observed are insignificant. Although the GA2 could be wrongly qualified as weaker because the cross section of PVA2 was more angular and thus diameter measured results into under estimating the cross-sectional area. Compared to the GA crosslinking the effect arising from the acidic bath with PVA is more significant. The average property values are higher and they have less deviation. The acidic bath increases the Young's modulus by even 200 MPa. The poor values reached by Guar4 with wider cross section further verifies the poor orientation.

The differences in the dopes cannot be properly correlated to the rheological results as there is more variables involved due to using different coagulation baths and attempted crosslinking. The differences between the 2 and 4 wt% corresponding dopes seem to arise from the increased entanglement degree which also affects LVR, yield stress, storage modulus, consistency and the non-Newtonian index. Thus seems that the $\tan\delta$, G^* and η^* were the least representative of the spinnability in this work. The difference between the 2 and 4

wt% dopes can be further studied from the maximum force and elongation that don't take the fiber diameter into consideration. Thus it answers if the 2 wt% dopes actually are stronger in comparison or if the underestimated cross section only makes it look like it. The force and elongations are presented in Table 9.

Table 9.Maximum force and maximum elongation of the filaments.

	maximum force [N]		maximum elongation [%]	
dope	mean	stdev	mean	stdev
PVA2	1.15	0.220	38.9	0.158
GA2	1.27	0.153	48.5	0.087
PVA4 neutral	1.79	0.480	43.7	0.228
PVA4 acidic	1.72	0.262	39.1	0.151
GA4	1.83	0.167	43.2	0.113
Guar4	1.11	0.532	20.1	0.070

The results show that the higher concentration leads to better ultimate force. When comparing the maximum force to the wt% the PVA2 and GA2 reaching 68 to 69 % of the force of corresponding 4 wt% filament indicates that they have slightly better reinforcing effect. The most probable cause for this is their easier orientation due to less entanglements, which effect on better orienting in lower shear can be seen from the flow curves. Also higher contraction caused by drying of the low concentration dopes when drying under tension could also favor the orientation.

The effect of GA can be seen to be more significant for the 2 wt% dopes. The effect was especially significant on the elongation. This could be understood to mean that only low crosslinking was reached, as high crosslinking would prevent relative movement of the chains. In regards of maximum forces there wasn't as significant difference between the dopes. The PVA4 neutral reached even slightly higher absolute strength due to the better orientation of PVA4 acidic not overcoming the effects of wider diameter. The difference from orientation isn't so important when the best orientation reached is still quite preliminary.

The values of the best filaments, PVA2 and GA2, are compared to previous filaments made using PVA and CNF in the Table 10 that were presented in the material information part of the literature review. This is because properly comparable PVA filaments could not be spun due to the consistency resulting mainly from the CNF fibers. Also the previously prepared filaments are made using

different CNF types (SCNF, TOCN and EFP) and most also used significantly lower concentration. Thus they are not ideally comparable, especially as most of them have been subjected to both wet and heat drawing inducing more strength. The filaments in this work were not even oven dried as the GA4 filaments exhibited charring in 120 °C oven due to residual acid.

Table 10. Other PVA/CNF composite fibers.

Filament	PVA/SCNF [6]	PVA/TOCN [9]			PVA/GA/EFP [8]		PVA2	GA2
PVA (mw/wt%)	85,000-24,000/9	75,000/10			195,000/5	195,000/4.4	195,000/1	
CNF (l/d/wt%)	15 – 28 /0.54	100/0.1			---/5	---/6.7	50 – 100/1	
GA wt% to solids	0	0			0.05	0.04	0	10
total draw ratio	27	20	10	3	0	0	0	0
Young's modulus [GPa]	32.3	57	32.5	5	2.3	3.4	1.38	1.22
Max tensile stress [GPa]	0.828	1.7	1	0.25	0.039	0.079	0.125	0.132
strain at break [%]	5.25	5.25	8.5	---	2.5	4.9	38.9	48.5

The values reached with Young's modulus are at best 4 % and the maximum strength 15% of the PVA/SCNF filaments prepared by Peng et al. and similarly only fraction of the PVA/TOCN filaments prepared by Endo et al. [6, 9]. Although as Endo et al. have reported values for filaments drawn to different draw ratios the significant effect of drawing can be seen [9]. This was already highlighted in the spinning setup and phenomena to be the most relevant stage in inducing the orientation and thus strengthening to the filament. When the effect of drawing is taken into account the fibers in this work could be comparable to the ones prepared by Peng et al. and Endo et al. if they were not drawn [9, 6]. This because the transition from draw ratio 3 to 10 exhibits significant increase both in Young's (5 to 32 GPa) modulus and tensile stress (0.25 to 1) and the effect of drawing then diminishes as it is taken further. If similar magnitude of increase could be expected the filaments could be easily comparable. [9]

If the drawing capability of the filaments is connected to the strain at break as the strain value reached can be seen to decrease the further the PVA/TOCN filaments are drawn [9]. the high strain rates recorded with the prepared filaments in this work would indicate that they have good drawing capability. If the crosslinking of

could be executed further it could potentially increase the Young's modulus to comparable with PVA/GA/EFP by Spoljaric et al., when in return decreasing the elongation. The maximum tensile stress could also be seen to lower with increased crosslinking degree, as it can have prevented the orientation when done prior to spinning. [8]

Even though the tensile testing gives indications that some crosslinking occurred with the GA2 and GA4, the dopes were further studied. The *IR spectroscopy* was used to compare the PVA and GA dopes together and to the spectra of pure CNF (1.35 wt%) and PVA (raw material flakes). The spectras are shown in the Figure 42 bellow.

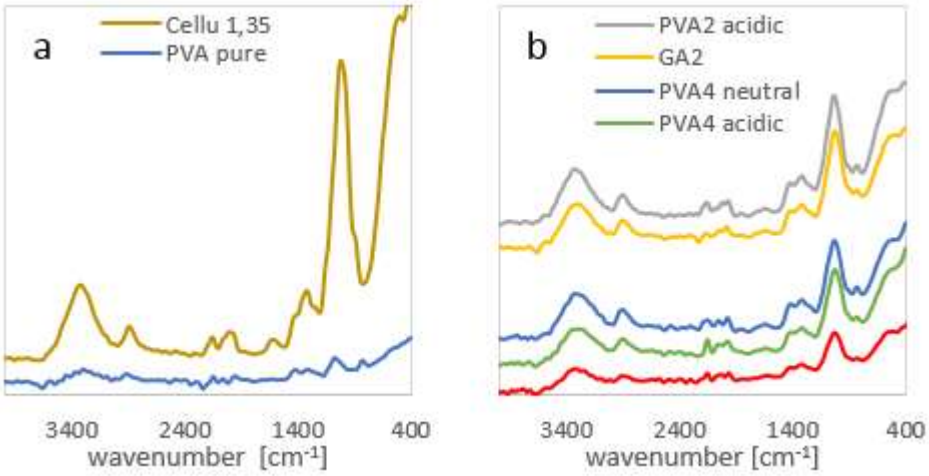

Figure 42. The IR spectra for a) raw materials b) the filaments.

From the spectra it is obvious that the filaments are the combinations of the PVA and CNF spectra so that both materials are present in the surface. The peak intensities around 3300 cm^{-1} visibly changes between the PVA and GA equivalents. This would indicate that GA in the dope resulted into more PVA being present on the surface. Similar trend was seen for PVA4 in acidic bath. Thus it indicates that acidic conditions and GA crosslinking caused there to be more PVA present on the surface. This could mean that the sedimentation observed in the coagulation bath could have been caused by PVA stripped from the filament with the mass transfer of water out. The intensities of the hydroxyl group stretching visible from peat at 3300 cm^{-1} is shown in Figure 43.

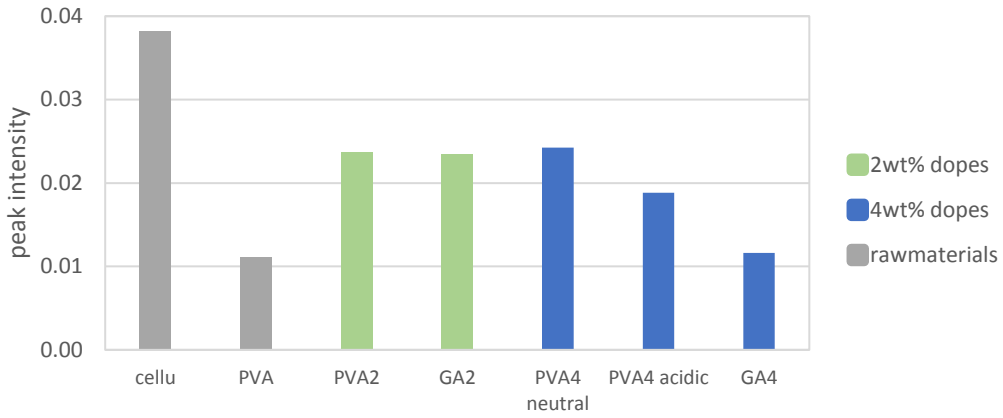

Figure 43. Intensities of the IR spectra's for the OH-group stretching

The 4 wt% dopes have clear trend of increased PVA on the surface which is affected both the acid crosslinking and the glutaraldehyde. Explaining the differences seen in the SEM between the PVA filaments spun in acidic and neutral baths. The difference in the 2 wt% dopes is almost non-existent. In addition to more PVA on the surface nothing else can be seen. The peaks indicating of GA and PVA crosslinking are not visible. For this there should be an intense duplet at 2931 and 2863 cm^{-1}, narrowing of the 3300 cm^{-1} peak as hydrogen bonding decreases and the 1075 cm^{-1} peak being replaced by two peaks at 1250 cm^{-1} [8]. The absence of these changes doesn't exclude some crosslinking occurring inside the filament or extremely low degree of crosslinking on the surface. Although it can also indicate that crosslinking didn't occur due to glutaraldehyde dissolcing into the ethanol before crosslinking ca occur [41].

In *the ^{13}C NMR* only the dopes spun in acidic baths (PVA2, GA2, PVA4 and GA4) were compared as with the PVA4 spun into neutral bath the sample amount was not sufficient. The samples were compared against each other to mainly compare the peak at 91.4 ppm that has previously been used as indication of crosslinking by Spoljaric et al.. This comes from glutaraldehyde participating in acetal linkage, which is it's method of crosslinking hydroxyl groups as presented in material information portion of literature review. [8] The Spectra of the PVA and GA filaments are shown in Figure 44.

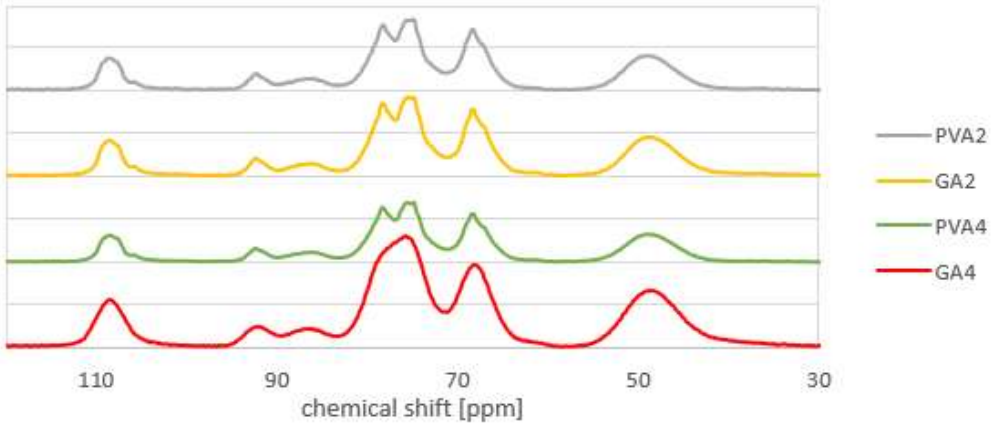

Figure 44. The ^{13}C NMR spectras for the PVA and GA dopes.

Unfortunately the resolution of Figure 44 wasn't good and especially for the GA4 the peaks were inaccurate and blunt. Thus making the comparison of the peaks harder. Otherwise the spectras are highly similar to previous filaments prepared with PVA, CNF and glutaraldehyde by Spoljaric et al. where the spectras were much more defined. In the spectra the peaks 107.7, 91.6, 86.3, 77.7, 74.1 and 67.6 are related to CNF, when the peaks related to PVA are 79.3, 73.6, 67.7 and 47.6.

Of which due to peaks overlaying each other the peak at 47.6 resulting from C_2 is best indicative of PVA and the peaks 86.3 from C_4 amorphous zones and 107.7 from C_1 correspond best to CNF. The increasing prominence of 91.4 can be used as indication of crosslinking [8]. Although due to poor resolution visual evaluation could not be done. At least there isn't significant peaks indicating of the presense of unreacted glutaraldehyde [58]. This could either indicate of significantly low glutaraldehyde concentration in the resulting filaments or successful crosslinking.

11 Conclusions and future applicability

The effect of consistency in 1:1 CNF to polymer containing dopes were tested by changing the solids content from 2 to 4 wt% and changing the matrix composition. Pure PVA matrix acted as the baseline when guar was used to increase the high molecular weight content and crosslinking was tested by introducing GA as crosslinking agent. The crosslinking was tested both with acidic coagulation bath and introducing the acid into the dope before spinning into neutral bath. For

reference the PVA/CNF dopes forming the baseline were spun into both neutral and acidic baths to compare if it had an effect. Prior to the spinning the dope masses were tested for rheology (amplitude and frequency sweep as well as steady shear measurements) that was compared to the spinnability in the gel spinning process and the quality of the formed products in tensile testing.

Best to the spinnability correlated the gel strength, storage modulus and LVR values. Other parameters also having some correlation to spinnability were zero shear, consistency value (k), viscosity at high shear rates and structure formation in the shear rate curve. Of these the gel strength could act as stand alone for comparing which one should be best spinnable, when the others provide explanations for the observed differences in the spinnability. Some rheological parameters instead didn't have observable correlations in this work but could prove to be usefull with other dopes or spinning system parameter ranges. These were the dynamic and longest relaxation times, tanδ, complex modulus, complex viscosity and shear rate at wall.

The gel strength presented by yield stress from amplitude sweep correlated well with the filament formation ability in the air gap. Higher strength favoured the form retention of the fluid jet after the needle. The strength range of 35 – 45 Pa allowed the formation of incipient filaments instead of droplets in the air gap and range of 60 – 80 Pa allowed the filament to continue into the coagulation bath without breaking via an air gap. Higher gel strength of 80 Pa was also needed in the neutral coagulation bath for the filament to retain its shape during the 24 h immersion time. The acid in the coagulation bath instead allowed even the weakest one with 20 Pa gel strength to retain the filament shape. Thus acidity could be used to enhance the spinnability. Optimizing the coagulation conditions will affect the lowest needed gel strength whereas the gel strength required for using the air gap will most likely be less affected by changing parameters. The viscosity values in flow curve at high shear rate also roughly correspond to the dopes ability to retain the filament shape. Although as the dopes experience different shear rates in the spinning system it is not as usable as gel strength.

The storage modulus values from frequency sweep instead gives indications of entanglement degree and dispersion state. The entanglement degree is related to

the storage modulus value, where a value lower than expected from the concentration and molecular weight, indicates a possibility of poor dispersion. Especially the 4 wt% dope containing guar didn't show expected entanglement degree increase that should result from the higher molecular weight portion. Thus it is expected that CNF dispersion was not ideal and resulted in poor reinforcement of the formed filaments. The effective network from zero shear also indicates that concentration increase in guar containing dopes didn't increase network as expected. Proving the inefficient network formation. The acid containing dopes didn't exhibit similar dispersion problems as the acid increasing the interactions was added after the dispersion of CNFs in the matrix. Although the flow curve would suggest that the interactions formed by acid break off easily. Optimal entanglement degree also needs to be found as inadequate entanglements or excess hinder the reached reinforcement. From the 2 and 4 wt% dope sets can be seen that the amount of entanglements affected the gel strength. With 2 wt% dopes it increased with the increasing entanglements whereas with 4 wt% dopes it decreased. The PVA4 seemed to have the most optimal entanglement degree as it resulted into the best gel strength.

Acid crosslinking in the dope also resulted them to appear most solid like with the shortest *LVR lengths*. The increased entanglement degree affects dopes similarly. From the results it would seem that lower gel strength requires longer LVR. The 2 wt% dopes with low gel strength required twice as long LVR compared to 4 wt% dopes. With further study a gel strength to LVR ratio could possibly be found but for these dopes the 2 wt% required the LVR to continue to 2 % strain value when the 4 wt% dopes the LVR up to value 1 % strain was sufficient. These LVR values alone don't ensure successful spinning as the 2 wt% dopes required the acid in the bath to increase viscosity/solid like behaviour to retain the shape over the 24 h immersion. Thus the filament formation is still highly dependent on the coagulation bath conditions.

The stability test indicated that no GA based crosslinking occurred in the crosslinker containing dopes as during the 20 minute time frame their behaviour didn't noticeably differ from the other dopes. This indicated that if crosslinking occurred it should have occurred in the coagulation bath over the 24 h immersion. The IR spectrometry and ^{13}C NMR measurements couldn't accurately determine if

crosslinking had occurred. The most significant difference between the PVA and GA dopes was the more constant and slightly enhanced tensile properties of the dry filaments. As the peaks indicating the lack of pure GA in the filaments, it would indicate that either all the GA reacted or some was dissolved in the coagulation bath. Most likely only small degree of crosslinking was reached in the filaments. In the future the effect of crosslinking could be further studied as it had positive effect on the filaments. Possible routes could be ensuring crosslinking over longer time period or attempting to optimize for faster crosslinking. Cold coagulation bath containing crosslinker could ensure good coagulation and throughout crosslinking over longer time period. Hotter coagulation bath could compromise coagulation but in case coagulation occurred it could result in crosslinking before all crosslinker was dissolved.

The rheological parameters couldn't be properly correlated to the resulting filament properties as only few of the dopes yielded filaments in the end. Most of the formed filaments were affected by the acid coagulation bath and thus could not be correlated to properties measured without the effect from the acid. Only the PVA4 and Guar4 dopes spun to neutral bath could be compared. And due to this only the visible effect from entanglements affecting the orientation and attained strength could be seen. The increased entanglement degree in Guar4 filaments resulted into wider cross section and poor tensile properties. Comparing the PVA4 dopes spun to acid and neutral baths it can be seen that the acid bath retained the inner orientation better in the coagulation bath, as the crossection was smaller and tensile properties increased. The tensile properties could be in the same range as previous CNF containing filaments if additional drawing could be induced to the filaments.

Of the parameters that were not found to be usable in this work most probably would be more important if the dopes were not considered as gel in low frequencies. So if the dopes were liquid like in low frequency or shear values $\tan\delta$, shear at wall and the relaxation times would become more important. In that case they would probably determine the spinnability ranges for the dopes or just plain determine if the dope is spinnable in the chosen condition. Of the parameters the complex modulus and complex viscosity gave least information of the used dopes.

Bibliography

[1] Suurnäkki, A., Cellulosefromfinland.fi, http://cellulosefromfinland.fi/design-driven-value-chains-in-the-world-of-cellulose/, 2.1.2017.

[2] Martoia, F., Perge C., Dumont, P.J.J., Orgeas, L., Fardin, M.A., Manneville, S. and Belgacem, M.N., Heterogeneous flow kinematics of cellulose nanofibril suspensions under shear, Soft matter 11 (2015) 4742 - 4755.

[3] Dimic-Misic, K., Micro and nanofibrillated cellulose (MNFC) as additive in complex suspensions: influence on rheology and dewatering, Doctoral Dissertation, Aalto University publication series Doctoral Dissertations 73/2014, Helsinki 2014, 281 s.

[4] Haward, S.J., Sharma, V., Butts, C.P., McKinley, G.H., Rahatekar, S.S., Shear and Extensional Rheology of Cellulose/Ionic Liquid Solutions, Biomacromolecules 13 (2012) 1688 - 1699.

[5] Kangas, H., Cellulosefromfinland.fi, http://cellulosefromfinland.fi/nanocellulose/, 2.1.2017.

[6] Peng, J., Ellingham, T., Sabo, R., Turng, L. and Clemons, C.M., Short cellulose nanofibrils as reinforcement in polyvinyl alcohol fiber, Cellulose 21 (2014) 4287 - 4298.

[7] Anonymous, Cellulosefromfinland.fi, http://cellulosefromfinland.fi/nanocellulose-filaments-for-composite-reinforcement/, 2.1.2017.

[8] Spoljaric, S., Auvinen, H., Orelma, H., Pere, J. and Seppälä, J., Enzymatically fibrillated cellulose pulp-based monofilaments spun from water; enhancement of mechanical properties and water stability, Cellulose 24 (2017) 871 - 887.

[9] Endo, R., Saito, T. and Isogai, A, TEMPO-oxidized cellulose nanofibril/poly(vinyl alcohol) composite drawn fibers, Polymer 54 (2013) 935 - 941.

[10] Uddin, A.J., Araki, J., Gotoh, Y., Characterization of the poly(vinyl alcohol)/cellulose whisker gel spun fibers, Composites: Part A 42 (2011) 741 - 747.

[11] Chen, Y., Xu, C., Huang, J., Wu, D., Lv, Q., Rheological properties of nanocrystalline cellulose suspensions, Carbohydrate Polymers 157 (2017) 303 - 310.

[12] Carnecki, P., Thermal and rheological characterization of cellulose spinning dopes modified with nanosilica and antibacterial agents, Polym. Adv. Technol. 18 (2007) 845 - 852.

[13] Niu, R., Gong, J., Xu, D., Tang, T. and Sun, Z., Influence of molecular weight of polymer matrix on the structure and rheological properties of graphene oxide/polydimethylsiloxane composites, Polymer 55 (2014) 5445 - 5453.

[14] Saastamoinen, J., Influence of the solute's molecular weight distribution on the spinnability of cellulose-ionic liquid solutions, Master's thesis, School of Electrical Engineering, Espoo 2011, 60 s.

[15] Eirich, F.R., Rheology Theory And Applications Vol III, Academic Press Inc, Brooklyn 1960, ss 569 - 587.

[16] de Haan, A.B., Process Technology - An Introduction, De Gruyter, Delft 2015, ss 366 - 368.

[17] Liu, S., Jiang, H., Du, W. and Pan, D., Spinnability in Pre-gelled Gel Spinning of Polyacrylonitrile Precursor Fibers, Fibers and Polymers 13 (7) (2012) 846 - 849.

[18] Chae, H.G., Newcomb, B.A., Gulgunje, P.V., Liu, Y., Gupta, K.K., Kamath, M.G., Lyons, K.M., Ghoshal, S., Pramanik, C., Giannuzzi, L., Sahin, K., Chasiotis, I. and Kumar, S., High strength and high modulus carbon fibers, Carbon 93 (2015) 81 - 87.

[19] Tang, C., Saquing, C.D., Harding, J.R. and Khan, S.A., In Situ Cross-Linking of Electrospun Poly(vinyl alcohol) Nanofibers, Macromolecules 43 (2010) 630 - 637.

[20] Nic, M., Jirat, J., Kosata, B. and A. Jenkins, IUPAC GoldBook, https://goldbook.iupac.org/html/G/G02600.html, 27.06.2017.

[21] Gupta, V.B. and Kothari, V.K., Manufactured Fibre Technology, Springer Science & Business Media, delhi 2012, ss 1 - 50.

[22] Bralla, J.G., Handbook of Manufacturing Processes - How Products, Components and Materials are Made, Industrial press, New York 2007, ss. 385 - 387.

[23] Imura, Y., Hogan, R.M.C. and Jaffe, M., Dry spinning of synthetic polymer fibers, in Advances in filament yarn spinning of textiles and polymers, Woodhead Publishing Limited, Cambridge 2014, ss. 187 - 202.

[24] Morrison, F.A., Understanding Rheology, Oxford University Press, New York 2001, ss 382 - 390.

[25] Hashim, A.N., Liu, F., Abed, M.M.R., Li, K., Chemistry in spinning solutions: Surface modification of PVDF membranes during phase inversion, Journal of Membrane Science 425 - 426 (2012) 399 - 411.

[26] Quin, J. and Chung, T., Effect of dope flow rate on the morphology, separation performance, thermal and mechanical properties of ultrafiltration hollow fibre membranes, J. Membr. Sci. 157 (1999) 35 - 51.

[27] Zhou, L., He, H., Li, M., Song, K., Cheng, H.N. and Wu, Q., Morphological influence of cellulose nanoparticles (CNs) from cottonseed hulls on rheological properties of polyvinyl alcohol/CN suspensions, Carbohydrate Polymers 153 (2016) 445 - 454.

[28] Hauru, L.K.J., Hummel, M., Nieminen, K., Michud, A. and Sixta, H., Cellulose regeneration and spinnability from ionic liquids, Soft Matter 12 (2016) 1487 - 1495.

[29] Shenoy, S.L., Bates, D.W., Frisch, H.L. and Wnek, G.E., Role of chain entanglements on fiber formation during electrospinning of polymer solutions: good solvent, non-specific polymer–polymer interaction limit, Polymer 46 (2005) 3372 - 3384.

[30] Zhang, S., Li, F. and Yu, J., Rheological properties of cellulose-NaOH complex solutions: from dilute to concentrated states, Cellul. Chem. Technol. 45 (5-6) (2011) 313 - 320.

[31] Han, J., Lei, T. and Wu, Q., High-water-content mouldable polyvinyl alcohol-borax hydrogels reinforced by well-dispersed cellulose

nanoparticles: Dynamic rheological properties and hydrogel formation mechanism, Carbohydrate Polymers 102 (2014) 306 - 316.

[32] Tanpichai, S. and Oksman, K., Cross-linked nanocomposite hydrogels based on cellulose nanocrystals and PVA: Mechanical properties and creep recovery, Composites: Part A 88 (2016) 226 - 233.

[33] Nechyporchuk, O., Belgacem, M.N. and Pignon, F., Rheological properties of micro-/nanofibrillated cellulose suspensions: Wall-slip and shear banding phenomena, Carbohydrate polymers 112 (2014) 432 - 439.

[34] Rakesh, G. and Deshpande, A.P., Rheology of crosslinking poly vinyl alcohol systems during film formation and gelation, Rheol Acta 49 (2010) 1029 - 1039.

[35] Fonseca dos Reis, E., Campos, F.S., Pereira Lage, A., Cerqueira Leite, R., Guilherme Heneine, L., Luiz asconcelos, W., Ines portela Lobato, Z. and Sander Mansur, H., Synthesis and Characterization of Poly (Vinyl Alcohol) Hydrogels and Hybrids for rMPB70 Protein Adsorption, Material Research 9 (2) (2006) 185 - 191.

[36] Anonymous, Sigma-Aldrich, http://www.sigmaaldrich.com/catalog/substance/mowiol569812345900289511?lang=fi&region=FI, 12.1.2016.

[37] Thombare, N., Jha, U., Mishra, S. and Siddiqui, M.Z., Guar gum as a promising starting material for diverse applications: A review, Int. J. Biol. Macromol. 88 (2016) 361 - 372.

[38] Lv, R., Kong, Q., Mou, H. and Fu, X., Effect of guar gum on stability and physical properties of orange juice, Int. J. Biol. Macromol. 98 (2017) 565 - 574.

[39] Szopinski, D. and Luinstra, G A., Viscoelastic properties of aqueous guar gum derivative solutions under large amplitude oscillatory shear (LAOS), Carbohydrate Polymers 153 (2016) 312 - 319.

[40] King, H., geology.com, http://geology.com/stories/13/guar-beans-and-hydraulic-fracturing/, 03.01.2017.

[41] Anonymous, Alibaba.com, https://www.alibaba.com/product-detail/Gluteraldehyde-Glutaraldehyde-Sterilization-Glutaraldehyde-Solution-50_60542619628.html?s=p, 3.1.2017.

[42] Thombare, N., Jha, U., Mishra, S. and Siddiqui, M.Z., Guar gum as a promising starting material for diverse applications: A review, Int. J. Biol. Macromol. 88 (2016) 361 - 372.

[43] Franck, A., TA Instruments, http://www.tainstruments.com/pdf/literature/AAN016_V1_U_StructFluids.pdf, 11.1.2016.

[44] Hill, A., Malvern, http://www.atascientific.com.au/eventsandtraining/eventsandtraining/wp-content/uploads/2013/01/Rheology-Basics-Introduction-to-Rheology-and-Kinexus.pdf, 12.13.2016.

[45] Anonymous, TA Instruments, http://pages.mtu.edu/~fmorriso/cm4655/TAInstruments/2013TA_10stepstogoodrheolmeasurements.pdf, 11.14.2016.

[46] Anonymous, Centre for industrial rheology, http://www.rheologyschool.com/advice/rheology-glossary, 10.1.2016.

[47] Anonymous, TA Instruments, http://www.tainstruments.com/pdf/literature/RS23.pdf, 11.1.2016.

[48] Yang, M.C., Scriven, L.E. and Macosko, C.W., Some Rheological Measurements on Magnetic Iron Oxide Suspensions in Silicone Oil, Journal of Rheology 30 (1986) 1015 - 1029.

[49] Castro, M., Giles, D.W., Macosko, C.W. and Moaddel, T., Comparison of methods to measure yield stress of soft solids, J. Rheol. 54 (81) (2010) 81 - 94.

[50] Hummel, M., Michud, A. and Sixta, H., Extensional rheology of cellulose-ionic liquid solutions, Annu. Trans. Nord. Rheol. Soc. 19 (2011) 313 - 319.

[51] Anonymous, Centre for industrial rheology, http://www.rheologyschool.com/testing/testing-examples, 10.1.2016.

[52] Idris, A., Ismail, A.F., Gordeyev, S A. and Shilton, S.J., Effect of rheological behavior of cellulose acetate spinning solutions on

performance of reverse osmosis hollow fiber membranes, Jurnal Teknologi 37 (2002) 1-14.

[53] Henke Sass Wolf, Anonymous, Henke Sass Wolf, https://www.henkesasswolf.de/cms/en/med_consumables_dental/syringes_needles/disposable_syringes/hsw_norm_ject_2/, 1.14.2017.

[54] Anonymous, Terumo pharmaseutical solutions, http://www.terumo-europe.com/en-emea/pharmaceutical-solutions/needles/hypodermic-needles/neolus®-hypodermic-needles, 1.14.2017.

[55] Anonymous, B Braun, https://www.bbraun.com/content/dam/b-braun/global/website/products-and-therapies/oem/brochures/Syringes_and_Needles_en_Edition_01-2014.pdf.bb-.46351419/Syringes_and_Needles_en_Edition_01-2014.pdf, 1.14.2017.

[56] Anonymous, Suomalainen kirjakauppa, http://www.suomalainen.com/webapp/wcs/stores/servlet/fi/skk/kontaktimuovi-40cm-x-5m-p519696--77, 11.12.2016.

[57] Anonymous, GraphPad, https://graphpad.com/quickcalcs/Grubbs1.cfm, 2.15.2017.

[58] Whipple, E.B. and Ruta, M., Structure of Aqueous Glutaraldehyde, J. Org. Chem 39 (12) (1974) 1666 - 1668.

Table 1. Cellulose raw material information.

cellulose	Cup [g]	cup+sample [g]	Dry [g]	dryweight [wt%]	mean [wt%]	standard deviation
driedCellu	1.886	7.499	2.225	4.521	4.521	0.000361
driedCellu	1.903	6.912	2.215	4.521		
undriedCellu	1.885	9.083	2.009	1.362	1.360	0.001946
undriedCellu	1.893	10.184	2.032	1.358		

Table 2. Polymeric raw material solutions information from measured amounts.

polymer solution	rawPVA4			rawPVA3/Guar1	
	BATCH1	BATCH2	BATCH3	BATCH1	BATCH2
water [g]	336.020	336.080	336.220	335.960	336.000
PVA4 [g]	14.004	14.006	14.030	10.510	10.503
Guar [g]	---	---	---	3.501	3.502
PVA4 [wt%]	4.001	4.001	4.006	3.003	3.001
Guar [wt%]	---	---	---	1.000	1.000
dryweight [wt%]	4.001	4.001	4.006	4.004	4.001
mean [wt%]	4.002			4.002	
standard deviation	0.00235			0.00116	

Table 1. Specific contents of raw dopes used to prepare the dopes used.

materials	rawDopes							
	A	B	A	B	C	B	A	B
	PVA2		PVA4				Guar2	Guar4
water [g]	4.41	4.45	17.36	17.4	17.5	17.56	4.56	17.37
rawPVA4 [g]	75.01	74.95	150.09	150	150.04	150.34	---	---
rawPVA3/ Guar1 [g]	---	---	---	---	---	---	74.17	150.02
Rawcellu consentration [wt%]	1.360	1.360	4.521	4.521	4.521	4.521	1.360	4.521
raw cellulose [g]	220.6	220.64	132.81	132.72	132.77	132.71	220.64	132.79
PVA4 [wt%]	1.001	1.000	2.001	2.000	2.000	2.002	0.744	1.500
Guar1 [wt%]							0.248	0.500
cellulose [wt%]	1.000	1.000	2.000	1.999	1.999	1.996	1.002	2.000

Table 2. Spesific dope contents.

rawDopes/ materials		Dopes							
		PVA2	GA2	Guar2	Ga+acid2	PVA4	GA4	Guar4	GA+acid4
A	PVA2	***			15.64				
B	PVA2		150.45		134.98				
A	PVA4					***			
B	PVA4						300.12		
C	PVA4								150
A	Guar2			***					
B	Guar4							***	
	GA [ml]		0.6		0.6		2.4		1.2
	HCL [ml]				1.2				1.4

*** = unqualified amount of the dope was used as it was

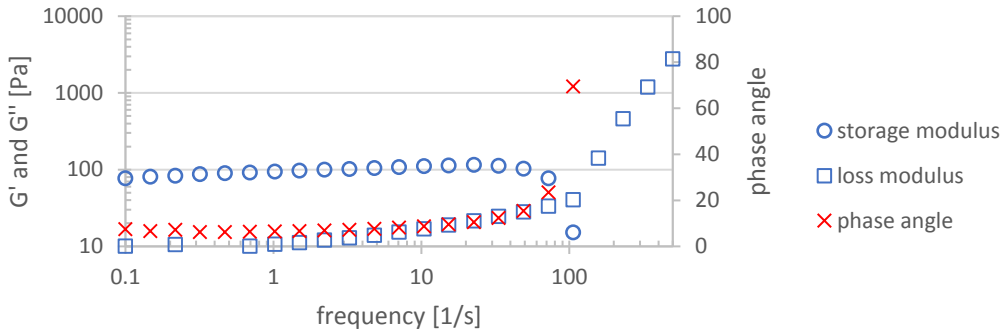

Figure 1. PVA2 frequency sweep.

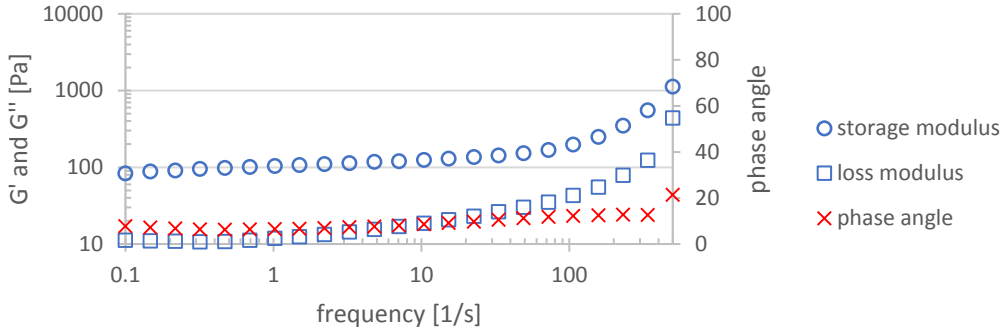

Figure 2. GA2 frequency sweep.

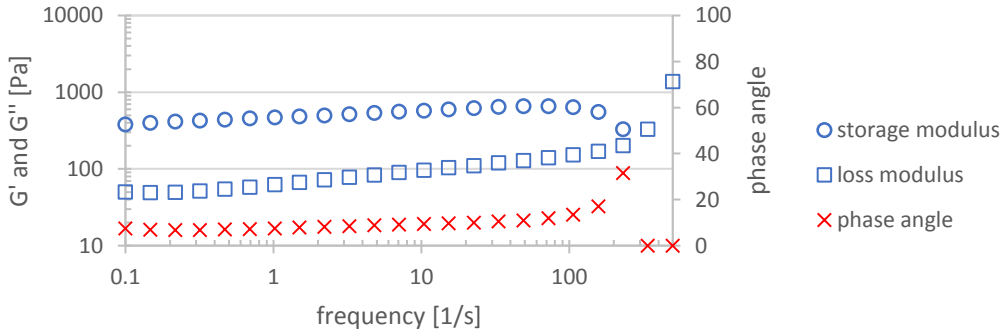

Figure 3. Guar2 frequency sweep.

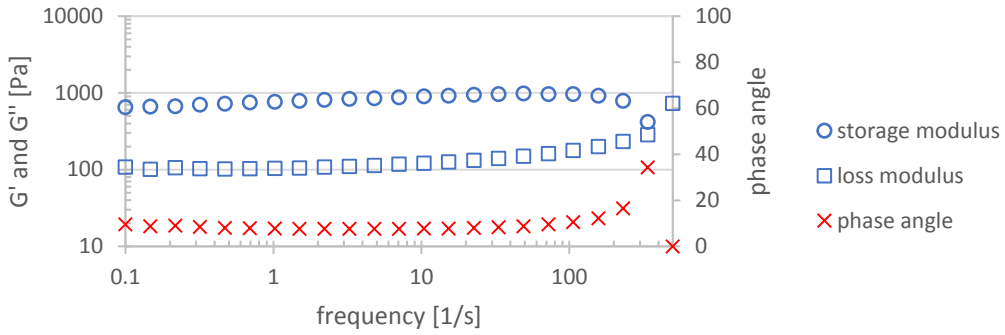

Figure 4. GA+acid2 frequency sweep.

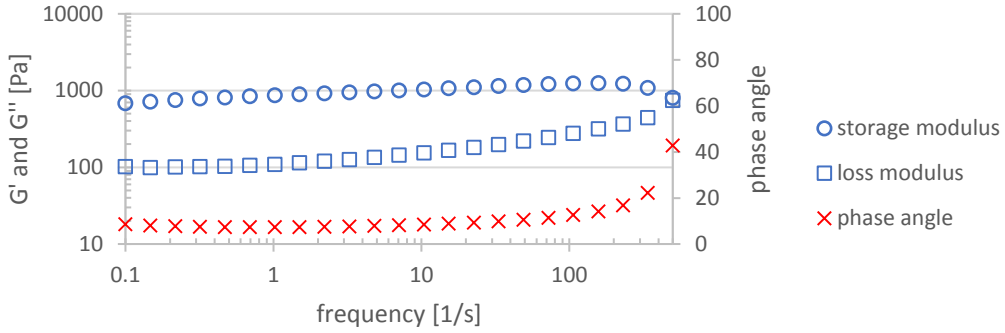

Figure 5. PVA4 frequency sweep.

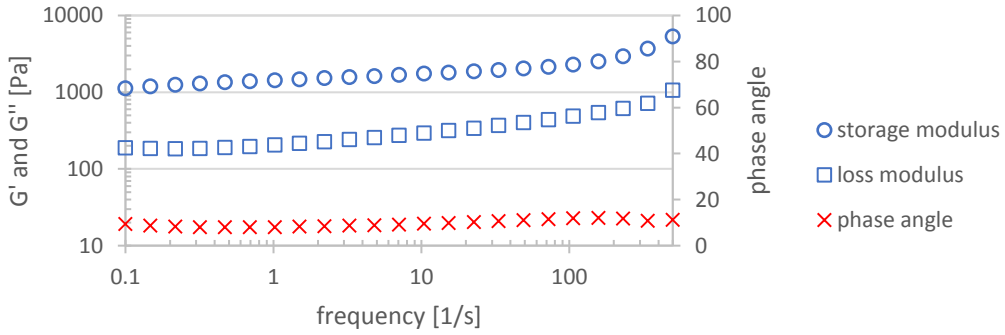

Figure 6. GA4 frequency sweep.

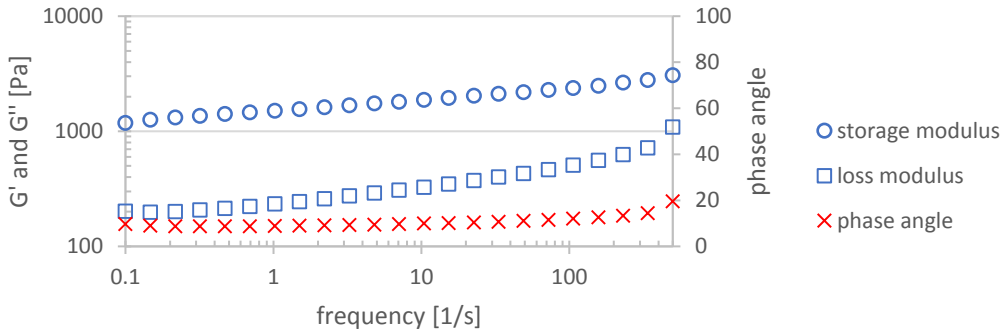

Figure 7. Guar4 frequency sweep.

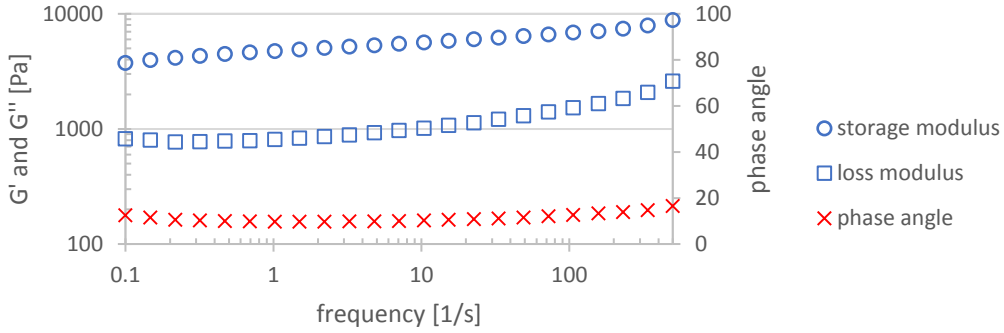

Figure 8. GA+acid4 frequency sweep.

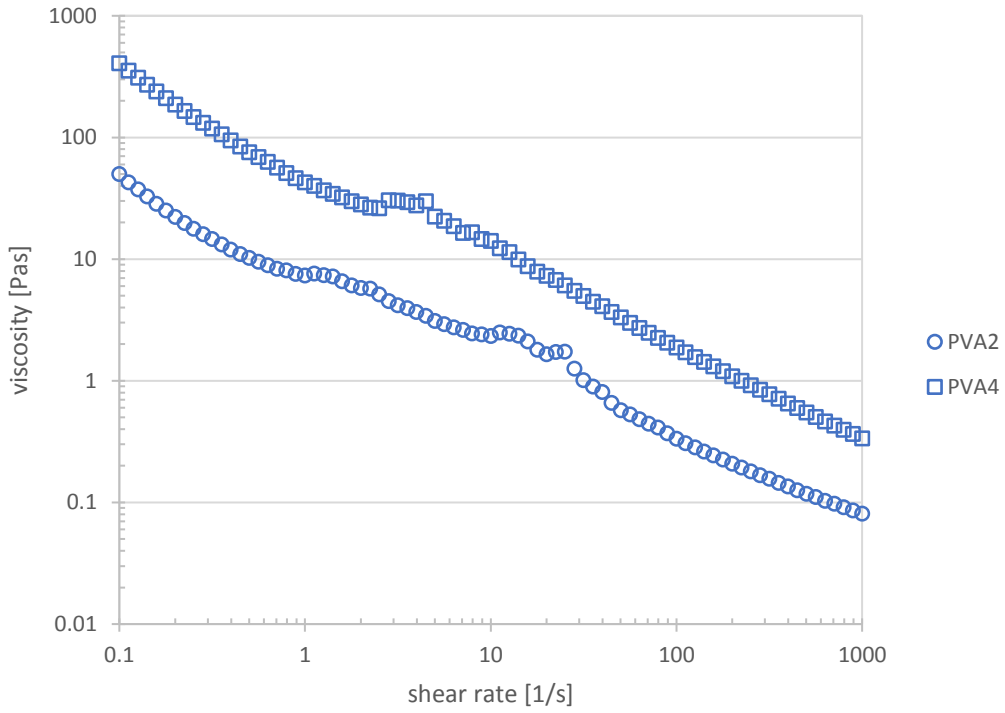

Figure 1. The PVA flow diagrams.

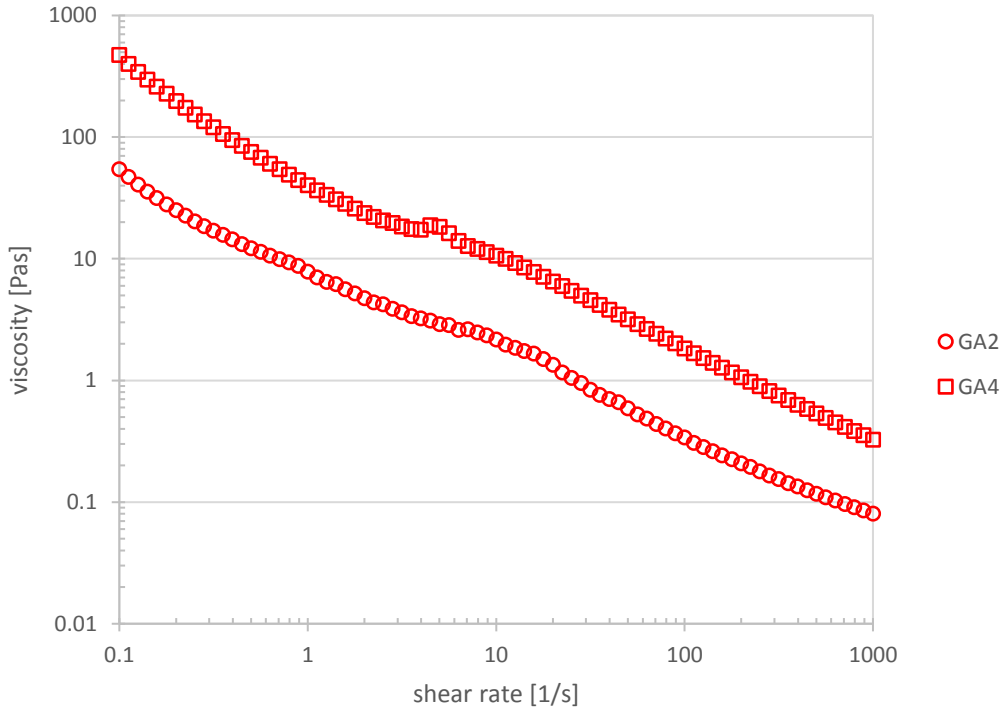

Figure 2. The GA flow diagrams

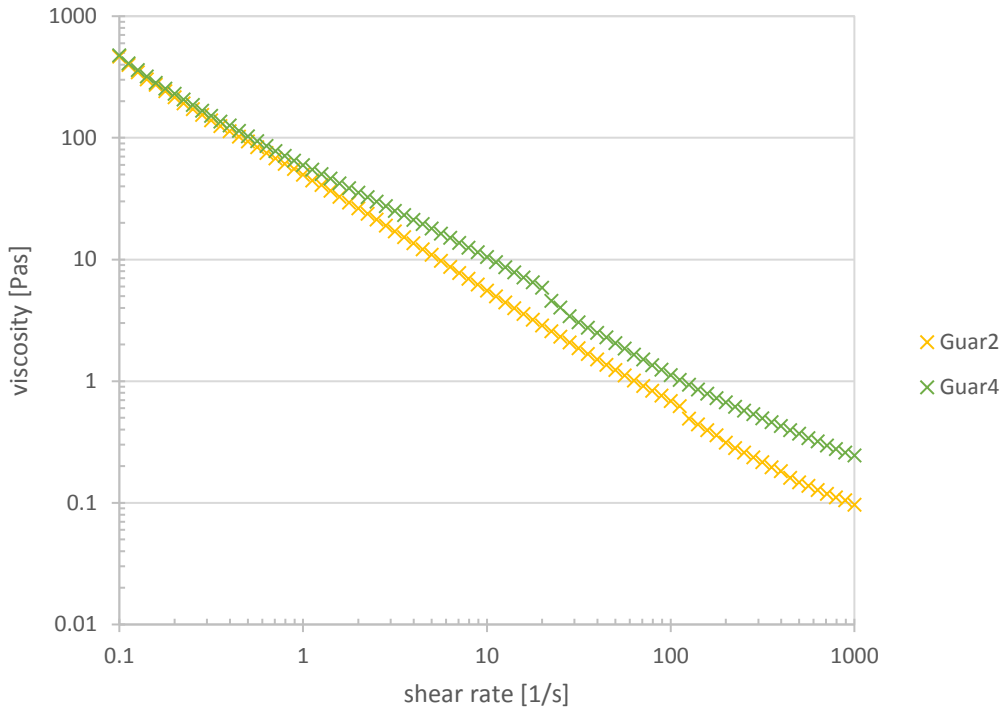

Figure 3. Guar flow diagrams.

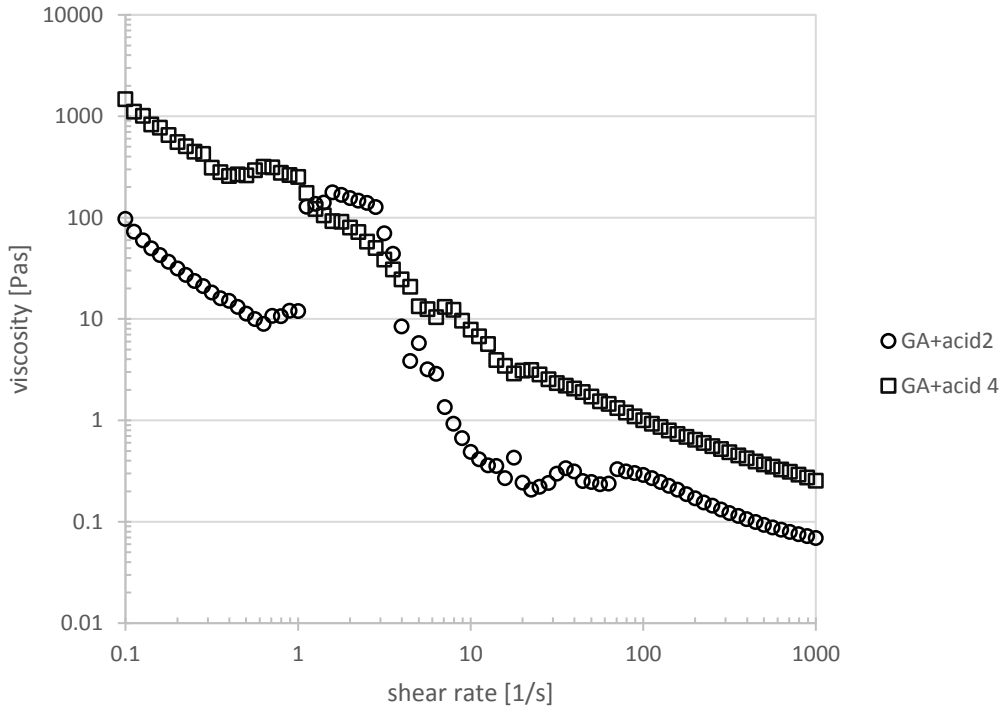

Figure 4. GA+acid flow diagrams.

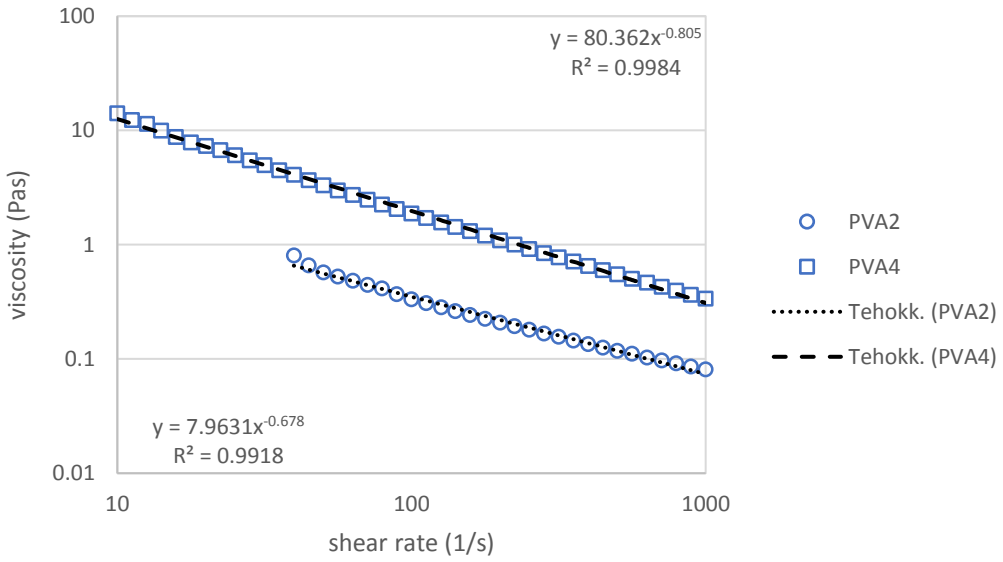

Figure 1. PVA flow curves fitted with powerlaw functions at high shear rates.

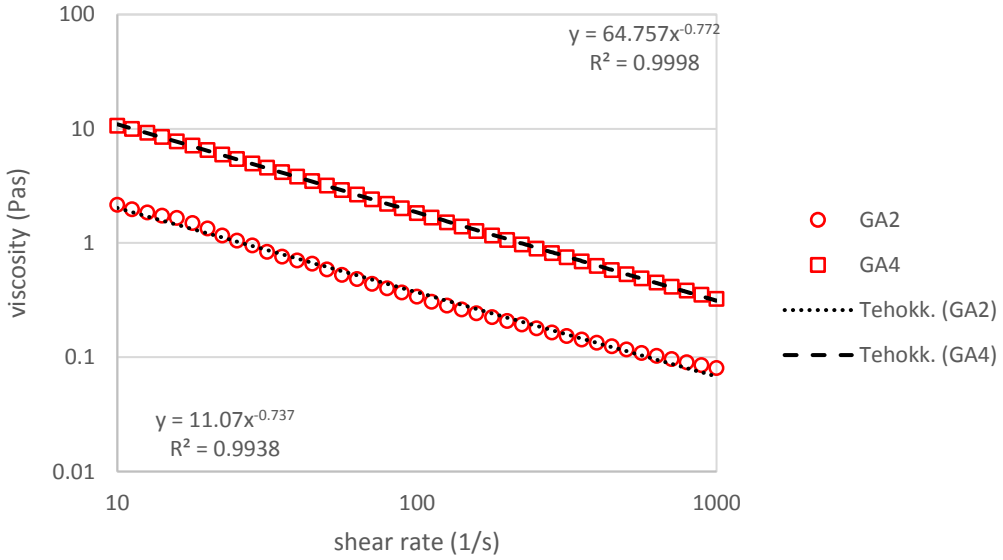

Figure 2. GA flow curves fitted with powerlaw functions at high shear rates.

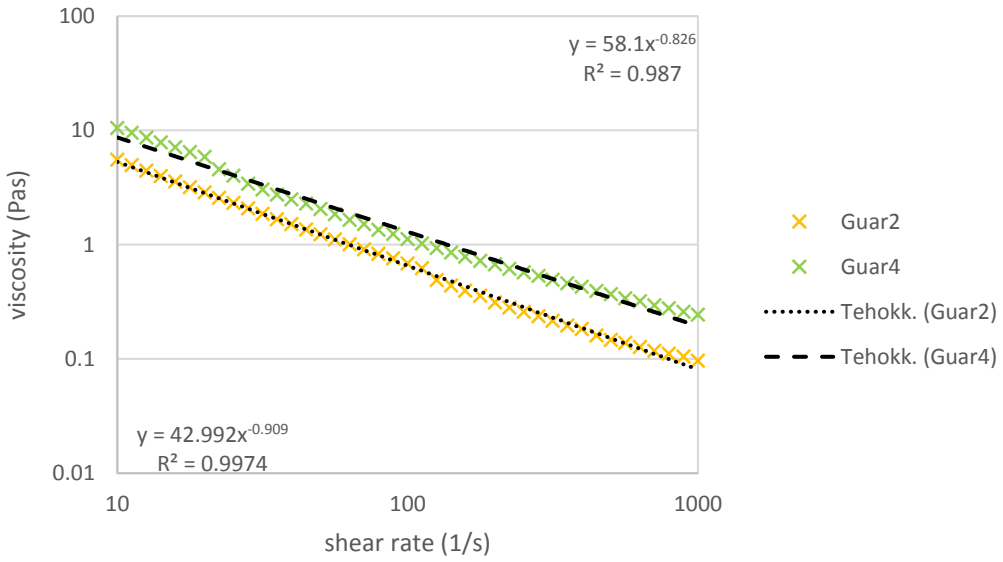

Figure 3. Guar flow curves fitted with powerlaw functions at high shear rates.

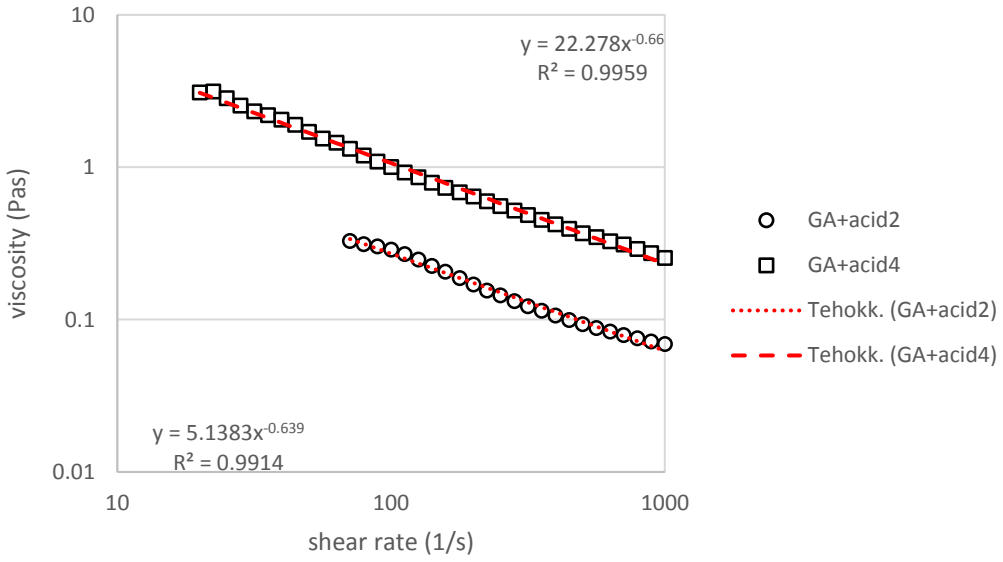

Figure 4. GA+acid flow curves fitted with powerlaw functions at high shear rates.

Table 11. Breaking mass data

sample	needle	Mean mass of 10 drops	standard deviation
PVA2	thin	0.1117	0.0026
	normal	0.1542	0.0026
	short	0.1477	0.0038
GA2	thin	0.1164	0.0186
	normal	0.1538	0.0043
	short	0.1475	0.0060
Guar2	thin	0.0818	0.0035
	normal	0.1267	0.0050
	short	0.1228	0.0065
GA+acid2	thin	0.1036	0.0056
	normal	0.1368	0.0041
	short	0.1381	0.0024
PVA4	thin	0.1324	0.0032
	normal	0.2182	0.0034
	short	0.2546	0.0804
GA4	thin	0.1218	0.0064
	normal	0.2230	0.0071
	short	0.2216	0.0035
Guar4	thin	0.1079	0.0059
	normal	0.2092	0.0072
	short	0.2006	0.0083
GA+acid4	thin	0.1182	0.0053
	normal	0.1918	0.0112
	short	0.2135	0.0057

Table 12. Air gap lengths for the dopes

dope	needle	needle position	water position	critical length
PVA2	thin	2.00	2.10	0.10
	normal	1.80	2.00	0.20
	short	0.00	0.20	0.20
GA2	thin	2.00	2.10	0.10
	normal	1.80	2.00	0.20
	short	0.00	0.20	0.20
PVA4	thin	2.00	3.13	1.13
	normal	1.80	3.50	1.70
	short	0.00	1.80	1.80
GA4	thin	2.00	2.95	0.95
	normal	1.80	3.25	1.45
	short	0.00	1.55	1.55
Guar2	thin	2.00	2.10	0.10
	normal	1.80	1.90	0.10
	short	0.00	0.20	0.20
Guar4	thin	2.00	4.30	2.30
	normal	1.80	3.90	2.10
	short	0.00	2.30	2.30
GA+acid2	thin	2.00	2.10	0.10
	normal	1.80	1.90	0.10
	short	0.00	0.10	0.10
GA+acid4	thin	2.00	3.10	1.10
	normal	1.80	3.20	1.40
	short	0.00	1.50	1.50

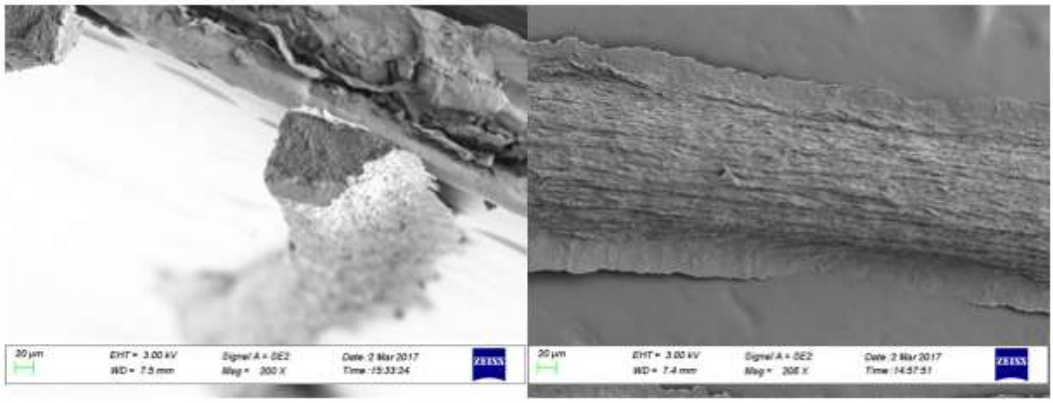

Figure 1. PVA2 cross section and side view.

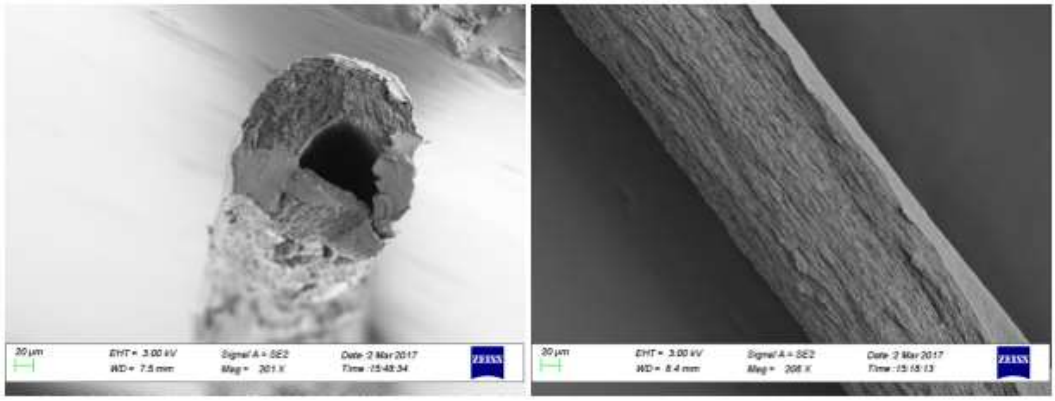

Figure 2. PVA4 acidic with bubble cross section and side view.

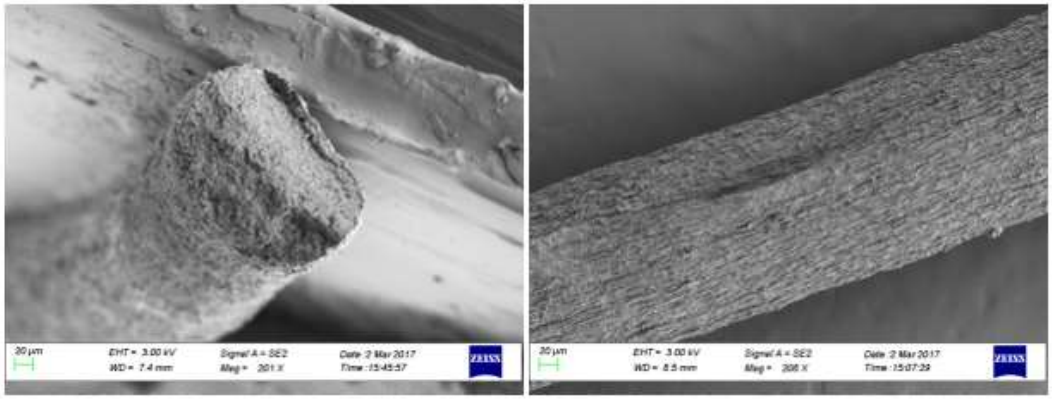

Figure 3. PVA4 neutral cross section and side view.

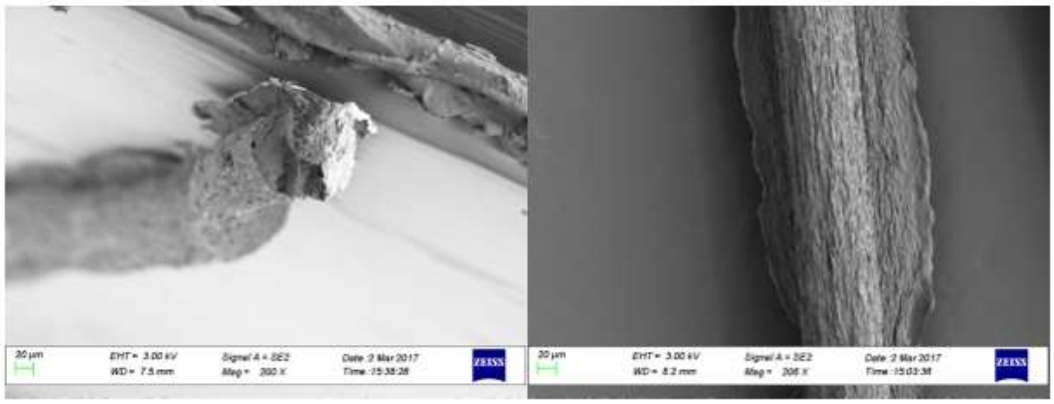

Figure 4. GA2 cross section and side view.

Figure 5. GA4 cross section and side view.

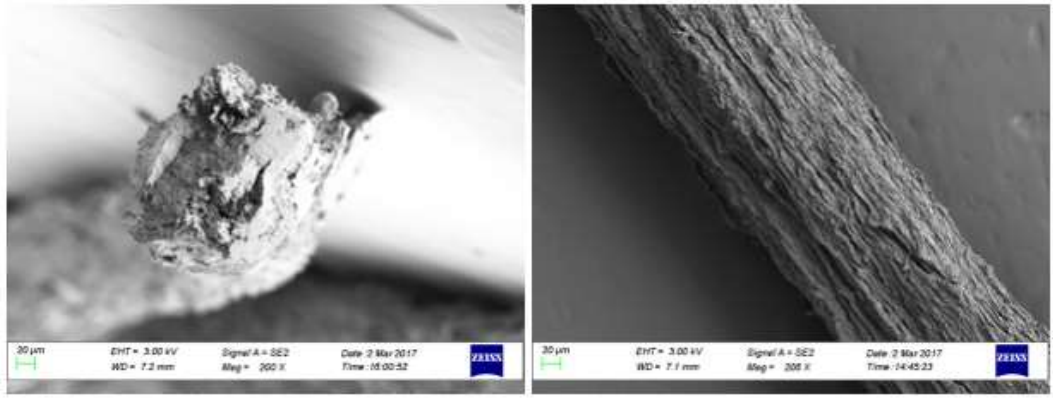

Figure 6. Guar4 cross section and side view.

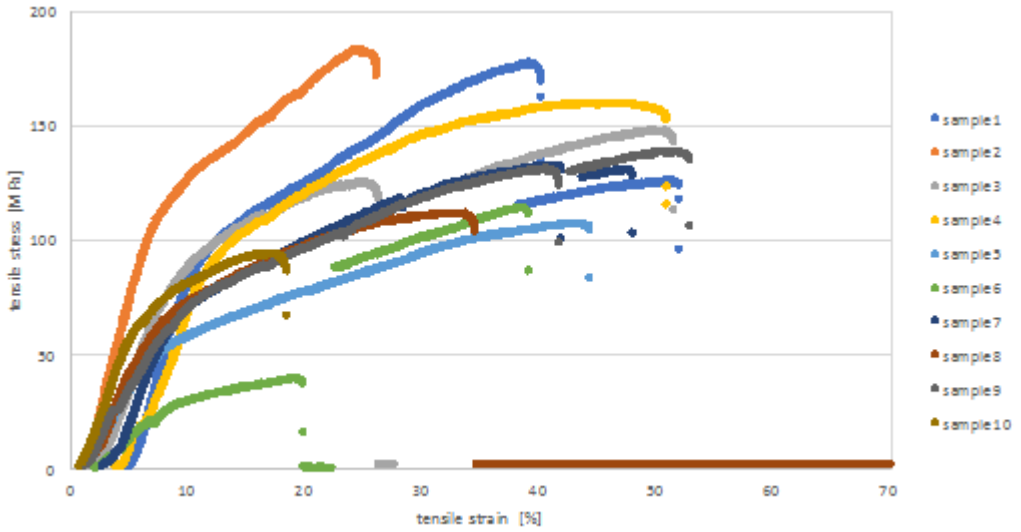

Figure 1. Tensile test results for PVA2.

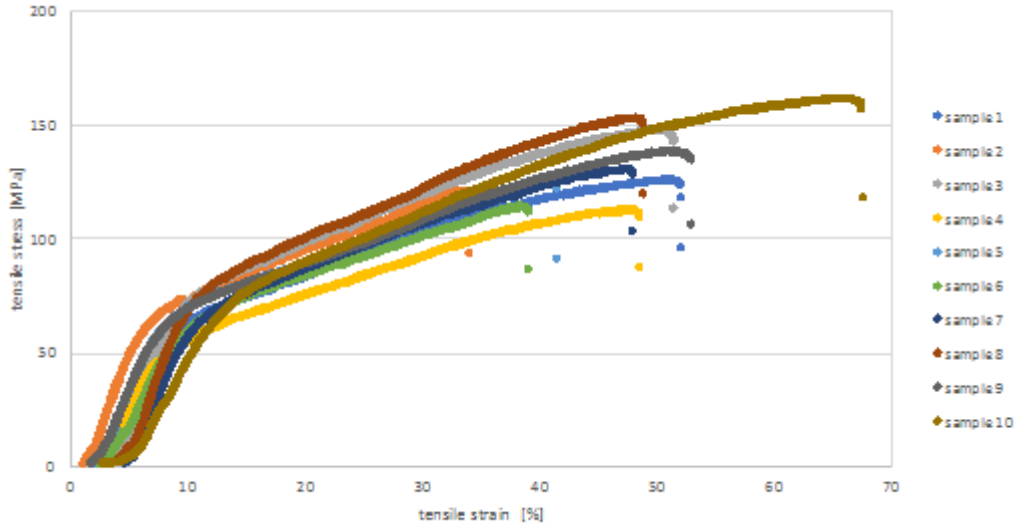

Figure 2. Tensile test results for GA2

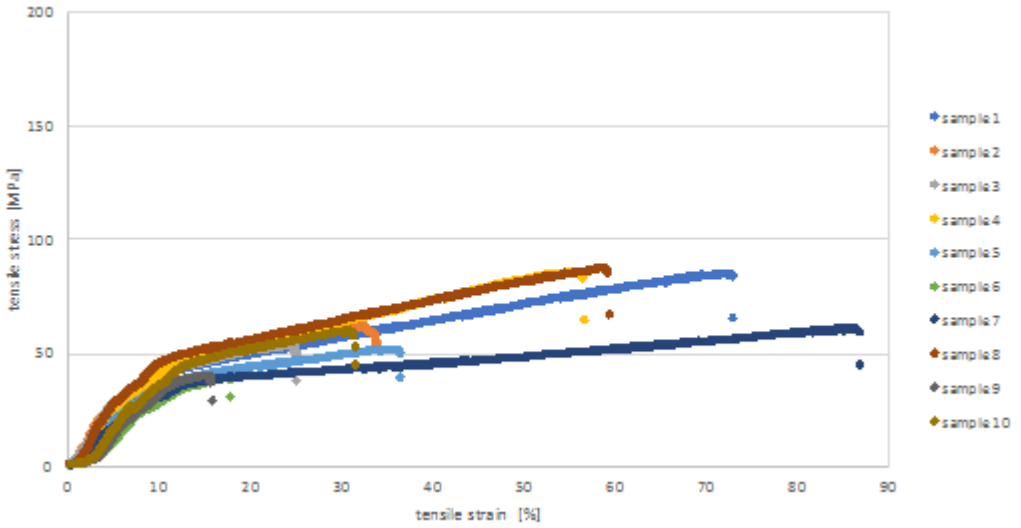

Figure 3. Tensile test results for PVA4 neutral.

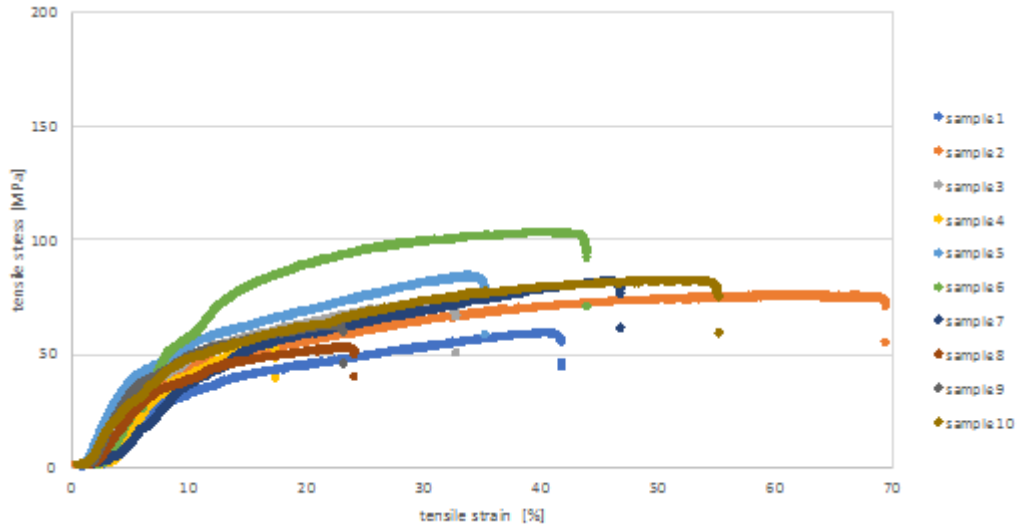

Figure 4. Tensile test results for PVA4 acidic.

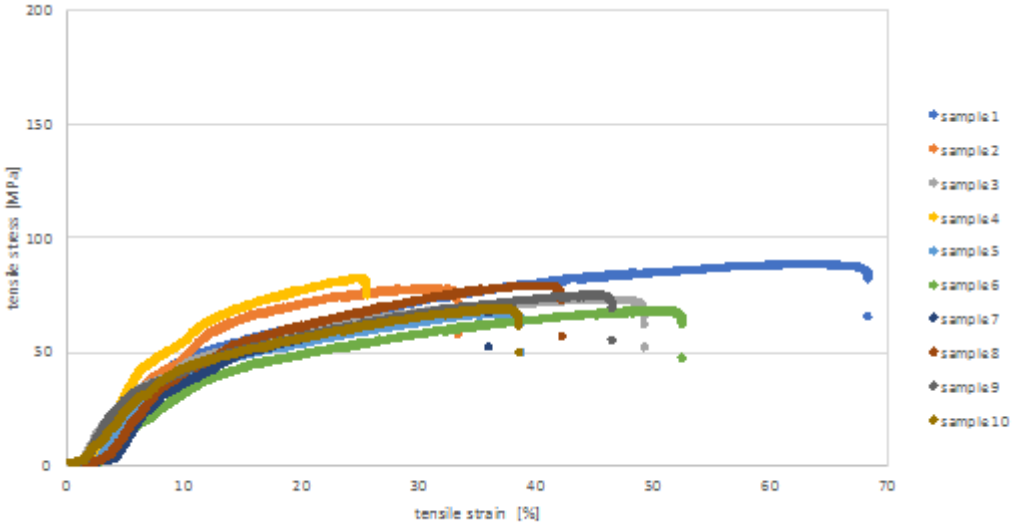

Figure 5. Tensile test results for GA4.

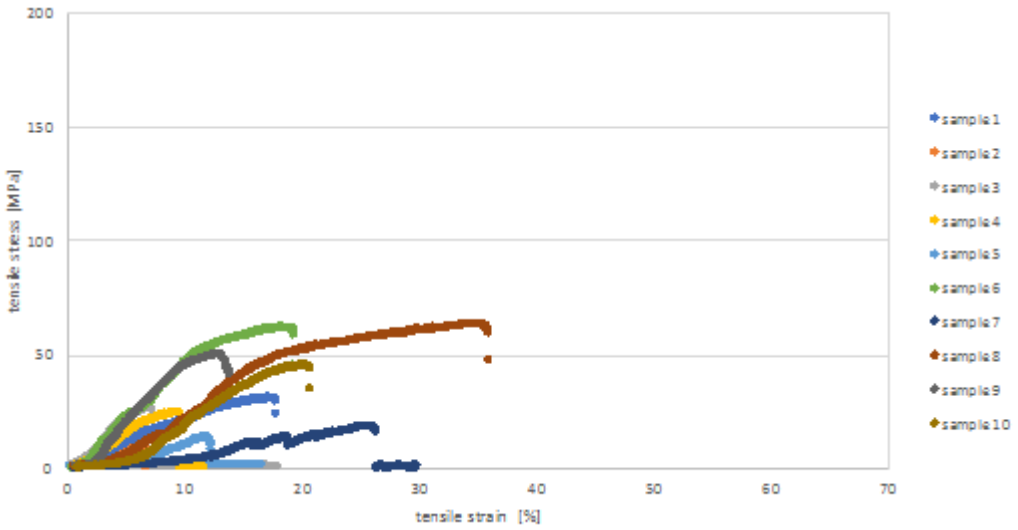

Figure 6. Tensile test results for Guar4.